University of Latvia

Faculty of Biology

Janis Leitans

Doctoral Thesis

Structural investigations of carbonic anhydrases for design of specific inhibitors

Promotion to the degree of Doctor of Biology

Molecular Biology

Supervisor: Dr. biol. Kaspars Tars

Riga, 2019

This Doctoral Thesis is a summary of publications.

The doctoral thesis was carried out at Latvian Biomedical Research and Study Center from 2013. to 2019.

The research was supported by the Latvian-Lithuanian-Taiwanese collaboration project “Design of Anticancer Pharmaceutical Compounds Using Structure and Energetics of Lead – Target Interaction”.

Supervisor: Prof. Kaspars Tārs

Reviewers:

1. Prof. Yean-Yves Winum
2. Prof. Kristaps Jaudzems
3. Dr. biol. Kalvis Brangulis

Chairman of the Doctoral Committee	Prof. Jānis Kloviņš	_____/ /
Secretary of the Doctoral Committee	Dr. biol. Daina Eze	_____/ /

Abstract

Carbonic anhydrases (CAs) are widespread metalloenzymes that catalyze the interconversion of a water molecule and carbon dioxide into bicarbonate and hydrogen ions. In mammals, CAs are involved in many vital processes such as regulation of pH and fluid balance and transport of carbon dioxide. However, activity of some CA isoforms can also promote several pathologies.

The enzymatic activity of human CA isoform II (hCA II) is associated with glaucoma. It increases the concentration of the bicarbonate ion in the eye, followed by intake of Na^+ ions and water flow along the gradient, thereby increasing intraocular pressure. Increased intraocular pressure is damaging to the eye nerve, which can lead to complete blindness. hCA II inhibitors are used as anti-glaucoma medicaments, able to decrease intraocular pressure.

Human CA isoform IX (hCA IX) is produced in a limited number of normal tissues, while it is significantly overexpressed in many solid tumors. The enzymatic activity of hCA IX helps to maintain the pH of hypoxic tumor cells within normal range and lowers the pH level of the extracellular matrix, thus accelerating tumor growth and metastasis. Therefore, specific hCA IX inhibitors potentially could be used to suppress cancer growth and metastasis.

Ideally, inhibition of CAs should be selective and targeted to specific isoforms. Medically used CA inhibitors have high affinity to most mammalian CA isoforms, thus making a long list of undesired side effects. In order to design an isoform selective inhibitor, accumulation of structural data is of crucial importance. Milligram amounts of pure enzyme are needed for structural studies and therefore efficient expression and purification protocols must be used. For hCA II highly efficient expression and purification system is already available and protein crystals can be produced easily. We have co-crystallized hCA II in complex with multiple CA inhibitors, not only giving further understanding for ligand-protein interactions, but also discovering a new type of CA ligands.

At the time, there was only one protein production and purification system for hCA IX with a rather poor outcome. We managed to create a new expression and purification system for catalytic domain of hCA IX. Crystals were obtained with multiple CA inhibitors, not only notably increasing the available structural data about interactions of diverse inhibitors with the enzyme, but also providing a new perspective for further structural and functional studies of hCA IX.

Kopsavilkums

Ogļskābes anhidrāzes (CA) ir plaši izplatīti ar metāla jonu saistītie enzīmi, kas katalizē atgriezenisko reakciju, kurā ūdens molekula un ogļskābā gāze veido bikarbonāta un ūdeņraža jonus. Zīdītājos tās piedalās daudzos vitāli svarīgos procesos, kā piemēram pH regulēšanā un CO_2 transportēšanā, tomēr dažu CA aktivitāte ir saistīta ar vairākām patoloģijām.

Cilvēkos sastopamā CA II izoforma (hCA II) tiek saistīta ar glaukomu. hCA II enzimātiskā aktivitāte paaugstina bikarbonāta jonu koncentrāciju acī, tam seko Na^+ jonu pieplūdums un ūdens plūsma gradienta virzienā, tādējādi paaugstinot intraokulāro spiedienu. Paaugstinātais intraokulārais spiediens bojā redzes nervu, kas var novest pie pilnīga redzes zuduma. hCA II inhibitori tiek izmantoti kā anti-glaukomas medikamenti, lai samazinātu slimības izraisītās sekas.

Cilvēkos sastopamā ogļskābes anhidrāzes IX izoforma (hCA IX) tiek producēta nelielā skaitā veselo audu, bet tās ekspresija ir ievērojami palielināta daudzos audzēju veidos. hCA IX enzimātiskā aktivitāte palīdz uzturēt normālu pH līmeni hipoksiskajās audzēja šūnās, vienlaikus samazinot pH audzēju vidē, tādejādi paātrinot audzēju attīstību. Specifiski hCA IX inhibitori varētu tikt izmantoti, lai kavētu audzēju attīstību.

Ideāli, CA inhibēšanai vajadzētu būt mērķētai uz specifisku izoformu. Medicīnā plaši izmantotie CA inhibitori ir ar augstu afinitāti pret vairumu zīdītājos sastopamo CA izoformu, līdz ar to, veidojot daudzas nevēlamas blaknes. Lai izveidotu izoformas selektīvu inhibitoru, ir būtiski akumulēt strukturālos datus. Strukturālo pētījumu priekšnosacījums ir miligramos mērāms attīrītā proteīna daudzums, līdz ar to, nepieciešama efektīva ekspresijas un attīrīšanas sistēma. hCA II esošā ekspresijas, attīrīšanas un kristalizācijas sistēma ir pietiekoši efektīva kristalogrāfijas vajadzībām. Mēs esam kokristalizējuši hCA II kompleksā ar vairākiem CA inhibitoriem, ne tikai dodot plašāku ieskatu ligandu-proteīnu mijiedarbībās, bet arī atklājot jaunu CA ligandu tipu.

Promocijas darbu uzsākot, vienīgā aprakstītā hCA IX producēšanas un attīrīšanas sistēma bija ar vāju iznākumu. Mums izdevās izveidot jaunu hCA IX katalītiskā domēna ekspresijas un attīrīšanas sistēmu un iegūto proteīnu sakristalizēt ar dažādiem ligandiem. Iegūtie dati ne tikai ievērojami papildināja pieejamos strukturālos datus par hCA IX mijiedarbību ar dažādiem inhibitoriem, bet arī sniedza jaunas iespējas hCA IX strukturālajiem un funkcionālajiem pētījumiem.

Table of Contents

Abbreviations

3D – three (**3**) **d**imensional

Å – **Å**ngström

AMS - **a**cute **m**ountain **s**ickness

AZM – **a**ceta**z**ola**m**ide

CA – **c**arbonic **a**nhydrase

CCM - **c**arbon dioxide **c**oncentration **m**echanism

DMSO - **d**i**m**ethyl **s**ulf**o**xide

DNA – **d**eoxyribo**n**ucleic **a**cid

DTT - **d**i**t**hio**t**hreitol

GI - **g**astro**i**ntestinal

GPI - **g**lycosyl**p**hosphat**i**dylinositol

HIF - **h**ypoxia-**i**nducible **f**actor

HRE - **h**ypoxia-**r**esponsive **e**lement

IC – **i**ntra**c**ytoplasmic domain

IOP - **i**ntra**o**cular **p**ressure

IPTG - **i**so**p**ropyl-β-D-**t**hio**g**alactopyranoside

kDa - **k**ilo**da**lton

LB – **L**uria **b**roth

MBP - **m**altose **b**inding **p**rotein

Ni-NTA – **ni**ckel-**n**itrilo**t**riacetic **a**cid

NMR – **n**uclear **m**agnetic **r**esonance

OD – **o**ptical **d**ensity

PAGE – **p**oly**a**crylamide **g**el **e**lectrophoresis

PCR - **p**olymerase **c**hain **r**eaction

PDB - **p**rotein **d**ata **b**ank

PG – **p**roteo**g**lycan-like domain

RNA – **r**ibo**n**ucleic **a**cid

rpm – **r**evolutions **p**er **m**inute

RuBisCO - **r**ib**u**lose-1,5-**bis**phosphate **c**arboxylase/**o**xygenase

SDS – **s**odium **d**odecyl **s**ulfate

TEMED - **te**tra**m**ethyl**e**thylene**d**iamine

TEV – **t**obacco **e**tch **v**irus

TM – **t**rans**m**embrane segment

ZBG – **z**inc **b**inding **g**roup

Introduction

Carbonic anhydrases are widespread in all domains of life. They are ancient enzymes, increasing their diversity with each next level of organisms along the course of evolution. There are at least 16 mammalian CA isoforms with variable localization in cells and tissue, but responsibility for the catalysis of the same reaction. All mammalian CA isoforms share relatively high sequence homology and conservative active sites. Although CAs perform physiologically important functions in the organism, activities of some of the mammalian CA isoforms are associated with various diseases. hCA II is a widespread CA isoform, but it is involved in manifestation of glaucoma and acute mountain sickness (AMS) symptoms and it is also overexpressed in gastrointestinal stromal tumor. hCA IX is expressed in a very limited number of normal tissues, but its highly overexpressed in many solid tumors. It has been assumed that enzymatic activity of hCA IX favors tumor growth, thus inhibition of this CA isoform could abate tumor spread.

The first crystal structure of hCA II was solved in 1972. Now there are over 775 3D structures of hCA II available in the Protein Data Bank, making it one of the most structurally studied enzymes to date. Even so, selective hCA II inhibitors are yet to be achieved hCA II in many cases is considered an off-target isoform but, it is usually used as a primary test subject for new types of CA ligands.

Although due to its high expression levels in many tumor types hCA IX is the main target for isoform selective CA drug design, up until 2015 there was only one protein 3D structure available in the PDB. Judging from the available data, no other research group has managed to obtain new hCA IX crystals, not even in the previously described crystallization conditions. Also, the described baculovirus expression system has a poor outcome, limiting the available experiments from one purification batch. In order to improve that, we decided to develop a new hCA IX catalytic domain expression and purification system, suitable for crystallization studies.

The aim of this study was analysis of interactions of multiple ligands with the human carbonic anhydrase isoforms II and IX in order to use the results in rational, structure-based drug design.

Workflow:

1. Expression and purification of hCA II;
2. Cloning, expression and purification of hCA IX;
3. Crystallization of hCA II and hCA IX catalytic domain with multiple ligands;

4. Data collection of protein crystals;
5. Analysis of the collected X-ray data, ligand modeling and protein-ligand interaction determination.

1. Literature review

1.1. Carbonic anhydrases

Carbonic anhydrases (CAs) are metalloenzymes that catalyze the reversible reaction:

$$CO_2+H_2O \leftrightarrow HCO_3^- + H^+$$

The reaction occurs within seconds also without a catalyst, but apparently this is not fast enough to meet the physiological needs of organism. CAs are among the fastest enzymes known catalyzing up to 1 000 000 reactions per second (Berg et al., 2002) (Table 1). CAs are widespread in many different organisms and mostly are responsible for vital processes in the organism. Meanwhile enzymatic activity of some CA isoforms is associated with various pathologies and their inhibition could slow down or even prevent specific diseases (Deitmer et al., 2015; Pinard et al., 2015).

Table 1. Comparison of catalyzed reactions per second and rate enhancement of various enzymes. Adapted from (Berg et al., 2002).

Enzyme	Nonenzymatic half-life	Uncatalyzed rate (k_{un},s^{-1})	Catalyzed rate (k_{cat}, s^{-1})	Rate enhancement (k_{cat}/k_{un})
OMP decarboxylase	78 000 000 years	2.8×10^{-16}	39	1.4×10^{17}
Staphylococcal nuclease	130 000 years	1.7×10^{-13}	95	5.6×10^{14}
AMP nucleosidase	69 000 years	1.0×10^{-11}	60	6.0×10^{12}
Carboxypeptidase A	7.3 years	3.0×10^{-9}	578	1.9×10^{11}
Ketosteroid isomerase	7 weeks	1.7×10^{-7}	66 000	3.9×10^{11}
Triose phosphate isomerase	1.9 days	4.3×10^{-6}	4300	1.0×10^{9}
Chorismite mutase	7.4 hours	2.6×10^{-5}	50	1.9×10^{6}
Carbonic anhydrase	5 seconds	1.3×10^{-1}	1 000 000	7.7×10^{6}

1.2. CA enzymatic reaction

CAs are metalloenzymes, active site of which in most cases contain a Zn^{2+} ion, coordinated by four ligands. Zn^{2+} ion can be coordinated by various residues (histidine, cysteine, etc.) (Laitaoja et al., 2013), but in most CA isoforms it is coordinated by nitrogen atoms of three histidine imidazole rings while the fourth coordination site is occupied by a water molecule (Fisher et al., 2007; Supuran, 2012) (Figure 1.).

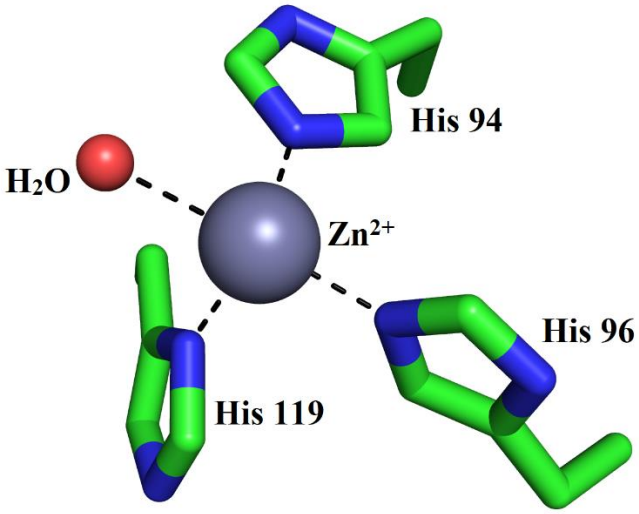

Figure 1. Coordination of zinc ion in human carbonic anhydrase isoform IX (PDB code 6FE2). The figure was prepared with the PyMOL Molecular Graphics System, Version 2.0 Schrödinger, LLC.

The reaction mechanism of CO_2 anhydrase is shown in Figure 2. When a water molecule is bound to the Zn^{2+} ion, it dissociates to OH^- group as a result of proton transfer. OH^- group makes a nucleophilic attack to electrophilic CO_2 forming a HCO_3^- ion. HCO_3^- stays weakly bound to Zn^{2+} ion until it is further replaced by a water molecule and the reaction cycle can start over again (Fisher et al., 2007; Supuran, 2012) (Figure 2.).

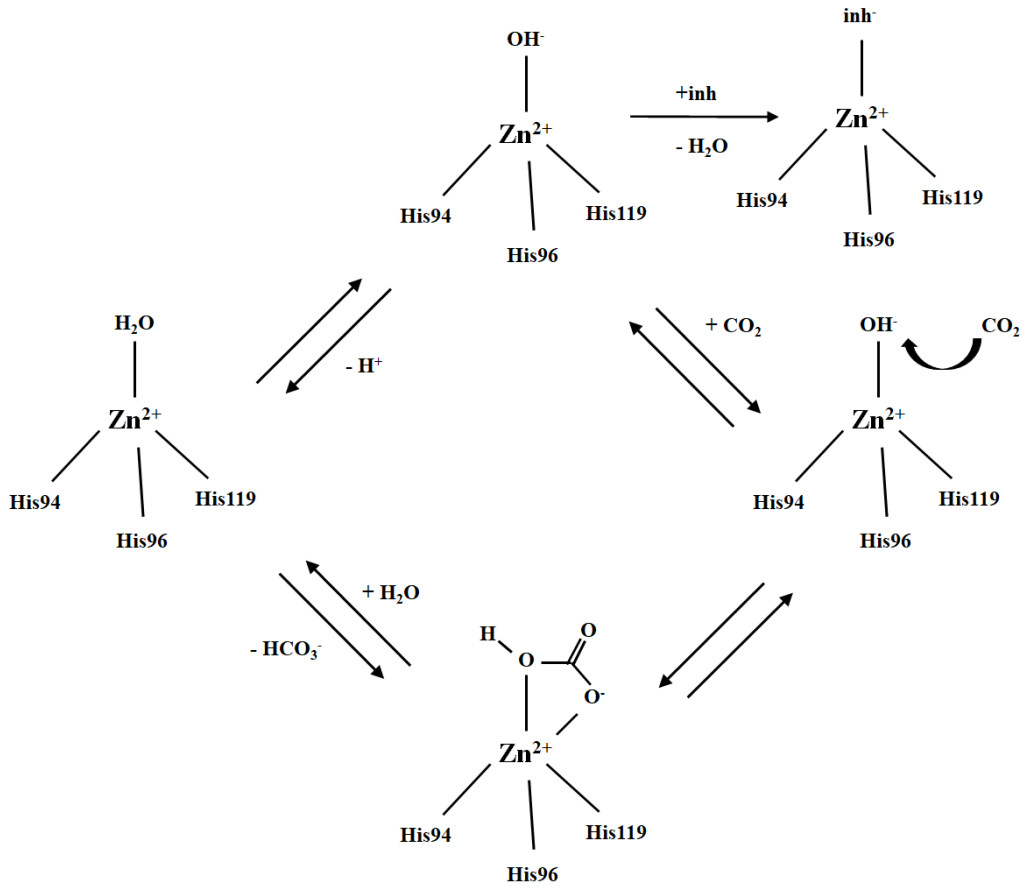

Figure 2. Enzymatic reaction of carbonic anhydrase. Adapted from (Supuran, 2012).

1.2.1. His64 proton shuttle

In case of CAs, speed of enzymatic reaction can be so vast that it becomes limited by substrate diffusion (Lindskog, 1997). A specific proton transfer mechanism greatly increases proton movements near the active site and allows the enzyme to bind a new substrate more quickly, therefore increasing the reaction speed (Maupin & Voth, 2007; Fisher et al., 2007; Tu et al., 2002). Movement of His64 (CA II numbering) side chain rotamer is significant for speed enchantment of catalytic reaction and has been proven by various kinetic measurements using hCA II His64→Ala mutants. Enzymatic reaction in those mutants ensued 10-50x slower than in the wild type hCA II (Tu et al., 1989; Roy & Taraphder, 2006). X-ray data has demonstrated that side chain of His64 has two alternative rotamers – "in" (closer to the active center) and "out" (further from the active center). As His64 "in" position is still too far from Zn^{2+} ion (~7.5 A) or Zn^{2+} bound water molecule it cannot carry out its proton transfer function directly. His64 proton transfer is achieved by a network of water molecules, forming a bridge in order to transfer the protons. His64 at its "in"

position obtains the proton from a nearby located water molecule and moves to the “out” position releasing the proton (Fisher et al., 2005) (Figure 3.).

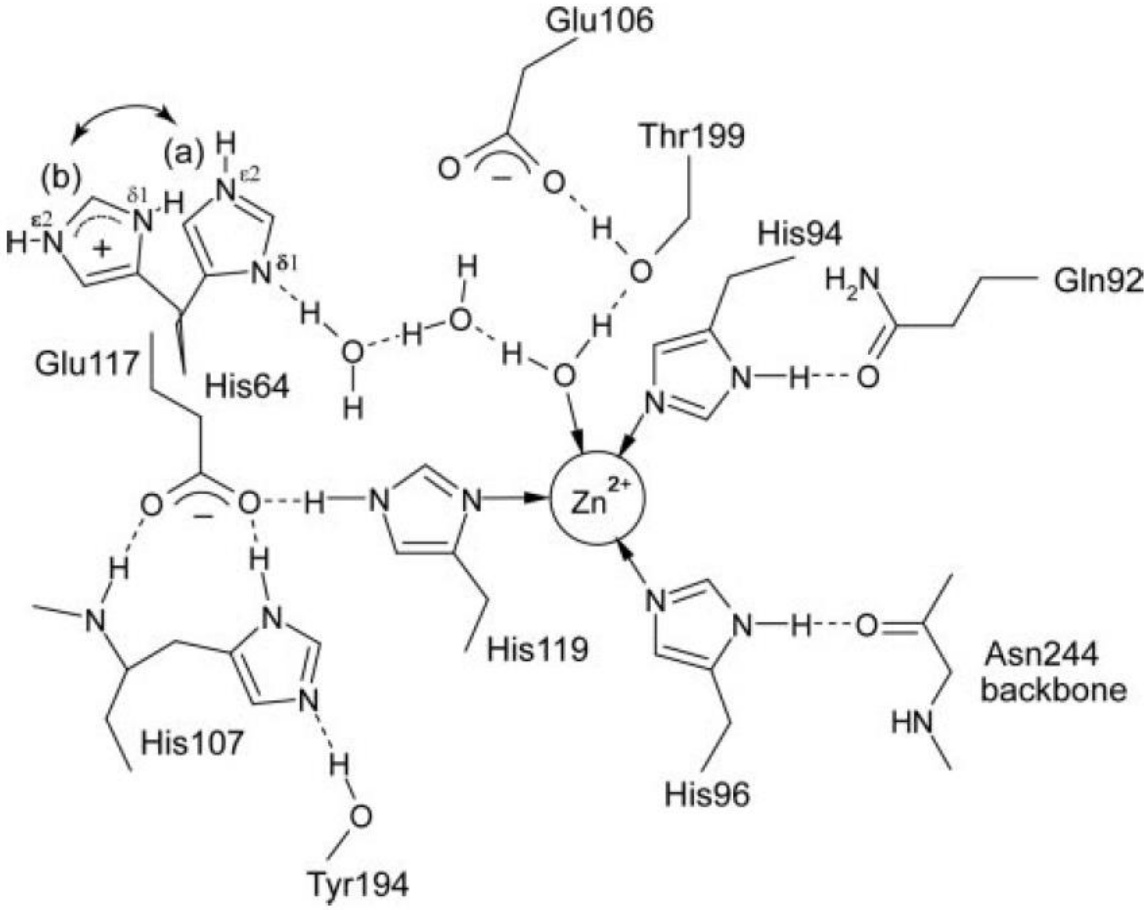

Figure 3. Solvent network of hCA II active site pocket and His64 proton shuttle mechanism Adapted from (Shimahara et al., 2007).

1.3. CA classification

Carbonic anhydrases are divided into 7 classes (α-, β-, γ-, δ-, ζ-, η-, and θ-CAs) (Capasso & Supuran, 2015; Kikutani et al., 2016; Supuran & Capasso, 2015; Aspatwar et al., 2018). CAs are structurally very diverse but the conjunctive element is the same catalytic reaction. Therefore, carbonic anhydrases are good examples of convergent evolution (Hewett-Emmett & Tashian, 1996; Liljas & Laurberg, 2000). CAs are evolutionarily ancient enzymes and pose higher and higher diversity along with increasing complexity of organisms (Banerjee & Deshpande, 2016).

1.3.1. β-CA

The β-class carbonic anhydrases are abundant among lower eukaryotes, prokaryotes, archaea and plants (Rowlett, 2010). Catalytic activity of β-CAs is relevant in photosynthesis. β-CAs help to regulate chloroplast pH levels and the CO_2 concentration mechanism (CCM) near RuBisCO (Bhat et al., 2017) (Figure 4.).

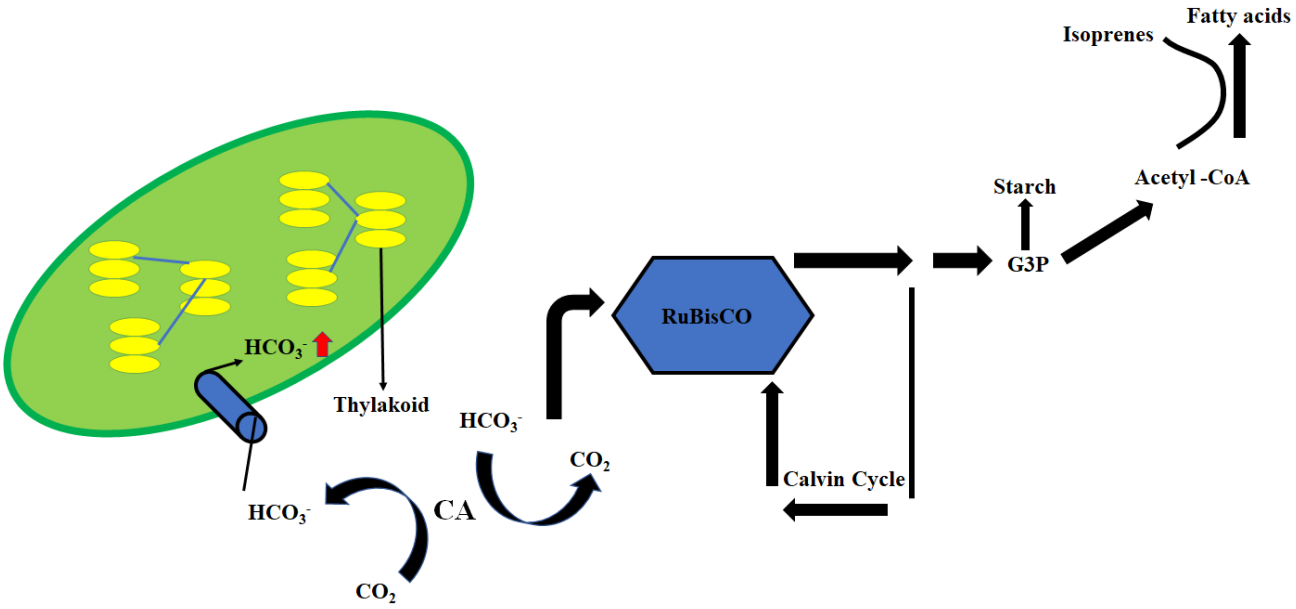

Figure 4. Role of the β-CAs explained involving RuBisCO. Adapted from (Bhat et al., 2017).

β-CAs are associated with ability of some plants to overcome cold temperatures and low light conditions and they also participate in immune responses to pathogens (Siedlecka et al., 1999). Structurally, β-CAs resemble a Rossmann fold, in which a central four-stranded parallel beta sheet with additional antiparallel strand is surrounded by alpha helices from both sides (Figure 5.). Catalytic zinc ion in β-CAs is coordinated by two cysteines and one histidine. Occasionally, Zn^{2+} ion in β-CAs can be coordinated by a fourth residue – aspartate, which renders the enzyme inactive at pH values below 8, but above pH 8.3 aspartate gets replaced by a water molecule thus re-activating the enzyme. (Huang et al., 2011; DiMario et al., 2017).

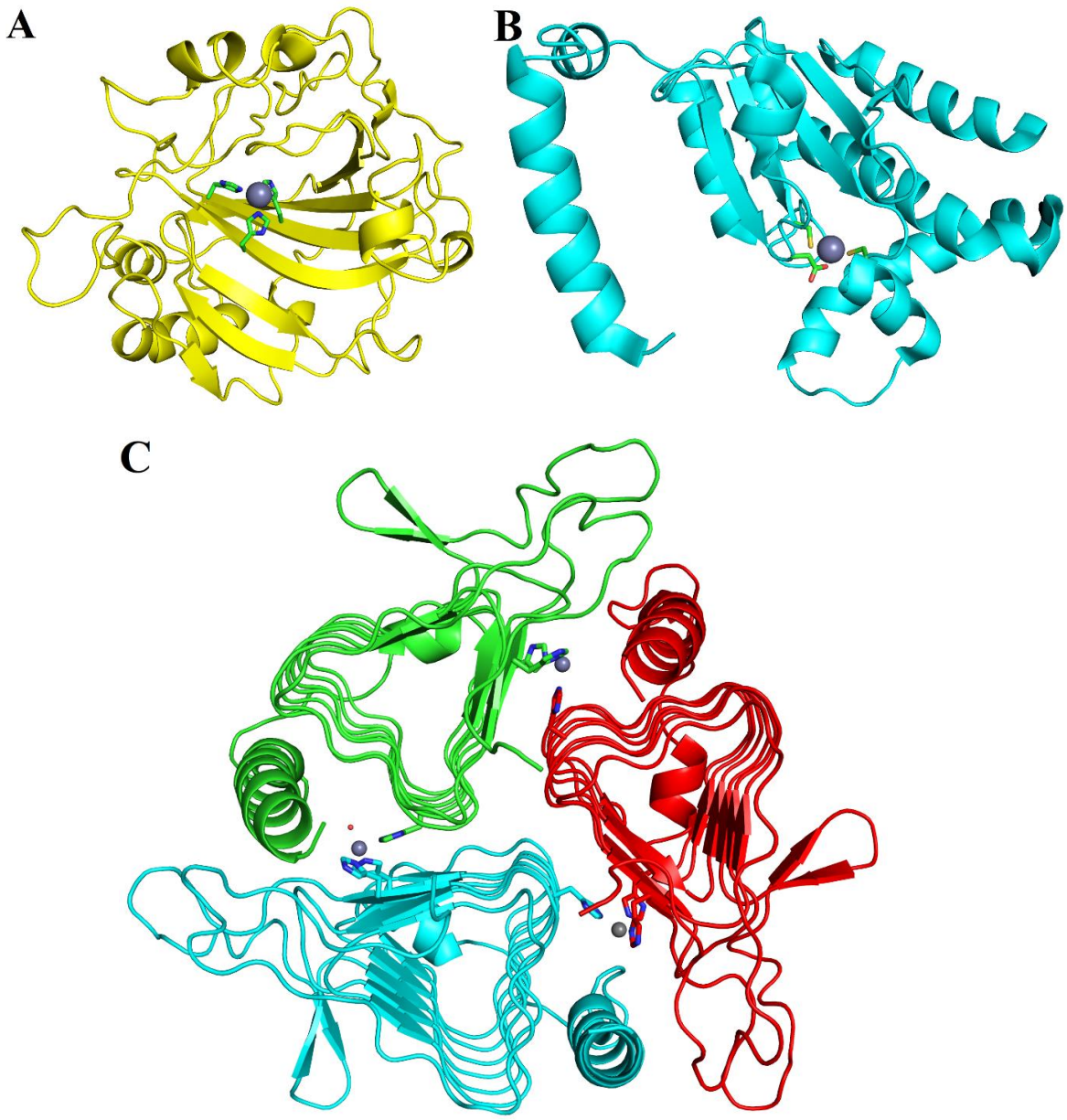

Figure 5. Tertiary structures of α-CA (panel A, PDB code 1CA2), β-CA (panel B, PDB code 1I6P) and γ-CA (panel C, PDB code 1QRG). Zn^{2+} ion coordinating residues are indicated. The figure was prepared with the PyMOL Molecular Graphics System, Version 2.0 Schrödinger, LLC.

Beta class CAs are found also in pathogens like *Salmonella typhimurium*, *Mycobacterium tubercolusis* and *Heliobacter Pylori* (Rowlett, 2010). Since β- CAs are involved in important functions of pathogens, specific inhibition could have antibacterial effect (Vullo et al., 2018). Antibacterial properties of CA inhibitors have been detected in studies on *S. Typhimurium* (Zimmerman & Ferry, 2008), potentially enabling development of CA-targeted antibiotics.

1.3.2. γ-CA

The γ-CA class is widely distributed in all three domains of life, however only a few of γ-CA enzymes have been studied kinetically or structurally, largely from Archaea domain (Ferry, 2010).

Structurally, monomers of γ-CAs are beta helices. Three monomers form a functionally active trimeric enzyme with three active sites located in between the monomers. Active site architecture of γ-CAs is somewhat similar to mammalian CAs, since Zn^{2+} is being coordinated by three histidines (Pena et al., 2010). Tested sulfonamides display weaker affinity to γ-CA than mammalian CA isoforms, which can be explained by different pocket conformation at the enzyme active site (Zimmerman & Ferry, 2008).

1.3.3. Other CA classes

δ- CA class can be found in marine diatoms (Del Prete et al., 2014a; Lapointe et al., 2008). ε- CA class has been identified in carboxysomal shell (So et al., 2004) of cyanobacteria and now are considered being highly modified β-CAs. η- family of CAs has been found in *Plasmodium* species and their enzymatic activity is considered to favor malaria (Reungprapavut et al., 2004; Krungkrai & Krungkrai, 2011), therefore they might be important targets for anti-malarial drugs. θ- class was recently identified in marine diatoms (Kikutani et al., 2016). ζ- class CAs also have been identified in marine diatoms. Structurally they somewhat resemble β-CAs both in respect to overall structure and metal coordination. ζ- class CAs are unique in their ability to use cadmium ion instead of zinc ion in their active sites, which might be an evolutionary advantage in zinc-depleted environments, often found in oceans (Alterio et al., 2015a).

1.3.4. α-CA

α-CA isoforms are found in many diverse organisms - algae, some bacteria and vertebrates, including mammals. α-CAs are structurally similar and their monomers are composed of seven alpha helices and 10 beta strands (Aggarwal et al., 2013). There are 16 α-CA isoforms identified in humans (hCAs) (Supuran, 2018a) with various localizations in the cell – cytosolic, mitochondrial, membrane-associated and secreted. Different hCA isoforms display remarkably different speeds of catalyzed reaction (Singh, 2018; Pinard et al., 2015) (Table 2). For example, CA Va isoform is considerably less active than hCA II, probably because of His64 → Ala mutation which disrupts the proton transfer mechanism and significantly lowers enzymatic activity (Heck et

al., 1996). CA VIII, X and XI isoforms are enzymatically inactive (carbonic anhydrase related proteins, CARPs) and their function in cell remains unclear, but it has been demonstrated that overexpression of CARPs in certain tissues corelate with cancer (Aspatwar et al., 2010). hCA isoforms are mostly involved in vital processes like pH and CO_2 homeostasis, bone resorption, calcification and other (Frost, 2014), but activity of some hCA isoforms are associated with various diseases (Pinard et al., 2015).

Table 2. Characteristics of hCA isoforms - catalyzed reaction speeds, current number of PDB entries, localization in cell and tissue. Adapted from (Supuran, 2008b).

Isoform	K_{cat}	PDB entries	Location (cell)	Location (tissue/organ)
hCA I	2.0×10^5	32	cytosol	Red blood cells, GI tract
hCA II	1.4×10^6	775	cytosol	Red blood cells, lung, eye, brain, osteoclasts, GI tract. kidney, testis
hCA III	1.0×10^4	6	cytosol	Skeletal muscle, adipocytes
hCA IV	1.1×10^6	12	Membrane bound, extracellularly located catalytic domain	GI tract, lung, kidney, colon, pancreas, brain capillaries, heart muscle
hCA Va	2.9×10^5	4 (murine)	mitochondria	liver
hCA Vb	9.5×10^5	-	mitochondria	kidney, heart and skeletal muscle, spinal cord, pancreas, GI tract
hCA VI	3.4×10^5	1	secretory	Salivary and mammary glands
hCA VII	9.5×10^5	6	cytosol	CNS
hCA IX	3.8×10^5	9	Transmembrane, extracellularly located catalytic domain	GI tract, several tumours

hCA XII	4.2×10^5	18	Transmembrane, extracellularly located catalytic domain	Eye, reproductive epithelia, renal, intestinal kidney, several tumours
hCA XIII	1.5×10^5	16	cytosol	Lung, brain, kidney, reproductive tract, gut
hCA XIV	3.1×10^5	4	Transmembrane, extracellularly located catalytic domain	Kidney, heart, skeletal muscle, brain, liver

Most of the mammalian CA isoforms are cytosolic, CA Va/Vb are localized in mitochondria while CA IX, CA XII and CA XIV are transmembrane proteins with an extracellular catalytic domain (Whittington et al., 2001; Alterio et al., 2009). CA IV is a GPI-anchored CA isoform with extracellular catalytic domain (Schneider et al., 2013). CA VI is the only α-CA isoenzyme which is secreted and can be found in saliva (Kivela et al., 1999).

All of the human α-CA isoforms have a relatively high sequence identity and it ranges from 23.1% to 60.5% (Pinard et al., 2015) (Table 3). Active site forming residues for hCA isoforms are highly conservative and it is the main problem for design of isoform selective hCA inhibitors (Supuran, 2012).

Table 3. Human carbonic anhydrase sequence homology in percent (lower left) and number of conserved residues (upper right). Adapted from (Pinard et al., 2015).

	hCA I	**hCA II**	**hCA III**	**hCA IV**	**hCA Va**	**hCA Vb**	**hCA VI**	**hCA VII**	**hCA IX**	**hCA XII**	**hCA XIII**	**hCA XIV**
hCA I	-	158	141	78	126	128	82	132	83	91	154	85
hCA II	60.5	-	152	88	133	138	90	147	85	89	157	96
hCA III	54.2	58.5	-	82	120	117	87	130	80	86	151	90
hCA IV	30.0	33.5	31.2	-	89	93	97	90	84	91	84	62
hCA VA	48.1	50.8	45.4	23.6	-	184	93	131	83	84	124	88
hCA VB	46.9	51.9	43.5	23.1	58.7	-	82	134	89	79	131	88
hCA VI	31.9	33.5	32.3	27.0	27.9	24.4	-	93	107	104	90	106
hCA VII	50.8	56.2	49.6	31.8	48.5	49.2	34.9	-	95	103	139	97
hCA IX	33.1	34.2	31.1	27.2	31.9	32.7	38.9	37.0	-	101	90	113
hCA XII	35.8	34.2	32.3	28.1	31.6	29.7	38.0	38.0	38.9	-	91	123
hCA XIII	59.2	59.6	57.7	28.2	46.2	47.7	33.2	52.7	35.0	34.7	-	98
hCA XIV	34.2	35.8	34.2	29.0	31.9	29.0	35.8	36.0	44.4	46.0	37.4	-

1.4. Active site of α-carbonic anhydrases

The active site of hCA is amphipathic, possessing both hydrophobic and polar parts (Krishnamurthy et al., 2008). It is thought that this is due to the extremely different properties of substrate vs products – CO_2 is a hydrophobic gas, while HCO_3^- and H^+ highly soluble ions. Therefore, CO_2 enters or exits the active site through the hydrophobic part while ions use the polar part. This property can be used in the design of specific "dual-tail" inhibitors occupying both parts of the active site. The goal for providing selectivity between similar isoforms is to orient the tails of ligands towards the region which differs most between target isoforms (Casey et al., 2004).

Table 4. Active site forming residues in hCAs (CA II numbering). Residues coordinating Zn^{2+} ion are marked in green, most variable residues between isoforms are marked in red. Adapted from (Tars & Matulis, *in press*).

Residue	**Isoform**											
	I	**II**	**III**	**IV**	**Va**	**Vb**	**VI**	**VII**	**IX**	**XII**	**XIII**	**XIV**
5	W	W	W	W	W	Y	W	W	W	W	W	W
7	Y	Y	Y	Y	W	Y	Y	Y	Y	Y	Y	Y
60	I	L	L	Q	W	W	V	T	R	T	S	H
62	N	N	N	N	N	N	N	N	N	N	N	N
64	H	H	K	H	Y	Y	H	H	H	H	H	H
65	S	A	T	S	L	S	T	S	S	S	S	T
67	H	N	R	M	Q	L	Q	Q	Q	K	N	Q
91	F	I	R	K	K	K	Q	K	L	T	R	A
92	Q	Q	Q	Q	Q	Q	Q	Q	Q	Q	Q	Q
94	H	H	H	H	H	H	H	H	H	H	H	H
96	H	H	H	H	H	H	H	H	H	H	H	H
119	H	H	H	H	H	H	H	H	H	H	H	H
121	A	V	V	V	V	V	V	V	V	V	V	V
131	L	F	F	V	Y	F	Y	F	V	A	F	L
135	A	V	L	Q	V	A	Q	A	L	S	A	A
141	L	L	I	I	L	L	L	L	L	L	L	L
143	V	V	V	V	V	V	V	V	V	V	V	V
198	L	L	F	L	L	L	L	L	L	L	L	L
199	T	T	T	T	T	T	T	T	T	T	T	T
200	T	T	T	T	T	T	T	T	T	T	V	T
202	P	P	P	P	P	P	P	P	P	P	P	P

Table 4. shows that only a few residues within the active site of hCAs have a relatively high diversity between hCA isoforms, making achieving of selectivity a challenging task. A very important factor for isoform selective drug design is an available three-dimensional (3D) model of the target protein. Most ligands are modeled based on known 3D structures, combined with additional data for ligand-protein interactions (Pinard et al., 2015).

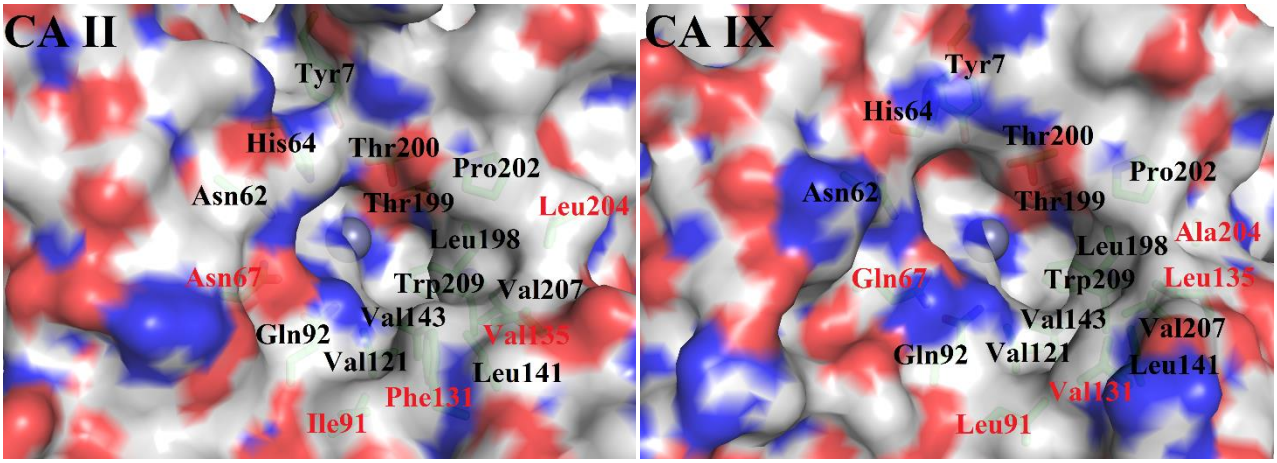

Figure 6. Comparison of active site pockets of hCA II (PDB code: 1CA2) and hCA IX (PDB code: 3IAI). Protein is visualized as a surface model, key residues forming the active site pocket are indicated. Residue labels in red indicate differences between hCA II and hCA IX. The figure was prepared with the PyMOL Molecular Graphics System, Version 2.0 Schrödinger, LLC.

Although active centers of all hCA isoforms are very similar there are some key residues which can be targeted for selectivity (Figure 6.). Some differences in the structure of active sites between CA isoforms can be also found in conservative regions, since the surrounding variable residues to some extent alter the overall 3D structure of the active site. Novel ligands can be modeled using protein–ligand docking software, trying to orient the ligand to the most diverse region between all α-CA isoforms (Tuccinardi et al., 2007).

1.5. Methods for structure determination of carbonic anhydrase

Even if the designed inhibitor binds well to the target enzyme, it is advisable to check the exact binding mode experimentally. Currently the most popular method for determination of protein-ligand interactions is X-ray crystallography. In case of monomeric CAs presumably NMR

could be used as well, but dimeric hCAs, like hCA IX or hCA XII are too large for analysis by solution NMR. The latest developments in cryo-electron microscopy (cryo-EM) allow structure determination at atomic resolution, but opposite to NMR currently it can be used only for large structures with size of at least 100 kDa. Neutron diffraction is yet another method of structure determination. In fact, hCA II is one of very few enzymes for which neutron diffraction structures have been determined. Although neutron diffraction has an advantage of revealing hydrogen positions, it requires extremely large crystals and very long data collection times, therefore in practice it can be successfully applied in very limited occasions.

To determine a 3D structure using x-ray crystallography the protein has to be crystallized first. Finding crystallization conditions is arduous and not every protein can be crystallized. Some hCA isoforms can be crystallized relatively efficiently, for example hCA II is easy to work with, as it can be easily produced in *E. coli*, it is highly soluble, can be purified without affinity tags and it crystallizes in a couple of days. Diffraction of hCA II crystals typically reaches atomic resolution (up to 0.9 Å) (Behnke et al., 2010; Avvaru et al., 2010). It is one of the most studied enzymes in the field of structural biology, with more than 775 structures available in the PDB. However, crystallization of other hCA isoforms is more challenging. Up until 2015 there was only one 3D structure available in the PDB for one of the main targets in CA drug design – tumor associated hCA IX (Alterio et al., 2009).

1.6. hCA II

hCA II is one of the 16 hCA isoforms and is encoded by the *CA 2* gene found in 8q21.2 region of 8th chromosome (Nakai et al., 1987). hCA II is a relatively widespread cytosolic CA isoform found in red blood cells, kidney, osteoclasts, eye, GI tract, lung, brain and elsewhere (Smith et al., 1999). hCA II has a fold and metal coordination pattern typical for all α-CAs (Avvaru et al., 2010) (Figure 7.).

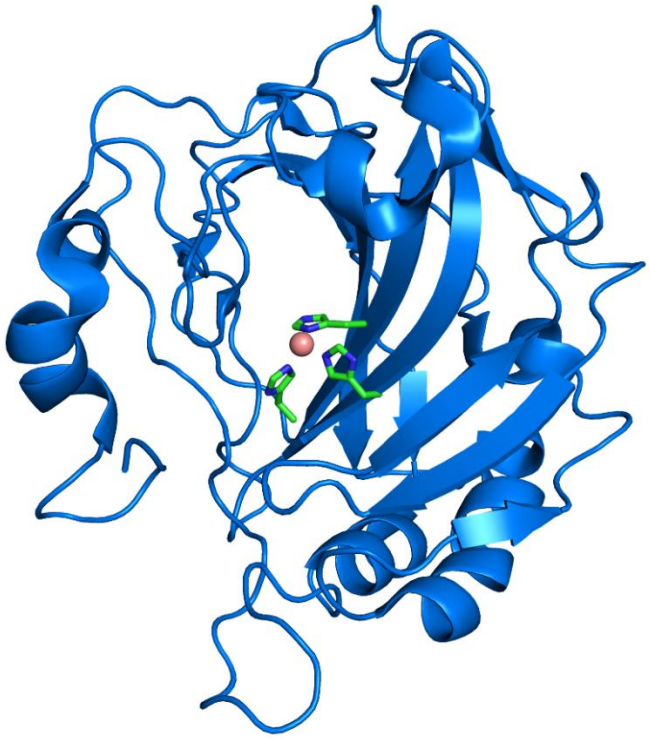

Figure 7. Tertiary structure of human carbonic anhydrase isoform II (PDB code: 3KS3). Zn^{2+} coordinating histidine residues are indicated. The figure was prepared with the PyMOL Molecular Graphics System, Version 2.0 Schrödinger, LLC.

hCA II is associated with various diseases by interfering with ion concentrations and influencing flow of water molecules. hCA II is associated with glaucoma (Kaur et al., 2002), acute mountain sickness (Taylor, 2011) and gastrointestinal stromal tumor (Parkkila et al., 2010). However, in most cases regarding the drug design, hCA II is considered an off-target isoform, since it is abundant in very many tissue types.

1.6.1. hCA II associated diseases

Glaucoma is a group of diseases characterized by a damage to optical nerve, which can lead to the loss of vision. The most important risk factor for development of glaucoma is increased intraocular pressure (IOP). Aqueous humor depends on the bicarbonate ion concentration in the eye. Human carbonic anhydrases (II, IV, XII) increase the bicarbonate ion concentration in the aqueous humor, followed by increase of Na^+ ion intake, which results in water flow along the gradient, thus increasing IOP (Mincione et al., 2008). Increased IOP damages the eye nerve and eventually leads to complete blindness (Maren, 1967). Although there is no cure for glaucoma, CA

inhibitors are used to ease the symptoms. Use of CA inhibitor acetazolamide (AZM) results in 25-30% decrease of the IOP, therefore lowering symptoms of glaucoma (Mincione et al., 2008). In medicine, the widely used CA inhibitor AZM is being sold under the trade name Diamox, treating various α-CA related diseases, including glaucoma (Jafarzadeh et al., 2014; Van Berkel & Elefritz, 2018). AZM has a poor selectivity and inhibits most of the human carbonic anhydrases, therefore common side effects include various symptoms like dizziness, lightheadedness, blurred vision, dry mouth, loss of appetite, nausea, vomiting, headache, diarrhea and many others (Katayama et al., 2002).

Enzymatic activity of hCA II is involved in acute mountain sickness (**AMS)** with symptoms present from approximately 2500 m (Taylor, 2011). High altitude caused hypoxia includes symptoms like troubled sleep, headache, dizziness, mental problems, weight loss, weakness and others. The exact mechanism of how CA inhibitor AZM reduces AMS symptoms is not known yet, but it has been associated with CA inhibition in the kidney (Leaf & Goldfarb, 2007).

Diuretics: it is known that inhibition of hCA II and membrane bound hCA IV and hCA XIV in humans work as diuretics (Supuran, 2008a; Carta & Supuran, 2013). By inhibiting those isoforms the available protons for the Na^+/H^+ antiporter, which regulate proton concentration in cell, decreases, resulting in transport of $NaHCO_3$ from the tubular lumen to the interstitial space, which increases water concentration and therefore induces diuretic effects (Puscas et al., 1999; Carta & Supuran, 2013).

Enzymatic activity of hCA II is involved in pH regulation in osteoclasts, therefore it is essential for optimal bone resorption (Kumar et al., 2007). It has been proved that *CA 2* gene deficiency in humans is related with osteopetrosis (Shah, et al., 2004). Therefore, hCA II inhibitors are used to treat **osteoporosis** (Pierce et al., 1991).

hCA II is overexpressed in **gastrointestinal stromal tumors** and therefore could be used as a biomarker for this particular type of cancer, or even as a target for inhibitors to slow tumor spread via destabilization of cancer cell pH (Parkkila et al., 2010).

1.7. hCA IX

Human carbonic anhydrase isoform IX (hCA IX) is encoded by the *CA9* gene found in the p12-p13 region of chromosome 9 (Nakagawa et al., 1998). *CA9* gene transcription is regulated by hypoxia-inducible transcription factor HIF-1 (Chiche et al., 2010; van den Beucken et al., 2009),

which is activated upon hypoxic conditions. HIF-1 is responsible for transcriptional control of *CA9* gene by binding to the *CA9* hypoxia-responsive element (HRE), which activates the *CA9* promoter and gene expression (Kaluz et al., 2009).

hCA IX is a transmembrane protein and consists of 4 domains (Alterio et al., 2009) (Figure 8.).

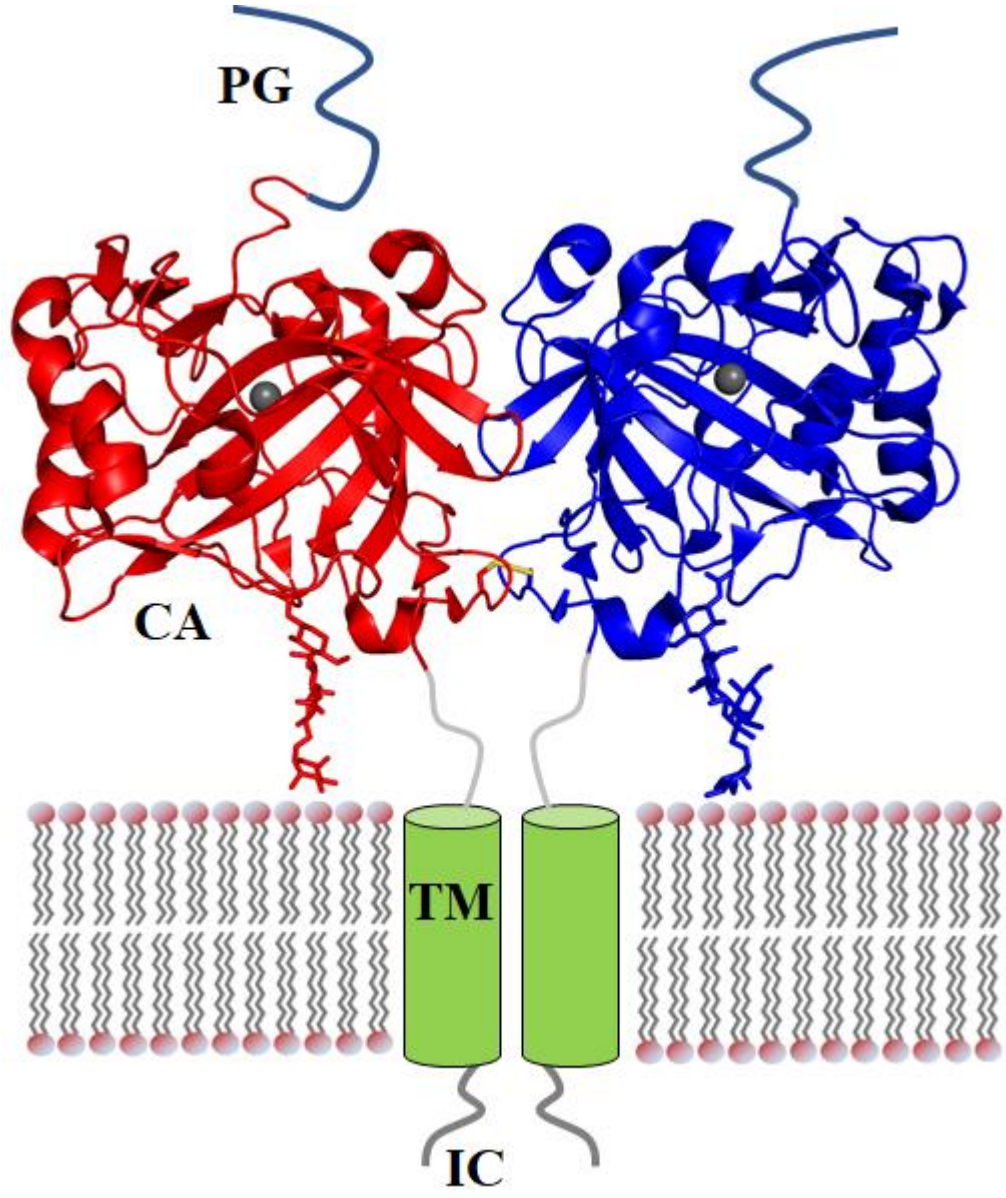

Figure 8. Proposed model of full length human carbonic anhydrase isoform IX. Adapted from (Tars & Matulis, *in press*).

Proteoglycan-like domain (PG) is an N-terminal component of hCA IX. It is unique in the hCA IX isoform and is not found in any other mammalian CAs. PG domain owes its name to some sequence similarity to aggrecan, which is a part of proteoglycan assembly. However, covalently linked carbohydrates have not been observed in CA IX PG domain, except for a single O-glycosylation site. Structurally, PG domain seems to be disordered with some parts possibly adapting polyproline type II helix conformation (Langella et al., 2018). Several functions have been attributed to PG domain. It has been demonstrated that PG domain is responsible for cancer cell adhesion, migration and spreading (Zavadova & Zavada, 2005; Csaderova et al., 2013). PG domain also influences the catalytic activity of enzyme. PG-less CA IX is roughly 2-3 times less active (Hilvo et al., 2008) and the optimum pH value of full-length enzyme is shifted from 7.0 to 6.5, thus making CA IX more efficient in acidic tissue, typical for hypoxic conditions (Innocenti et al., 2009).

The catalytic domain has relatively high amino acid homology to other mammalian CA isoforms and the obvious role of this domain is to perform the catalytic reaction (Hilvo et al., 2008). Transmembrane α helix (TM) is responsible for anchoring the catalytic domain (Morgan et al., 2007), while the intracellular fragment (IC) role is associated with location of the catalytic domain in the cell (Hulikova et al., 2009). No direct experimental data is available regarding IC structure, but modelling studies suggest that part of IC might be in helical conformation (Buonanno et al., 2017). IC domain has three phosphorylation sites - T406, S411, and Y412. The first two seem to regulate the enzymatic activity of CA IX, while the last one is involved in EGFR-induced signal transduction to PI3/Akt kinase pathway. IC tail has also been shown to interact with cullin-associated NEDD8-dissociated protein 1 (CAND1). It appears that CAND1 is stabilizing CA IX structure, since cells with lower CAND1 expression also have lower CA IX content (Buonanno et al., 2017).

Dimer formation is surprisingly different for hCA IX and hCA XII, although they are structurally similar and both are transmembrane proteins expressed in similar tissues. Another isoform - hCA VI also forms a dimer and its oligomerization form is very different from both hCA IX and hCA XII (Figure 9.). Dimer forming for hCA VI is stabilized by 11 hydrogen bonds and van der Waals forces (Pilka et al., 2012). In contrast, hCA XII is stabilized by 19 hydrogen bonds (Whittington et al., 2001) and hCA IX by 2 hydrogen bonds and one intermolecular disulfide bond. Available structural data has shown that the absence of a disulfide bond does not interrupt oligomerization of hCA IX (Alterio et al., 2009; Leitans et al., 2015).

Active site cavities in hCA IX and hCA XII dimers are relatively far from each other, but in case of hCA VI entrances of both active site cavities are oriented facing each other.

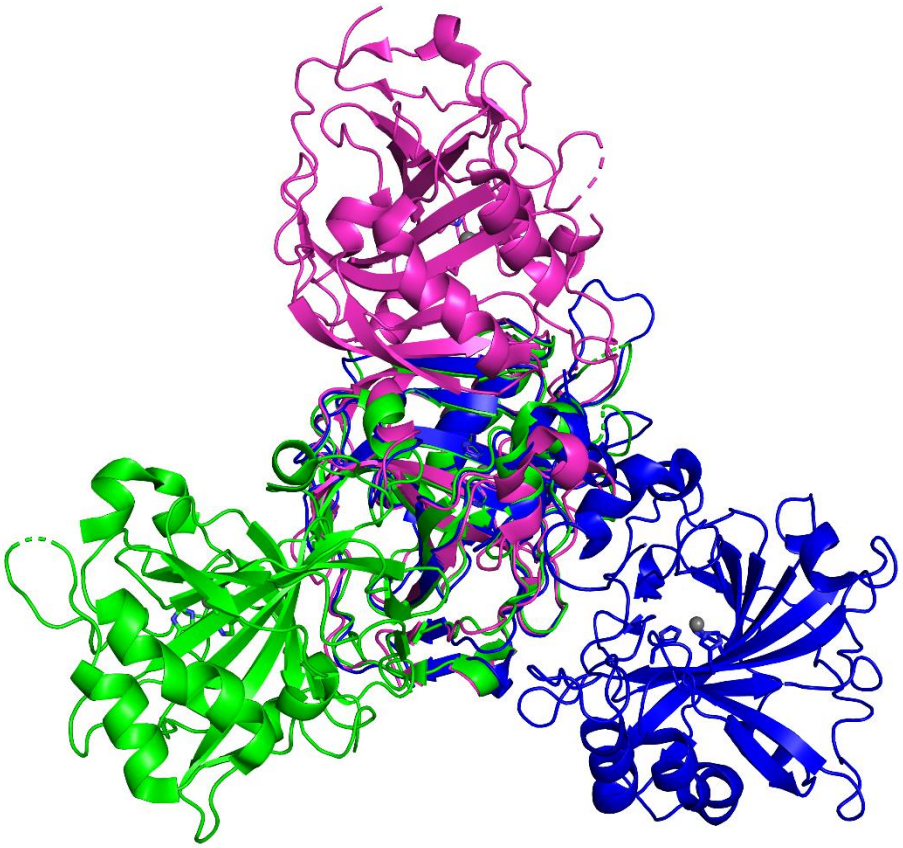

Figure 9. Superposed dimer structures of catalytic domains of hCA VI (purple, PDB code 3FE4), hCA IX (green, PDB code 6FE2) and CA XII (blue, PDB code 1JCZ). The figure was prepared with the PyMOL Molecular Graphics System, Version 2.0 Schrödinger, LLC.

hCA IX is overexpressed in many solid tumors including renal cell carcinoma (Bismar et al., 2003), breast cancer (Chia et al., 2001) and others (Figure 10.). Enzymatic activity of hCA IX favors tumor metastasis (Supuran, 2012; Chiche et al., 2009) and high expression of hCA IX correlates with poor prognosis and reduced disease-free interval following therapy (Bui et al., 2003). In limited amounts hCA IX can also be found in several normal tissues, notably gastrointestinal tract (Mahon et al., 2015).

Knockout *CA9* gene in mice in homozygous animals results in development of mild gastric hyperplasia (Gut et al., 2002). However, it does not disrupt mice development and gastric juice pH and secretions are kept at normal levels. Judging from these experiments, it has been promoted that

the disruption of *CA9* gene does not lead to serious abnormalities in development and sustainability, leading to concept that selective hCA IX inhibition also would not cause serious side effects (Leppilampi et al., 2005; Pan et al., 2006).

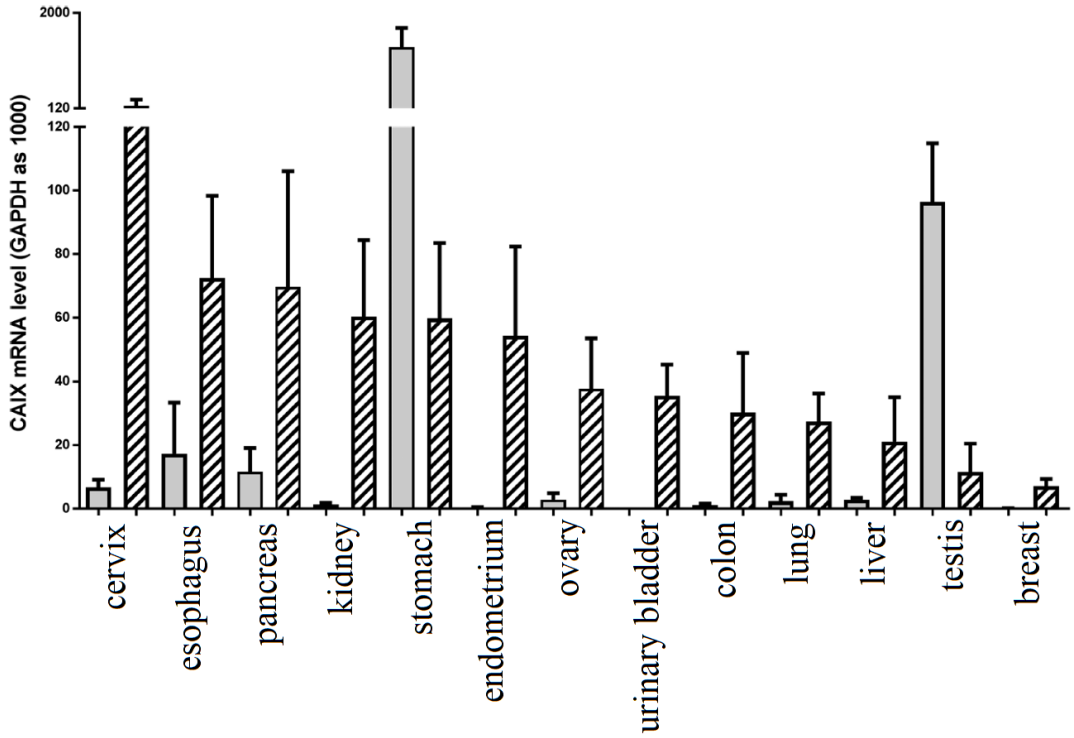

Figure 10. Expression of CA IX in various types of human cancer (grey bars) and normal tissue (striped bars). Adapted from (Mahalingam et al., 2018).

1.7.1. hCA IX targeting in anti-tumour drug design

Specific presence of CA IX on the surface of tumour cells can be targeted in two distinct ways. First, enzymatic activity of CA IX can be inhibited by small molecules, therefore slowing the catalytic reaction. Second strategy is to use CA IX as a cancer cell-targeting molecule. For example, specific anti-CA IX antibodies can mediate cancer cell destruction by antibody-dependent cell-mediated cytotoxicity, complement-dependent cytotoxicity and antibody-dependent cellular phagocytosis (Chang et al., 2015). Several monoclonal anti-CA IX antibodies have been shown to reduce tumour size in animal models. Anti-CA IX monoclonal antibody Girentuximab (known also as G250) displayed promising results in Phase I and Phase II clinical trials (Bleumer et al., 2004) but failed to display significant benefit in Phase III trials (Haas et al., 2017).

1.8. CA inhibitors

1.8.1. Ligand classification

Ligand binding to the active center of enzyme can lower the enzymatic activity. In principle it can be done in several ways - by interaction with key residues or co-factors required for catalytic activity, by changing the conformation of the active site or by slowing/blocking diffusion of substrates or products near the active site – (Srinivasan et al., 2019). "Classical" CA inhibitors are compounds that bind directly to the Zn^{2+} ion displacing the water molecule and therefore preventing the catalytic reaction. Sulfonamides are by far the most popular class of CA inhibitors. Like many classical CA inhibitors, sulfonamides are made of a zinc binding group, linker and a tail moiety (Pinard et al., 2015) (Figure 11.).

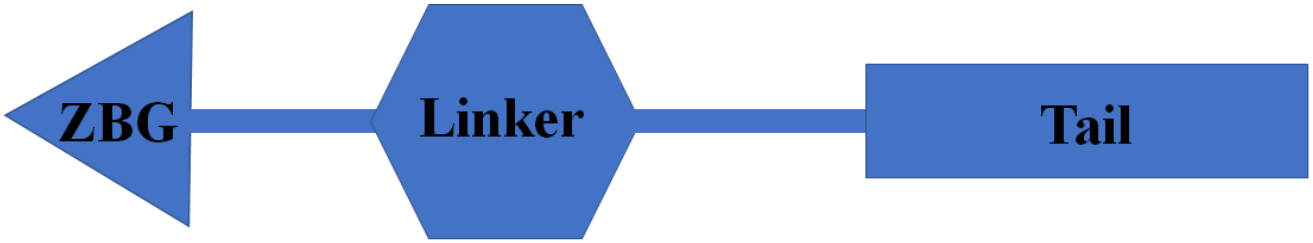

Figure 11. Schematic representation of classical CA inhibitors. Adapted from (Pinard et al., 2015).

In the case of sulfonamides ZBG is SO_2NH_2, where NH_2 moiety interacts with Zn^{2+}, also forming hydrogen bond with conservative α-CA residue Thr199 (Chakravarty & Kannan, 1994) (Figure 12.). The linker usually is an aromatic ring, it has little (if any) interaction with active site residues and mostly functions as a connector to the tail moiety. Tail moieties are very diverse, mostly modeled to target specific regions of active site (Scozzafava et al., 1999; Pinard et al., 2015).

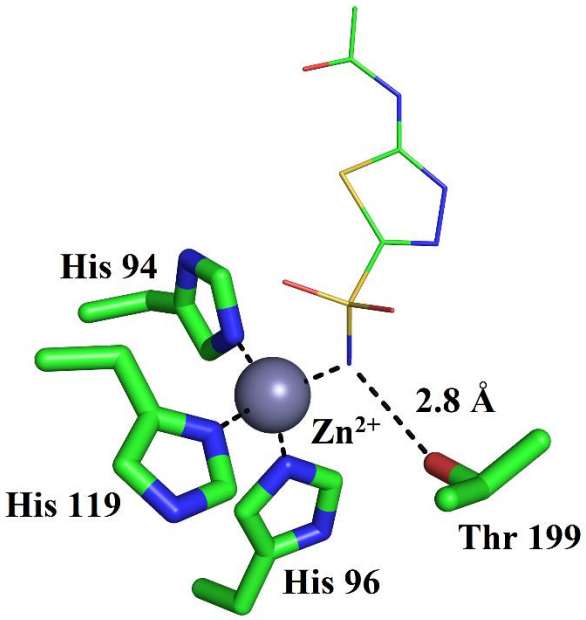

Figure 12. Binding mode of acetazolamide within the active site of hCA II (PDB code 3HS4). The figure was prepared with the PyMOL Molecular Graphics System, Version 2.0 Schrödinger, LLC.

It was discovered that the artificial sweetener saccharin can also inhibit some of the α-CA isoforms (Figure 13.). The inhibition mechanism of saccharine is similar to the sulfonamide binding mode - it also blocks the binding of water molecule to the Zn^{2+} ion. Although the binding mode is similar, differences in orientation of bound saccharin from sulfonamides can be useful for design of ligand tail orientation (Köhler et al., 2007).

Isoform	K_I [nM]	
	Acetazolamide	**Saccharin**
hCA I	250	18540
hCA II	12	5950
hCA IV	74	7920
hCA Va	63	10060
hCA Vb	54	7210
hCA VI	11	935
hCA VII	2.5	10
hCA IX	25	103
hCA XII	5.7	633
hCA XIV	41	773

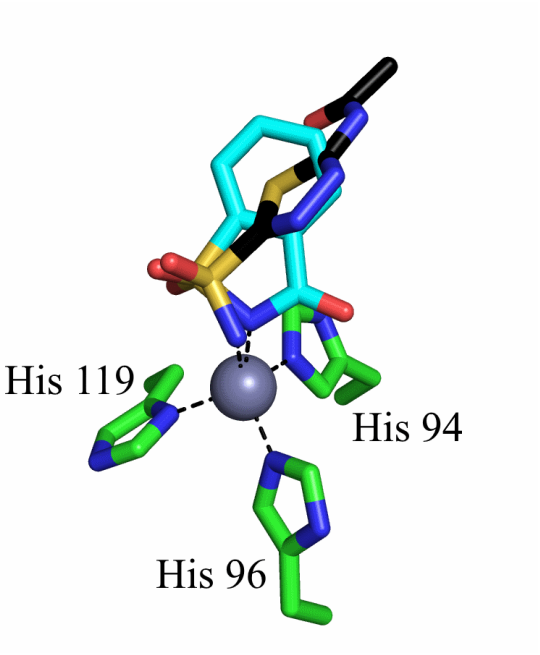

Figure 13. Inhibition constants of acetazolamide and saccharin on human carbonic anhydrase isoforms (left) (Köhler et al., 2007). Binding mode comparison of acetazolamide (PDB code 3HS4) and saccharine (PDB code 2Q1B) (right). The figure was prepared with the PyMOL Molecular Graphics System, Version 2.0 Schrödinger, LLC.

Sulfocoumarin type inhibitors present a different binding mode. Sulfocoumarins bind to CAs in hydrolyzed form and do not replace the zinc-bound water molecule, but interact with it via a hydrogen bond, thereby blocking the access of CO_2 molecule (Tars et al., 2013) (Figure 14.).

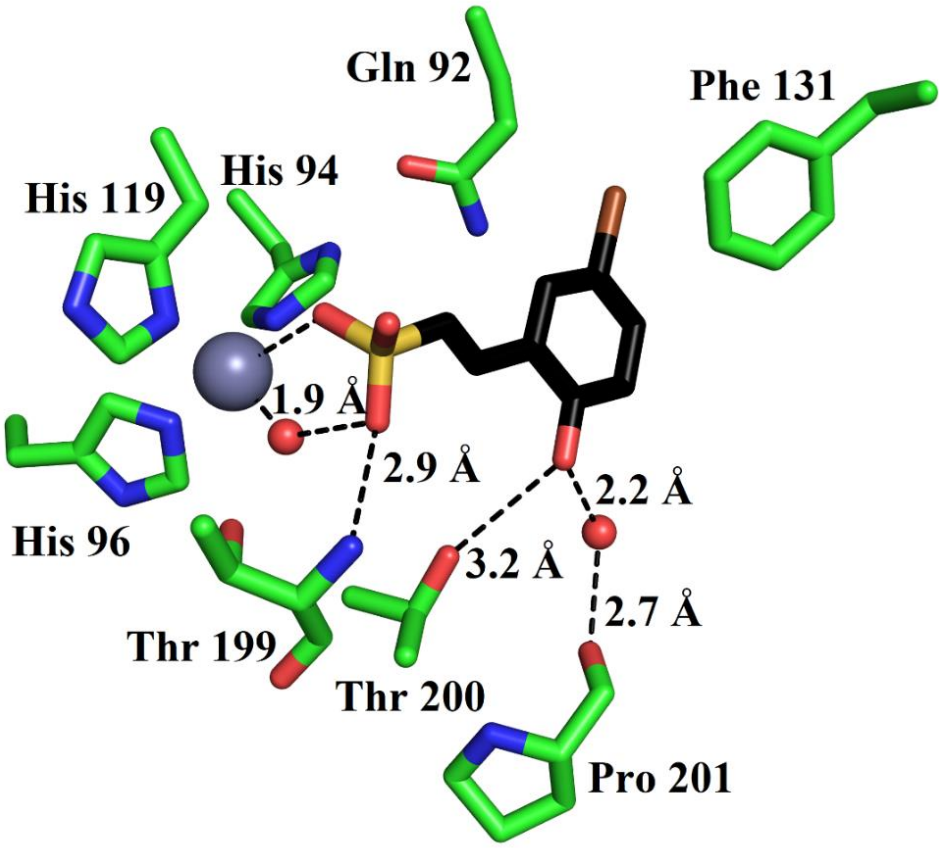

Figure 14. Binding mode of sulfocoumarin within the active site of carbonic anhydrase. Adapted from (Tars et al., 2013). The figure was prepared with the PyMOL Molecular Graphics System, Version 2.0 Schrödinger, LLC.

1.8.2. Novel aspects for the CA inhibitor design

Design of dual tail inhibitors is another useful approach in order to achieve isoform selective inhibitors (Figure 15.). This strategy makes use of both polar and hydrophobic parts of CA active site. If a compound contains both hydrophobic and polar tails it could be targeted as potentially covering more surface and gaining selectivity for the isoform (Tanpure et al., 2015).

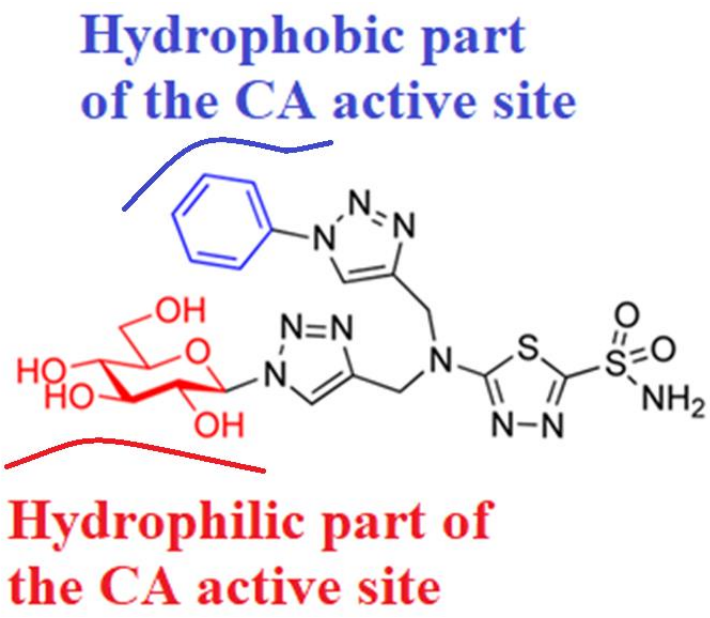

Figure 15. Dual tail ligand approach in CA drug design. Adapted from (Tanpure et al., 2015).

Many factors must be noted in designing of inhibitors. The inhibitor has to be with high selectivity and affinity to the target isoform and has to be able to cross the plasma membrane in the case of cytosolic isoforms. Often the designed compounds have poor solubility in water, which can make further studies difficult (Scozzafava et al., 1999).

Specificity of CA inhibitors can also be modulated by their capability to cross plasma membrane. Most of the CA isoforms are cytosolic, while tumor associated CA IX and CA XII are extracellular. Membrane impermeability can be achieved by addition of high molecular weight compounds that are too big for the membrane penetration (bulky compounds), charged molecules that are incapable of passing into the cytosolic environment (fluorescently labeled or cationic compounds) or glycoconjugates. In this way it is possible to partially address selectivity problems in respect to most of the CA isoforms (Mahon et al., 2015) (Figure 16.).

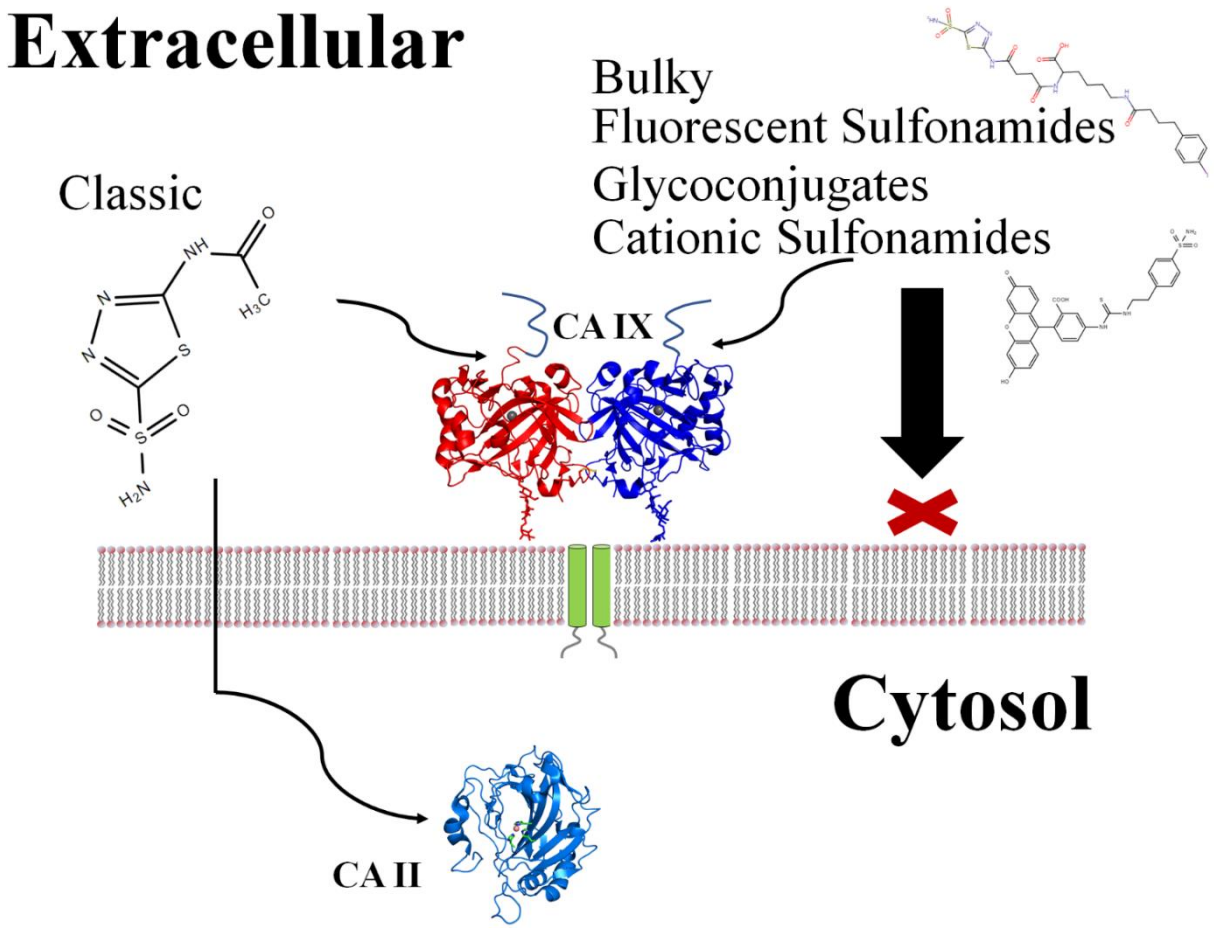

Figure 16. Classification of carbonic anhydrase inhibitors by their ability to cross plasma membrane. Adapted from (Mahon et al., 2015).

1.8.3. Approved CA inhibitor medications and ongoing clinical trials

Currently the most widely used CA inhibitor in medicine is acetazolamide, but it has poor selectivity and it strongly inhibits most of the human carbonic anhydrase isoforms (Hilvo et al., 2008) (Table 5). Dorzolamide (Serle, 1994), Methazolamide (Gudmundsdóttir et al., 2000), ethoxzolamide (García-Fernández et al., 2013), Dichlorphenamide (Kanski et al., 1968), Brinzolamide (Lusthaus & Goldberg, 2017), Topiramate (Aminlari et al., 2008), Sulpiride (Souza et al., 2008) and Zonisamide (De Simone et al., 2005) are other approved acetazolamide-like medications, with little specificity regarding different CA isoforms and mostly used to treat hCA II related diseases. For example, dorzolamide is a topical drug, which can be used as eye drops in case of glaucoma. Dorzolamide was developed to circumvent systemic side effects of

acetazolamide, which has to be taken orally. Dorzolamide has a reputation of first drug used for human therapy, discovered by structure-aided drug design.

Some other CA inhibitors have reached clinical trials. Indisulam is a chloroindolyl sulfonamide. It showed promising results in Phase I trial (Raymond et al., 2002), but Phase II trial was terminated in 2016 (Talbot et al., 2007).

Table 5. Inhibition constants of most popular CA inhibitors. Adapted from (Supuran, 2008b).

K_I(nm)	**hCA I**	**hCA II**	**hCA III**	**hCA IV**	**hCA VA**	**hCA VB**	**hCA VI**	**hCA VII**	**hCA IX**	**hCA XII**	**mCA XIII**	**hCA XIV**
Acetazolamide	250	12	$2x10^5$	74	63	54	11	2.5	25	5.7	17	41
Methazolamide	50	14	$7x10^5$	6200	65	62	10	2.1	27	3.4	19	43
Ethoxzolamide	25	8	$1x10^6$	93	25	19	43	0.8	34	22	50	2.5
Dichlorphenamide	1200	38	$6.8x10^5$	15000	630	21	79	26	50	50	23	345
Dorzolamide	50000	9	$7.7x10^5$	8500	42	33	10	3.5	52	3.5	18	27
Brinzolamide	45000	3	$1.1x10^5$	3950	50	30	0.9	2.8	37	3.0	10	24
Indisulam	31	15	10400	65	79	23	47	122	24	3.4	11	106
Topiramate	250	10	$7.8x10^5$	4900	63	30	45	0.9	58	3.8	47	1460
Sulpiride	12000	40	10600	$6.5x10^5$	174	18	0.8	3630	46	3.9	295	110
Zonisamide	56	35	$2.2x10^6$	8590	20	6033	89	117	5.1	11000	430	5250
SLC-0111	5080	960	-	286	-	-	-	-	45	4.5	-	-

Ureido-benzenesulfonamide compund SLC-0111 is now in Phase Ib/II clinical trials as anti-tumour drug candidate (Supuran, 2018b). Judging from the available data in literature, compound SLC-0111 has been tested *in vitro* for inhibition potential against hCAs I, II, IX and XII (Carta et al., 2017). Although SLC-0111 is a weaker hCA IX inhibitor than acetazolamide, it has significantly decreased affinity to isoforms I and II, which are considered as off-target isoforms in most cases (Pinard et al., 2015). Affinity to hCA XII can be considered as a bonus. hCA XII is another tumor associated hCA isoform and it has been proven that hCA XII works as a compensating mechanism in tumor cells if hCA IX activity is lowered (Chiche et al., 2009). However, compared to hCA IX, hCA XII has a wider distribution in normal tissue.

2. Materials and Methods

2.1. *E.coli* strains

E.coli **RR1**: *F^- leuB6 proA2 thi-1 araC14 lacY1 galK2 xyl-5 mtl-1 rpsL20 (Str^r) glnV44 $recA^+$ Δ(mcrC-mrr)* (Stratagene, USA)

E.coli **JM109***: F' traD36 proAB laclq Δ(lacZ)M15/ endA1 rec A1 gyrA96(Nalr) thi hsdR17($r_k^- m_k^+$) relA1 supE44 Δ(lac-proAB)* (Stratagene, USA)

E.coli **BL21 (DE3)**: *F^- ompT gal dcm lon $hsdS_B$($r_B^- m_B^-$) λ(DE3 [lacI lacUV5-T7 gene 1 ind1 sam7 nin5])* (Stratagene, USA)

Pichia pastoris **GS115** *his4* (Stratagene, USA)

2.2. Expression vectors

In this work pETDuet-1, pRSFDuet-1 and pPIC3.5K vectors were used (Invitrogen, USA).

2.3. Genes

Genes were obtained from gene synthesis service company GenScript (Japan).

2.4. Agarose gel electrophoresis

Agarose gel electrophoresis was performed using 1 % agarose (Thermo Fisher Scientific, USA) gels in 1x TAE buffer (1 mM EDTA, 40 mM Tris, 20 mM acetic acid) with additional 1 μg/mL ethidium bromide solution (Merck, Germany).

2.5. DNA fragment purification from agarose gel

DNA fragments were extracted from the agarose gel by using GeneJET Gel Extraction Kit (Thermo Fisher Scientific, USA) reagents and manufacturer provided user manual.

2.6. Digestion of the DNA using endonucleases

Restriction reaction was done following FastDigest (Thermo Fisher Scientific, USA) manual, using the necessary endonucleases.

2.7. DNA ligation

Gene ligation in the expression vector was done by following procedure:

Reaction mix:

Fragment DNA (25-100 ng/µl) 1-3 µl;

Expression vector DNA (25-100 ng/µl) 1-3 µl;

10x T4 DNA Ligase buffer (Thermo Fisher Scientific, USA) - 2 µl;

T4 DNA ligase (5 µ/µl) (Thermo Fisher Scientific, USA) - 1 µl;

Water – up to 20 µl

Ligation reaction was performed either for 1-2 h at room temperature, or overnight at +4° C.

2.8. Plasmid transformation in *E.coli*

Ligation mix (10-20 µl) was added to thawed competent cells and incubated for 10 min on ice. Heat shock was performed at 42° C for 35 seconds or two minutes depending on the cell type. After the heat shock cells were incubated on ice for two minutes. Afterwards 0.9 mL of LB medium (5 g/l Bacto yeast extract (Difco Laboratories), 10 g/l Bacto tryptone (Difco Laboratories), 10 g/l sodium chloride (Stanlab, Poland)) was added and cells were incubated for one hour at +37° C whilst slowly shaking the reaction mix. 100 µl of reaction mix was applied on LB agar plates (5 g/l Bacto yeast extract (Difco Laboratories), 10 g/l Bacto tryptone (Difco Laboratories), 10 g/l sodium chloride (Stanlab, Poland), 15 g/l Bacto agar (Difco Laboratories)) containing necessary antibiotic (kanamycin – 10 mg/mL or ampicillin - 20 mg/mL). Plates were incubated overnight at +37° C.

2.9. *E.coli* cultivation for plasmid DNA amplification

One colony from the Petri plates was transferred to 3 mL 2x TY (5 g/l Bacto yeast extract (Difco Laboratories), 16 g/l Bacto tryptone (Difco Laboratories), 5 g/l sodium chloride (Stanlab, Poland)) media containing necessary antibiotic (kanamycin – 10 mg/mL or ampicillin - 20 mg/ml) and incubated overnight at +37° C in a shaker (160-200 rpm) (Infors HT Multitron (Infors AG, Switzerland)).

2.10. Plasmid purification from *E.coli* cells using GeneJET Plasmid Miniprep Kit.

Plasmid DNA were isolated and purified using GeneJET Plasmid Miniprep Kit (Thermo Fisher Scientific, USA) following the user manual.

2.11. DNA sequencing

DNA sequencing was performed by following procedure:

Reaction mix:

Big Dye (Applied Biosystems) – 1 µl;

Big Dye 5x reaction buffer (Applied Biosystems) – 2 µl;

Primer (1-5 pmol/µl). – 1 µl;

Plasmid DNA (25-100 ng/µl)- 2 µl;

Water – up to 20 µl

PCR for sequencing was followed by standard protocol.

DNA precipitation and washing were performed by the following procedure:

Add 65 µl of 96% ethanol;

Incubate 10-15 min at -20° C;

Centrifugate 10-15 min, 13000 rpm using centrifuge 5418 R (Eppendorf, Germany);

Remove the supernatant;

Add 200 µl of 70% ethanol;

Remove the supernatant;

Centrifugate for 3 min, 13000 rpm using centrifuge 5418 R (Eppendorf, Germany);

Remove the supernatant;

Dry debris at 55° C;

11 µl of formamide solution was added (Sigma, USA). Samples were heated for 5 min at +95° C, proceeding with immediate cooling on ice. Samples were analyzed using 3130xl Genetic analyzer (Applied Biosystems) and sequences were visualized using FinchTV (Geospiza, USA).

2.12. *E.coli* cultivation for recombinant protein expression

One colony from Petri plates was transferred to LB medium (5 g/l Bacto yeast extract (Difco Laboratories), 10 g/l Bacto tryptone (Difco Laboratories), 10 g/l sodium chloride (Stanlab, Poland)), containing necessary antibiotic (kanamycin – 10 mg/mL or ampicillin - 20 mg/ml) and proceeded without shaking at +37° C overnight. The prepared *E.coli* cultivation material was added to 2x TY (5 g/l Bacto yeast extract (Difco Laboratories), 16 g/l Bacto tryptone (Difco Laboratories), 5 g/l sodium chloride (Stanlab, Poland)) at maximum 1/10 ratio. Cells were incubated at +37° C, 160-200 rpm (Infors HT Multitron (Infors AG, Switzerland)) till OD_{540} reached 0.6-0.8. Cells were induced with 0.2 mM IPTG (Thermo Fisher Scientific, USA) and grown for another 3-5 hours at +37° C, 160-200 rpm. Cell culture was harvested by centrifugation and stored frozen at -20° C.

2.13. *Pichia pastoris* cultivation for recombinant protein expression

Linearized DNA containing the target gene was added to competent cells and incubated 15 min in ice cold electroporation cuvette. Electroporation was done at 1.2 kV (Electroporator 2510, Eppendorf) immediately adding 1 mL YEPG medium (19 g/l peptone, 9.5 g/l yeast extract, 2 mL glucose) and incubating for 1 hour at 30° C. Cells were centrifugated at 8000 rpm (4° C), supernatant was removed and 1mL of distilled water was added to the cells. After resuspension, 100 µl was spread on RDB plates (850 mL/l agar, 20 mL/l glucose, 3.4g/l yeast nitrogen base, 10g/l ammonium sulphate, 10 mL/l amino acid mix (L-methionine, L-glutamine, L-lysine, L-leucine, L-isoleucine 5g/l), 0.4 mg/L biotin). First colonies appeared after 2-3 days of incubation at 30° C. To select for clones with multiple target gene integration , colonies from single plate were resuspended in 2-3 mL of YEP medium (20 g/l peptone, 10 g/l yeast extract), diluted 10x with distilled water and spread on YEPG agar plates (20 g/l peptone, 10 g/l yeast extract, 15 g/l agar, 20 mL/l glucose) containing 2-4 mg/ml geneticin. Plates were incubated for 2-5 days at 30° C and selected colonies were used for cultivation material preparation in YEPG medium with chloramphenicol (34 mg/l). The cultivation material was incubated for 3 days at 30° C without shaking.

The prepared cultivation material was added to BMGY medium at 1:100 ratio (16 g/l peptone, 11.4 g/l yeast extract, 10 g/l ammonium sulphate, 100 mL/l potassium phosphate buffer pH 6.0 (2.3 g K_2HPO_4, 11.8 g KH_2PO_4), 10 mL glycerol) with 34 mg/l chloramphenicol and incubated at 30° C; 250 rpm until OD_{590} reached 6-8. 1% methanol was added every 24 hours for 96 hours to induce protein synthesis. Cells were harvested by centrifugation and frozen until further use.

2.14. Cell lysis using French press

Cells were resuspended in lysis buffer solution (40 mM Tris 8.0, 200 mM NaCl, proceeding with three lysis cycles by French press at 20 000 psi using French Press cell disrupter (Thermo Electron, USA). Cell debris was removed by centrifugation for 60 min at 10 000 rpm, 4° C using centrifuge 5404 R (Eppendorf, Germany).

2.15. Protein purification using metal affinity chromatography

Lysed cell supernatant was purified using metal ion affinity Ni-NTA agarose columns (Thermo Fisher Scientific). Column was washed with cell lysis buffer solution, following wash

with lysis buffer containing 20 mM imidazole (AppliChem, Germany) and protein was eluted with lysis buffer containing 300 mM imidazole.

2.16. His-tag cleavage using TEV protease

TEV cleavage was performed for 1 hour at room temperature in 40mM Tris-HCl 8.0, 300 mM NaCl, 300 mM imidazole, 1 mM DTT buffer. In-house produced TEV protease was used at ratio 25-50 μg per 1 mg of the target protein.

2.17. Protein purification by gel filtration chromatography

Proteins were purified using Superdex 200 10/ 300 GL column (GE Healthcare Life Sciences, Japan) linked to ÄKTA chromatography system (Amersham Biosciences, UK). Column was pre-washed with 20 mM Tris-HCl 8.0, 200 mM NaCl. Flow rate was 1 mL/min, fraction size 1 mL.

2.18. Protein purification by using ion-exchange chromatography

For additional purification ion-exchange chromatography was performed - MonoQ TM column (GE Healthcare Life Sciences, Japan), salt gradient 0.1-0.5 M NaCl, flow rate 1 mL/min, fraction size 1 mL.

2.19. SDS-PAGE electrophoresis

Proteins were analyzed on SDS-PAGE electrophoresis by following procedure:

Main gel (10 %):

0.6 M Tris 8.8 (AppliChem, Germany)– 2 mL;

Water – 4.5 mL;

30 % acrylamide solution (Sigma, USA) – 3.3 mL;

10% SDS (AppliChem, Germany) – 0.1 mL;

10% ammonium persulfate (Sigma, USA) – 0.1 mL;

TEMED (AppliChem, Germany) – 0.01 mL.

After main gel is polymerized, upper layer of the gel (2%) is added:

0.6 M Tris 6.8 (AppliChem, Germany) – 0.5 mL;

Water – 3.75 mL;

30 % acrylamide solution (Sigma, USA) – 0.7 mL;

10 % SDS (AppliChem, Germany) – 0.05 mL;

10 % ammonium persulfate (Sigma, USA) – 0.07 mL;

TEMED (AppliChem, Germany) – 0.007 mL.

Samples were mixed with Laemmli sample loader (1% SDS (AppliChem, Germany), 40 mM Tris HCl pH 8.0, 0.05 % bromophenol blue (Merck, Germany), 2 % 2-Mercaptoethanol (Sigma, USA). 1x SDS running buffer (25 mM Tris (AppliChem, Germany), 192 mM glycine (AppliChem, Germany), 0.1% SDS (AppliChem, Germany)) was used and loaded samples were run on the SDS-PAGE electrophoresis until the bromophenol blue stain reached the bottom of the gel. Gel was washed in 30% ethanol, 10% acetic acid solution for 20 min and proteins were stained using the Coomassie blue G-250 solution (Serva, Germany) for 20 minutes. Afterwards, washing with water was proceeded in order to wash away unbound stain.

2.20. Protein desalting and concentration

Proteins were desalted to 20 mM Tris-HCl, pH 8.0 buffer and concentrated to 10 mg/mL using 10k amicon ultra centrifugal filter (Merck Millipore Ltd, Ireland) at 4900 rpm, +4° C using centrifuge 5404 R (Eppendorf, Germany).

2.21. Protein crystallization in complex with the ligands

Crystallization was performed using TECAN crystallization robot (Evonik Industries, Switzerland) (0.4+0.4 µl drops) by co-crystallization, sitting drop, vapor diffusion method. 5-10 mM inhibitor (final concentration, stock solution was prepared at 100 mM, dissolved in 100% DMSO (AppliChem, Germany)) was added to the protein solution before the crystallization.

2.22. Diffraction data collection and structure determination

Diffraction data were collected at MAX II and MAX IV (Lund, Sweden) or Bessy II (Berlin, Germany) synchrotrons. Images were indexed using MOSFLM (Leslie, 1992), scaled with SCALA (Evans, 1997) and molecular replacement was done using MOLREP (Vagin & Teplyakov, 1997). Ligand bond information was generated by LIBCHECK (Vagin et al., 1998). Ligand was manually fitted in the electron density using COOT (Emsley & Cowtan, 2004) followed by further REFMAC (Murshudov et al., 1997) runs. Structure was visualized using COOT (Emsley & Cowtan, 2004) and the PyMOL Molecular Graphics System, Version 2.0 Schrödinger, LLC.

3. Results

3.1. 5-Substituted-(1,2,3-triazol-4-yl) thiophene-2-sulfonamides strongly inhibit human carbonic anhydrases I, II, IX and XII: Solution and X-ray crystallographic studies

Various thiophene-sulfonamide derivatives were crystallized with hCA II in order to explain kinetic data displaying increase in selectivity for some of the hCA isoforms. In this work we published two of the determined crystal structures. Structure of hCA II in complex with compound with naphthyl moiety as a tail was determined at 1.35 Å resolution and with compound with phenyl cyano tail at 1.82 Å resolution. Both crystal structures displayed invariable orientation of sulfonamide group, interacting with Zn^{2+} ion and Thr199. Compound with naphthyl tail did not have any other polar interactions to stabilize ligand binding mode and ligand tail moiety orientation was achieved solely by hydrophobic and van der Waals contacts with residues Phe131, Val135, Pro202 and Leu204, fitting perfectly in the hydrophobic part of the enzyme active site. Comparing both structures, ligand binding differences can be noticed already starting from the thiophene ring, orientation of which in "cyano" and "naphthyl" structures differs by 180 degrees and the phenyl cyano tail is orientated towards the hydrophilic part of the enzyme active site pocket, while napthyl tail occupies the hydrophobic part. The compound with phenyl cyano tail also makes hydrogen bond with a highly conservative hCA residue Gln92, which according to the literature is a popular interaction (De Simone et al., 2013). Phenyl cyano tail also interacts with residues Val121, Phe131, Leu141, and Leu198. Due to the lack of cryoprotectant in the precipitant, 30% glycerol was added during flash freezing of crystals in liquid nitrogen. Apparently, the short soaking in cryoprotectant solution was long enough for a glycerol molecule to bind in the active site of hCA II in the same place as observed earlier for other hCA II structures (Avvaru et al., 2010). As glycerol is attached to the enzyme during cryoprotection it was assumed that it does not interfere with ligand binding and can be considered as an artifact.

The obtained results suggest that the binding mode of compound can be directly influenced purely from hydrophobicity of the tail moiety. The results can be used for rational design of selective hCA II inhibitors, harboring both napthyl and phenyl cyano tails, able to bind both parts of the active site of enzyme.

Crystal structures are deposited on PDB with access codes: 4BF1 and 4BF6.

Bioorganic & Medicinal Chemistry 21 (2013) 5130–5138

Contents lists available at SciVerse ScienceDirect

Bioorganic & Medicinal Chemistry

journal homepage: www.elsevier.com/locate/bmc

5-Substituted-(1,2,3-triazol-4-yl)thiophene-2-sulfonamides strongly inhibit human carbonic anhydrases I, II, IX and XII: Solution and X-ray crystallographic studies

Janis Leitans [a], Agnese Sprudza [b], Muhammet Tanc [c,d], Igor Vozny [b], Raivis Zalubovskis [b,*], Kaspars Tars [a], Claudiu T. Supuran [c,d,*]

[a] Biomedical Research and Study Center, Ratsupites 1, LV 1067 Riga, Latvia
[b] Latvian Institute of Organic Synthesis, Aizkraukles 21, LV-1006 Riga, Latvia
[c] Università degli Studi di Firenze, CSGI, Polo Scientifico, Laboratorio di Chimica Bioinorganica, Rm. 188, Via della Lastruccia 3, Sesto Fiorentino, 50019 Florence, Italy
[d] Università degli Studi di Firenze, NEUROFARBA Dept., Sezione di Scienze Farmaceutiche e Nutraceutiche, Sesto Fiorentino, 50019 Florence, Italy

ARTICLE INFO

Article history:
Received 18 May 2013
Accepted 16 June 2013
Available online 27 June 2013

Keywords:
Carbonic anhydrase
Enzyme inhibitor
Thiophene-2-sulfonamide
Click chemistry
X-ray crystallography
Sulfonamide

ABSTRACT

We report here a series of 2-thiophene-sulfonamides incorporating 1-substituted aryl-1,2,3-triazolyl moieties, prepared by click chemistry from 5-ethynylthiophene-2-sulfonamide and substituted aryl azides. The new sulfonamides were investigated as inhibitors of the zinc metalloenzyme CA (EC 4.2.1.1), and more specifically against the human (h) cytosolic isoforms hCA I and II and the transmembrane, tumor-associated ones hCA IX and XII: The new compounds were medium–weak hCA I inhibitors (K_Is in the range of 224–7544 nM), but were compactly, highly effective, low nanomolar hCA II inhibitors (K_Is of 2.2–7.7 nM). The tumor-associated hCA IX was inhibited with K_Is ranging between 5.4 and 811 nM, whereas hCA XII with inhibition constants in the range of 3.4–239 nM. The X-ray crystal structure of the adducts of two such compounds bound to hCA II (one incorporating 1-naphthyl, the other one 3-cyanophenyl moieties) evidenced the reasons of the high affinity for hCA II. Highly favorable, predominantly hydrophobic interactions between the sulfonamide scaffold and the hCA II active site were responsible for the binding, in addition to the coordination of the sulfamoyl moiety to the zinc ion. The tails of the two inhibitors adopted very diverse orientations when bound to the active site, with the naphthyltriazolyl moiety orientated towards the hydrophobic half of the active site, and the 3-cyanophenyl one pointing towards the hydrophilic half. These data may be used for the structure-based drug design of even more effective hCA II inhibitors, with potential use as antiglaucoma agents or as diuretics.

1. Introduction

Carbonic anhydrase (CAs, EC 4.2.1.1) catalyze the interconversion between CO_2 and bicarbonate by using a metal hydroxide nucleophilic mechanism.[1–3] They constitute a superfamily of metalloenzymes with five distinct genetic families known to date, the α-, β-, γ-, δ- and ζ-CAs, in organisms all over the tree of life. These enzymes differ in their preference for metal ions used within the active site for performing the catalysis: Zn(II) ions may be used by all five classes mentioned above, but the γ-CAs are probably Fe(II) enzymes (being active also with bound Zn(II) or Co(II) ions),[4,5] whereas the ζ-class uses Cd(II) or Zn(II) to perform the physiologic reaction catalysis.[6]

The inhibition and activation of CAs are well understood processes, with most classes of inhibitors binding to the metal center,[1–3] whereas activators bind at the entrance of the active site cavity and participate in proton shuttling processes between the metal ion – bound water molecule and the environment.[7] This leads to the enhanced formation of the metal hydroxide, catalytically active species of the enzyme.[7] Inhibitors generally bind to the metal ion from the enzyme active site in deprotonated state (as anions),[1–3] although alternative inhibition mechanisms in which the inhibitor interacts with the zinc-coordinated water molecule/hydroxide ion,[8–10] or does not interact at all with it,[11–13] have been recently described. The zinc-binders are the most investigated classes of CA inhibitors (CAIs), and they include the sulfonamides and their isosteres,[1–3,14,15] the dithiocarbamates,[16] the xanthates,[17] and the hydroxamates/carboxylates[18,19] (although some carboxylates may bind to the enzyme through the alternative inhibition mechanisms, which do not involve directly the metal ion).[8,9,11–13]

* Corresponding authors. Tel.: +371 67014826; fax: +371 67550338 (R.Z.); tel.: +39 055 457 3005; fax: +39 055 457 3385 (C.T.S.).
E-mail addresses: raivis@osi.lv (R. Zalubovskis), claudiu.supuran@unifi.it (C.T. Supuran).

0968-0896/$ - see front matter © 2013 Elsevier Ltd. All rights reserved.
http://dx.doi.org/10.1016/j.bmc.2013.06.041

Sulfonamide/sulfamate CAIs are in clinical use for decades as antiglaucoma,[20] diuretic,[21] antiobesity,[22] and antitumor agents,[23] targeting diverse of the various 16 CA isoforms known to date in humans.[1–3] Recently, targeting CAs from parasites (bacteria, fungi and/or protozoa among others) with specific inhibitors was proposed as an alternative for designing antiinfective agents with a new mechanism of action.[24]

Due to the high number of CA isoforms present in most organisms, and because the clinically used sulfonamides such as acetazolamide **AAZ**, methazolamide **MZA**; ethoxzolamide **EZA**, or dichlorophenamide **DCP** do not show selectivity for inhibiting any of the isoforms with pharmacologic applications,[1–3] there is a constant search for new compounds belonging to the CAI class, and the sulfonamides remain one of the most investigated such chemotype, due to their strong affinity for CAs, ease of synthesis, stability and lack of toxicity.[1–3]

Continuing our interest in sulfonamides as CAIs, we report here the synthesis of a series of 5-substituted-(1,2,3-triazol-4-yl)thiophene-2-sulfonamides, prepared by click chemistry from thiophenesulfonamides incorporating an alkyne functionality in the 5th position of the heterocyclic ring and aryl azides.

2. Results and discussion

2.1. Chemistry

Thiophene-2-sulfonamides were already investigated in the early 90s by Shepard et al.[25] in the search of topically-acting antiglaucoma CAIs.[26] One of the intermediates reported in this early paper was the dimethylacetamide protected sulfonamide group of 5-bromo-thiophene-2-sulfonamide **1**. This compounds has been used for the preparation of 4-acetylene-thiophene-2-sulfonamide (**4**), the alkyne component used for click chemistry purposes in this work.[27,28] Compound **4** may be prepared in a two step process: the first step involving the Sonogashira reaction of bromide **1** with trimethylsilylacetylene, whereas the second one, the trimethylsilyl (TMS) protecting group cleavage. Unfortunately several attempts to perform Sonogashira reaction with **1**, under various conditions did not provide the cross-coupling product, and only unreacted bromo derivative **1** was detected. The most probable cause of this lack of reactivity might be the unprotected sulfonamide group, therefore protection of sulfonamide NH_2 employing *N*,*N*-dimethylformamide dimethyl acetal was done as reported by Shepard et al.[25] and the protected intermediate **2** was isolated in 93% yield (Scheme 1). Reaction of compound **2** with trimethylsilylacetylene under Sonogashira condition afforded the cross-coupling product **3** in a 82% yield. The desired acetylene intermediate **4** was obtained by treatment of compound **3** with TBAF, when TMS cleavage and the simultaneous deprotection of the sulfonamide group took place, affording the key intermediate **4** in 50% yield.

Cu(I) catalyzed azide–alkyne cycloaddition or 'click chemistry' is a powerful tool for the regioselective synthesis of 1,4-substituted 1,2,3-triazoles.[27] After the first attempts to synthesize compound **5** under click chemistry conditions from alkyne **4** and phenylazide it was observed that the reaction takes place in 99% conversion yield, in 1:1 mixture ^{t}BuOH/H_2O and in the presence of sodium ascorbate, at 40 °C in seven days. However, when these reaction conditions were modified by the recently published discovery of using acetic acid as an additive in the Cu(I) catalyzed azide–alkyne cycloaddition,[28] the reaction took place with full conversion in 30 min at room temperature and compound **5** was isolated with a 96% yield. With these optimal conditions in hand, the entire series of triazoles **5–19** was prepared in 54–96% yields (Scheme 1).

Apart the phenyl group present in compound **5**, we incorporated various aryl such moieties in the new derivatives reported here, of types **5–19**, as it has been observed earlier[29,30] that the nature of the tails present in sulfonamide CAIs strongly influence the inhibitory properties and isoform selectivity of such derivatives. Thus we have chosen variously mono/-di-substituted phenyl

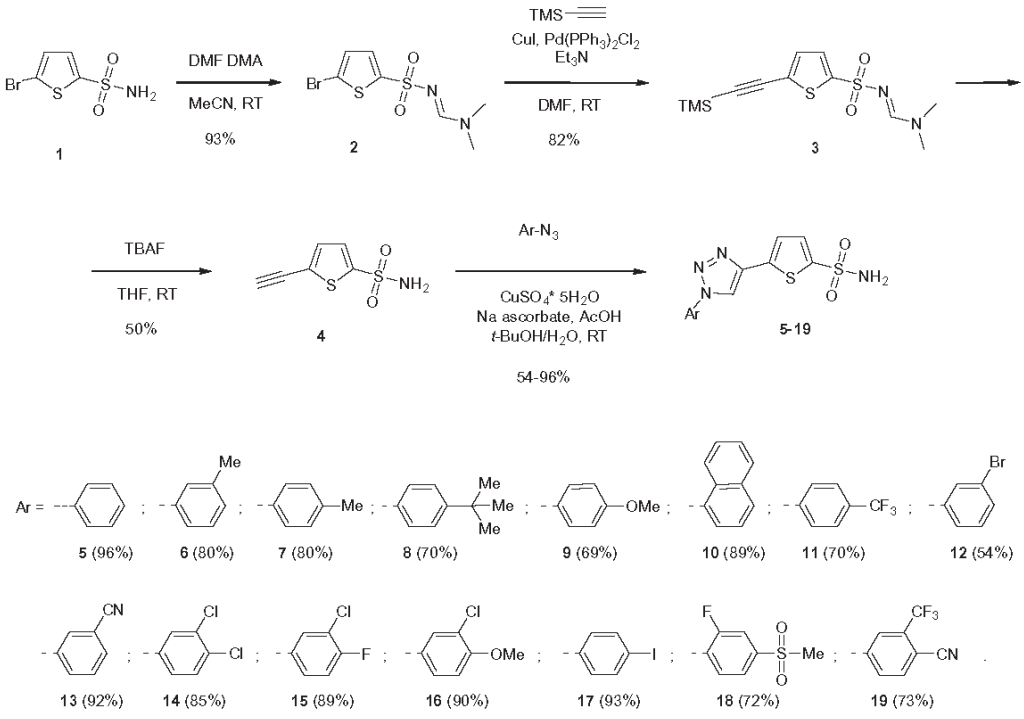

Scheme 1. Preparation of sulfonamides **5–19** from 1-bromo-thiophene-5-sulfonamide **1** by using click chemistry.

moieties (in diverse positions of the ring with respect to the azide moiety) as well as the naphthyl moiety (Scheme 1). In this way we introduced chemical diversity in the small library of thiophene-2-sulfonamide derivatives **5–19** reported here.

2.2. Carbonic anhydrase inhibition

Sulfonamides **5–19** reported here and acetazolamide **AAZ** as standard drug were assayed as inhibitors of four physiologically relevant CA isoforms, the cytosolic hCA I and II, as well as the transmembrane, tumo-associated ones CA IX and XII.[31] It should be mentioned that CA II and XII are targets for developing antiglaucoma drugs,[20] whereas CA IX (and XII) are antitumor drug targets.[23] hCA I is rather widespread in many tissues in humans, and it may be considered as an offtarget isoform.[1–3]

The following structure–activity relationship (SAR) can be evidenced from data of Table 1 regarding the CA inhibitory properties of sulfonamides **5–19**:

(i) hCA I was moderately inhibited by sulfonamides **5–19**, which showed inhibition constants in the range of 224–7544 nM, being thus similar (or less effective as hCA I inhibitors) to acetazolamide AAZ (K_I of 250 nM). The best inhibitors were **13** and **18** (incorporating 3-cyanophenyl and 4-methylsulfonyl-2-fluorophenyl moieties as Ar group) which showed (K_Is in the range of 224–289 nM, whereas the remaining compounds in the series were less effective, with K_Is in the range of 499–7544 nM (Table 1). It may be thus considered that the relatively weak inhibitory properties against the widespread isoform hCA I constitute a favorable feature of this class of CA is reported here.

(ii) The physiologically dominant isoform hCA II was highly inhibited by the new class of sulfonamides investigated here, with a flat (but excellent) inhibition profile. Indeed, the K_Is only ranged between 2.2 and 7.7 nM, making all these compounds highly effective hCA II inhibitors. Unexpectedly (however, see the X-ray crystallographic part for an explanation of this finding) all the substitution patterns present in compounds **5–19** lead to highly effective CAIs. All these compounds were better hCA II inhibitors compared to the clinically used drug **AAZ** (Table 1).

(iii) A more complicate SAR has been evidenced for the inhibition of the tumor-associated isoform hCA IX (Table 1). Several compounds, such as **5**, **9**, **12** and **17**, showed highly effective hCA IX inhibitory properties, with K_Is in the range of 5.4–10.9 nM. They incorporate phenyl, 4-methoxyphenyl-, 3-bromophenyl and 4-iodophenyl moieties. Another group of derivatives, among which **7**, **11**, **13**, **14** and **16**, showed inhibition constants in the range of 29.4–89.1 nM. They incorporate 4-tolyl, 4-trifluoromethylphenyl, 3-cyanophenyl, 3,4-dichlorophenyl and 3-chloro-4-methoxyphenyl moieties. It is obvius from these data that even small modifications of the Ar group from compounds **5–19**, lead to important changes in their affinity for CA IX (but not CA II, as mentioned above). For example, introduction of a 3-Cl atom in **9**, leading thus to **16**, had as a consequence a 12.8-times loss of hCA IX inhibitory activity of **16** compared **9** (Table 1). Weaker hCA IX inhibition was observed for compounds **6**, **8**, **10**, **15**, **18** and **19**, which had K_Is in the range of 101–811 nM. Apparently, bulkier Ar moieties (as the 1-naphthyl one present in **10**, the *tert*-butyl-phenyl present in **8**, etc.) lead to a loss of the hCA IX inhibitory activity for this series of sulfonamide CAIs.

(iv) hCA XII was also effectively inhibited by all sulfonamides investigated here, with K_Is in the range of 3.4–239 nM (Table 1). Most of the new sulfonamides were highly effective, low nanomolar hCA XII inhibitors, for example, compounds **5–7**, **9**, **10**, **13**, **15**, **17** and **18** (K_Is range of 3.4–9.6 nM). Several other derivatives, such as **8**, **12**, **14**, and **16** showed inhibition constants of 24.7–58.8 nM. Only two derivatives (**11** and **19**, both possessing CF_3 moieties in their molecules) were less effective as hCA XII inhibitors, with K_Is of 107.5–239 nM (Table 1). Thus, as for hCAII; most of the substitution patterns present in these new sulfonamides as Ar moieties (except those from **11** and **19**) lead to quite effective hCA XII inhibitors.

(v) Except for the offtarget isforms hCA I, which is generally poorly inhibited by sulfonamides **5–19**, the remaining three isoforms (hCA II, IX and XII) are well inhibited by the compounds reported here, with hCA II inhibition being in the low nanomolar ramnge for all compounds, followed by hCA XII inhibition (most derivatives low nanomolar inhibitors), whereas for hCA IX both highly effective as well as less effective inhibitors have been detected in this small series of derivatives.

Table 1
Inhibition data of isoforms hCA I, II, IX and XII with sulfonamides **5–19** and a standard, clinically used sulphonamide (acetazolamide **AAZ**), by a stopped-flow CO_2 hydrase assay[31]

Compound	K_I (nM)[a]			
	hCA I	hCA II	hCA IX	hCA XII
5	499	6.1	7.2	7.3
6	1434	3.8	560	6.2
7	526	3.5	43.6	8.8
8	2540	2.9	713	45.4
9	746	6.3	6.4	8.4
10	750	2.4	101	7.4
11	3055	2.9	89.1	107.5
12	2420	7.7	10.9	30.3
13	289	4.5	29.4	6.0
14	2132	3.2	63.5	24.7
15	2464	3.0	395	6.6
16	4273	2.7	81.9	58.8
17	709	2.9	5.4	9.6
18	224	2.7	140	3.4
19	7544	2.2	811	239
AAZ	250	12	25	5.6

[a] Errors were in the range of 5–10% of the reported values, from three different assays.

2.3. Protein X-ray crystallography

In order to rationalize some of the very interesting inhibition data reported above, we have resolved the high resolution X-ray crystal structures for the adducts of two of these inhibitors (**10** and **13**) bound to hCA II (Tables 2 and 3 and Figs. 1–3).

The crystal structure of hCA II in complex with compound the 1-naphthyl derivative **10** was solved at 1.35 Å resolution (Table 2). The obtained electron density clearly revealed the expected features of inhibitor (Fig. 1). Apart from interaction between the deprotonated sulfonamide moiety and the metal ion, and the hydrogen bond between the NH moiety of the sulfonamide and the OH of Thr199 (present in all other sulfonamide–hCA II complexes)[1a,2a,3a,30,32] **10** was not involved in other polar contacts with protein. This is one of the few cases in which positioning of the ligand within the hCA II active site was achieved solely by hydrophobic and van der Waals interactions (Fig. 1). Interestingly, the binding mode of **10** is quite different from that, observed in another similar compound **13**, (Fig. 2, see latter in the text). The naphthyl moiety of **10** fits perfectly well in a hydrophobic pocket of the protein evidenced earlier for the binding of other sulfonamide CAIs,[1a,2a,3a,30,32] with residues Phe131, Val135, Leu204 and Pro202 being in van der Waals contact with the naphthyl tail of the inhibitor (Fig. 2).

The crystal structure of CA II in complex with compound **13** was solved at 1.82 Å resolution (Table 3). The obtained electron density was good for most of the molecule except for the phenylcyano group, where it was weaker but still interpretable (Fig. 2). Along the interactions with the metal ion and Thr199 (as mentioned

Table 2
Data processing, refinement and validation statistics for the hCA II–**10** complex

Space group	$P2_1$
Cell dimensions	
a (Å)	42.3
b (Å)	41.5
c (Å)	72.2
β (°)	104.3
Resolution (Å)	20–1.34
Highest resolution shell (Å)	1.34–1.41
Number of reflections	50,792
Number of reflections in test set	2615
Completeness (%)	93 (80*)
R_{merge}	0.05 (0.17)
$\langle I/\sigma I \rangle$	12.7 (4.3)
Average multiplicity	2.0 (1.2)
R-factor	0.13 (0.19)
R_{free}	0.18 (0.24)
Average *B* factor (Å^2)	11.7
Average *B* factor for inhibitor (Å^2)	11.0
<*B*> from Wilson plot (Å^2)	8.5
Number of protein atoms	2094
Number of inhibitor atoms	24
Number of solvent molecules	305
R.m.s. deviations from ideal values	
Bond lengths (Å)	0.022
Bond angles (°)	2.41
Outliers in Ramachandran plot (%)	0.41

[a] Values in parenthesis are for the high resolution bin.

Table 3
Data processing, refinement and validation statistics for the hCA II–**13** complex

Space group	$P2_1$
Cell dimensions	
a (Å)	42.4
b (Å)	41.5
c (Å)	72.2
β (°)	104.2
Resolution (Å)	20–1.82
Highest resolution shell (Å)	1.82–1.86
Number of reflections	20,916
Number of reflections in test set	1122
Completeness (%)	99.3 (86.8*)
R_{merge}	0.17 (0.36)
$\langle I/\sigma I \rangle$	21.9 (3.4)
Average multiplicity	7.5 (2.8)
R-factor	0.14 (0.21)
R_{free}	0.20 (0.30)
Average *B* factor (Å^2)	12.2
Average *B* factor for inhibitor (Å^2)	15.6
<*B*> from Wilson plot (Å^2)	8.1
Number of protein atoms	2080
Number of inhibitor atoms	22
Number of solvent molecules	296
R.m.s. deviations from ideal values	
Bond lengths (Å)	0.019
Bond angles (°)	2.14
Outliers in Ramachandranplot (%)	0.40

[a] Values in parenthesis are for the high resolution bin.

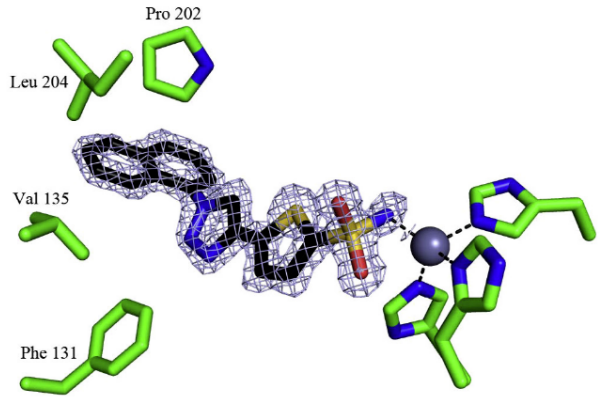

Figure 1. Binding of **10** within the hCA II active site. The zinc ion is shown as a gray sphere and its coordinating histidines (His94, 96 and 119) are shown in green. Residues 131, 135, 204 and 205 participating in hydrophobic and van der Waals contacts with inhibitor are indicated. For the sake of clarity, $2F_o-F_c$ electron density is shown only for ligand, contoured at 1 and calculated in the absence of ligand. The figure prepared by using Pymol (DeLano The PyMOL Molecular Graphics System San Carlos, CA, USA, DeLano Scientific).

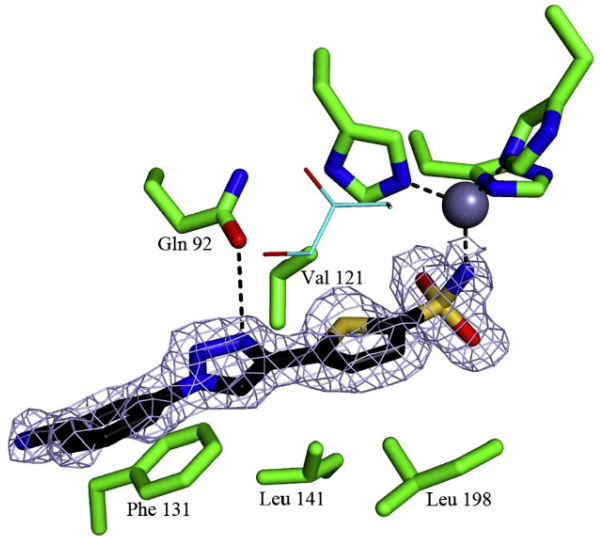

Figure 2. Binding of **13** within the hCA II active site. The zinc ion is shown as a gray sphere and its coordinating histidines (His94, 96 and 119) are shown in green. Residues 92, 121, 131, 141 and 198 participating in hydrogen bonding, hydrophobic and van der Waals contacts with the inhibitor are also indicated. A glycerol molecule bound to the enzyme is shown as a thin stick model with sky blue carbon atoms. For the sake of clarity, $2F_o-F_c$ electron density is shown only for ligand, contoured at 1 and calculated in the absence of ligand. The figure was prepared by using Pymol (DeLano, The PyMOL Molecular Graphics System San Carlos, CA, USA, DeLano Scientific).

above for **10**), compound **13** was involved in another polar contact with the protein, that is, a hydrogen bond with Gln92, an amino acid residues known to be involved in the binding of sulfonamide CAIs.[3a,30,32] A number of hydrophobic and van der Waals interactions are present as well in this adduct, and involved the following amino acid residues: Val121, Leu141, Phe131, and Leu198 (Fig. 2). In the electron density map of active site, we also located a glycerol molecule, in a near identical location as reported earlier in a number of CA II structures by McKenna's group.[33] As shown by these researchers, the glycerol is bound within the enzyme active site during the cryo-protection of the protein crystal, before freezing, and that does not affect the binding of the sulfonamide inhibitor.[33]

It should be also noted the very different orientation of the two inhibitors **10** and **13**, when bound to the hCA II active site (Fig. 3). Only the sulfamoyl moieties of the two compounds are superimposable, whereas the rest of the molecule is not (even at the level of the thiophene ring, rather close to the metal ion). Indeed, the aryl–triazolyl moieties of the two compounds adopt highly diverse orientation within the hCA II active site cavity, being completely non-superimposable. The 3-cyanophenyl group of **13** is oriented more towards the hydrophilic half of the active site and the triazole ring participates in the hydrogen bonding with the oxygen of the $CONH_2$ moiety of Gln92 (Figs. 2 and 3). On the contrary, the naphthyl (and triazole ring) of **10** are orientated towards the

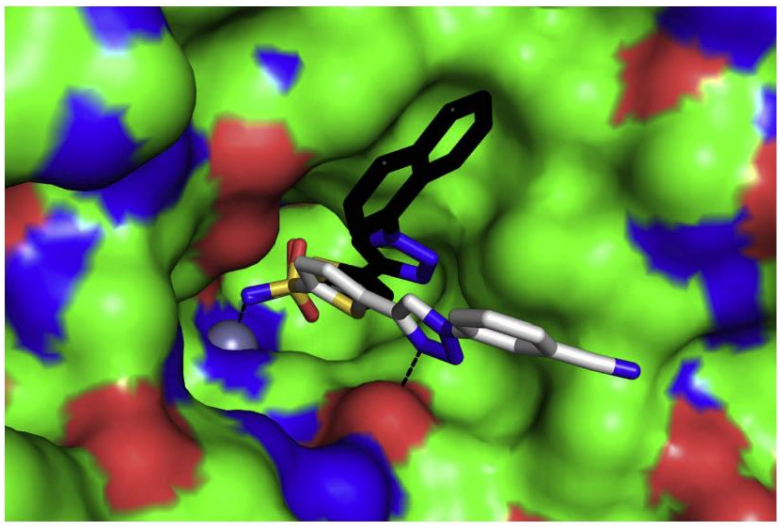

Figure 3. Comparison of the binding modes of **10** and **13** when bound to hCA II. Sulfonamide **10** is shown with black carbons and **13** with gray carbons. The protein is shown as a surface model, coloured according to surface atoms (carbon-green, nitrogen-blue, oxygen-red) and the zinc ion is sown as a gray sphere. Interactions of the sulfonamide group with the metal ion and a hydrogen bond of the triazole ring of **13** to the oxygen of the Gln92 residue are also shown.

hydrophobic half of the hCA II active site, occupying completely this binding pocket. The perfect fit of the aryl–triazolyl moiety of these compounds within the hCA II active site, may explain the excellent inhibition profile of all these compounds against the dominant CA isoforms, as shown above in Section 2.2.

3. Conclusions

We report here a series of 2-thiophene-sulfonamides incorporating 1-substituted aryl-1,2,3-triazolyl moieties, prepared by click chemistry from 5-ethynylthiophene-2-sulfonamide and substituted aryl azides. The new sulfonamides were investigated as inhibitors of the zinc metalloenzyme CA, and more specifically against the cytosolic isoforms hCA I and II and the transmembrane, tumor-associated ones hCA IX and XII: The new compounds were medium–weak hCA I inhibitors (inhibition constants in the range of 224–7544 nM), but were compactly, highly effective, low nanomolar hCA II inhibitors (K_Is in the range of 2.2–7.7 nM). The tumor-associated hCA IX was inhibited with K_Is ranging between 5.4 and 811 nM, whereas hCA XII with inhibition constants in the range of 3.4–239 nM. The X-ray crystal structure of the adducts of two such compounds complexed to hCA II (one incorporating 1-naphthyl, the other one 3-cyanophenyl moieties) evidenced the reasons of the high affinity for this enzyme. Highly favorable, predominantly hydrophobic interactions between the sulfonamide scaffold and the hCA II active site were responsible for the binding, in addition to the coordination of the sulfamoyl moiety to the zinc ion. The tails of the two inhibitors adopted very diverse orientations when bound to the active site, with the naphthyltriazolyl moiety orientated towards the hydrophobic half of the active site, and the 3-cyanophenyl pointing towards the hydrophilic half. These data may be used for the structure-based drug design of even more effective hCA II inhibitors, with potential use as antiglaucoma agents or as diuretics.

4. Experimental protocols

4.1. Chemistry

Reagents and starting materials were obtained from commercial sources and used as received. The solvents were purified and dried by standard procedures prior to use; petroleum ether of boiling range 40–60 °C was used. Flash chromatography was carried out using Merck silica gel (230–400 mesh) or reversed phase PR18 (25–40 μm). Thin-layer chromatography was performed on silica gel, spots were visualized with UV light (254 and 365 nm). Melting points were determined on an OptiMelt automated melting point system. IR spectra were measured on a Shimadzu FTIR IR Prestige-21 spectrometer. NMR spectra were recorded on Varian Mercury (400 MHz) spectrometer with chemical shifts values (δ) in ppm relative to TMS using the residual DMSO-d_6 signal as an internal standard. HRMS data were obtained with a Q-TOF micro high-resolution mass spectrometer with ESI (ESI^+/ESI^-).

*5-Bromo-N-[(E)-(dimethylamino)methylidene]thiophene-2-sulfonamide (**2**)*[25]*:*

To a solution of 5-bromothiophene-2-sulfonamide (**1**) (7.00 g, 28.91 mmol) in acetonitrile (50 mL) *N,N*-dimethylformamide dimethyl acetal (5.50 mL, 41.34 mmol) was added. The mixture was stirred at room temperature for 24 h. Solvent evaporation in vacuum afforded **2** (7.98 g, 93%) as light yellow solid. Mp 104–105 °C. IR (KBr, cm^{-1}) ν_{max}: 1631 (N=C), 1331 (S=O), 1142 (S=O), 1127 (S=O); ^1H NMR (400 MHz, DMSO-d_6) δ: 2.94 (s, 3H), 3.16 (s, 3H), 7.27 (d, J = 3.9 Hz, 1H), 7.36 (d, J = 3.9 Hz, 1H), 8.21 (s, 1H); ^{13}C NMR (100 MHz, DMSO-d_6) δ: 35.3, 41.1, 117.1, 130.6, 131.0, 145.7, 160.0.

*N-[(dimethylamino)methylidene]-5-[2-(trimethylsilyl)ethynyl)]thiophene-2-sulfonamide (**3**):*

To a solution of compound **2** (2.00 g, 6.73 mmol) in dry DMF CuI (0.13 g, 0.68 mmol), $Pd(PPh_3)_2Cl_2$ (0.24 g, 0.34 mmol), trimethylsilylacetylene (1.35 mL, 9.46 mmol) and Et_3N (4.70 mL, 33.78 mmol) were added. The mixture was stirred at room temperature under an argon atmosphere for 48 h, diluted with EtOAc (30 mL), filtered though a celite plug. Saturated aqueous NH_4Cl (50 mL) was added and the product was extracted with EtOAc (3 × 50 mL). The organic extract was washed with H_2O (2 × 50 mL) and brine (50 mL), dried over Na_2SO_4, solvent driven off in vacuum. Purification of the crude product by silica gel chromatography (EtOAc/PE 2:1) afforded **3** (1.75 g, 82%) as light brown solid. R_f = 0.7 (EtOAc/PE 2:1). Mp 120.5–121.5 °C. IR (KBr, cm^{-1}) IR (KBr, cm^{-1}) ν_{max}: 2147 (C≡C), 1635 (N=C), 1345 (S=O), 1148 (S=O); ^1H NMR (400 MHz, DMSO-d_6) δ: 0.24 (s, 9H), 2.95 (s, 3H), 3.17 (s, 3H), 7.32 (d, J =

3.9 Hz, 1H), 7.43 (d, J = 3.9 Hz, 1H), 8.22 (s, 1H); ^{13}C NMR (100 MHz, DMSO-d_6) δ: −0.45, 35.3, 41.1, 96.0, 101.9, 126.0, 130.0, 133.2, 145.7, 160.0; HRMS (ESI) $[M+H]^+$: m/z Calcd for ($C_{12}H_{19}N_2O_2S_2Si$) 315.0657. Found 315.0652.

*5-Ethynylthiophene-2-sulfonamide (**4**)*[34]:

To a solution of compound **3** (1.00 g, 3.18 mmol) in dry THF (30 mL) 1 M TBAF in THF (6.36 mL, 6.36 mmol) was added. The mixture was stirred at room temperature for 3 h, diluted with H_2O (30 mL), extracted with EtOAc (3 × 25 mL). The organic phase was washed with brine (25 mL), dried over Na_2SO_4, solvent was driven off in vacuum. Purification of the crude product by silica gel chromatography (EtOAc/PE 1:1) afforded **4** (0.30 g, 50%) as brown solid. R_f = 0.8 (EtOAc/PE 1:1). Mp 125.5–126.5 °C. IR (KBr, cm^{-1}) ν_{max}: 3330 (NH), 3233 (NH), 2100 (C≡C), 1341 (S=O), 1150 (S=O); ^{1}H NMR (400 MHz, DMSO-d_6) δ: 4.81 (s, 1H), 7.38 (d, J = 3.9 Hz, 1H), 7.47 (d, J = 3.9 Hz, 1H), 7.83 (s, 2H); ^{13}C NMR (100 MHz, DMSO-d_6) δ: 75.4, 87.6, 125.4, 130.0, 133.3, 146.5.

General procedure for the synthesis of 1,2,3-triazolylderivatives of sulfamoylthiophene

To a solution of 5-ethynylthiophene-2-sulfonamide (**4**) (1 equiv) in 1:1 ^{t}BuOH/H_2O (10 mL per 1.07 mmol of **4**) corresponding arylazide (1 equiv) and solution of $CuSO_4{\cdot}5H_2O$ (1.3 equiv) in H_2O (1.5 mL per 1.36 mmol) were added. The mixture was stirred at room temperature for 5 min before solution of sodium ascorbate (4 equiv) in H_2O (2 mL per 4.27 mmol) was added. The mixture was stirred at room temperature for another 15 min before AcOH (20 equiv) was added and stirring was continued for 30 min. Solvent was driven off in vacuum and the crude product was purified by reversed phase chromatography (C-18, H_2O–MeCN gradient MeCN 10–90%) with followed re-crystallization from MeCN/H2O.

*5-(1-Phenyl-1H-1,2,3-triazol-4-yl)thiophene-2-sulfonamide (**5**)*

Compound **5** was prepared according to the general procedure from **4** (0.20 g, 1.07 mmol), azidobenzene[35,36] (0.13 g, 1.07 mmol), $CuSO_4{\cdot}5H_2O$ (0.34 g, 1.36 mmol), sodium ascorbate (0.85 g, 4.27 mmol) and AcOH (1.22 mL, 21.36 mmol) as a yellowish solid (0.31 g, 96%). Mp 287–288 °C. IR (KBr, cm^{-1}) ν_{max}: 3324 (NH), 3238 (NH), 1335 (S=O), 1151 (S=O); ^{1}H NMR (400 MHz, DMSO-d_6) δ: 7.46 (d, J = 3.7 Hz, 1H), 7.50 (d, J = 3.7 Hz, 1H), 7.51–7.56 (m, 1H), 7.61–7.67 (m, 4H), 7.92–7.96 (m, 2H), 9.32 (s, 1H); ^{13}C NMR (100 MHz, DMSO-d_6) δ: 120.0, 120.2, 124.1, 129.1, 129.6, 130.0, 135.6, 136.4, 141.7, 147.0; HRMS (ESI) $[M+H]^+$: m/z Calcd for ($C_{12}H_{11}N_4O_2S_2$) 307.0323. Found 307.0325.

*5-[1-(3-Methylphenyl)-1H-1,2,3-triazol-4-yl]thiophene-2-sulfonamide (**6**):*

Compound **6** was prepared according to the general procedure from **4** (0.20 g, 1.07 mmol), 1-azido-3-methylbenzene[37] (0.14 g, 1.07 mmol), $CuSO_4{\cdot}5H_2O$ (0.34 g, 1.36 mmol), sodium ascorbate (0.85 g, 4.27 mmol) and AcOH (1.22 mL, 21.36 mmol) as a yellowish solid (0.27 g, 80%). Mp 222–223 °C. IR (KBr, cm^{-1}) ν_{max}: 3309 (NH), 1340 (S=O), 1151 (S=O); ^{1}H NMR (400 MHz, DMSO-d_6) δ: 2.43 (s, 3H), 7.33–7.37 (m, 1H), 7.50 (d, J = 3.9 Hz, 1H), 7.51–7.54 (m, 1H), 7.60 (d, J = 3.9 Hz, 1H), 7.70–7.74 (m, 1H), 7.76–7.79 (m, 3H), 9.33 (s, 1H); ^{13}C NMR (100 MHz, DMSO-d_6) δ: 20.9, 117.3, 120.2, 120.6, 124.2, 129.7, 129.8, 130.8, 136.3, 136.8, 139.8, 141.4, 144.4; HRMS (ESI) $[M+H]^+$: m/z Calcd for ($C_{13}H_{13}N_4O_2S_2$) 321.0480. Found 321.0505.

*5-[1-(4-Methylphenyl)-1H-1,2,3-triazol-4-yl]thiophene-2-sulfonamide (**7**):*

Compound **7** was prepared according to the general procedure from **4** (0.20 g, 1.07 mmol), 1-azido-4-methylbenzene[35] (0.14 g, 1.07 mmol), $CuSO_4{\cdot}5H_2O$ (0.34 g, 1.36 mmol), sodium ascorbate (0.85 g, 4.27 mmol) and AcOH (1.22 mL, 21.36 mmol) as a light brown solid (0.27 g, 80%). Mp 275–276 °C. IR (KBr, cm^{-1}) ν_{max}: 3324 (NH), 3233 (NH), 1340 (S=O), 1153 (S=O); ^{1}H NMR (400 MHz, DMSO-d_6) δ: 2.39 (s, 3H), 7.41–7.46 (m, 2H), 7.50 (d, J = 3.9 Hz, 1H), 7.59 (d, J = 3.9 Hz, 1H), 7.78 (s, 2H), 7.79–7.83 (m, 2H), 9.29 (s, 1H); ^{13}C NMR (100 MHz, DMSO-d_6) δ: 20.7, 120.1, 120.2, 124.2, 130.4, 130.9, 134.1, 136.9, 138.9, 141.4, 144.4; HRMS (ESI) $[M+H]^+$: m/z Calcd for ($C_{13}H_{13}N_4O_2S_2$) 321.0480. Found 321.0527.

*5-[1-(4-tert-Butylphenyl)-1H-1,2,3-triazol-4-yl]thiophene-2-sulfonamide (**8**):*

Compound **8** was prepared according to the general procedure from **4** (0.20 g, 1.07 mmol), 1-azido-4-*tert*-butylbenzene[38] (0.19 g, 1.07 mmol), $CuSO_4{\cdot}5H_2O$ (0.34 g, 1.36 mmol), sodium ascorbate (0.85 g, 4.27 mmol) and AcOH (1.22 mL, 21.36 mmol) as a light brown solid (0.27 g, 70%). Mp 213–214 °C. IR (KBr, cm^{-1}) ν_{max}: 3303 (NH), 1341 (S=O), 1152 (S=O); ^{1}H NMR (400 MHz, DMSO-d_6) δ: 1.34 (s, 9H), 7.50 (d, J = 3.9 Hz, 1H), 7.59 (d, J = 3.9 Hz, 1H), 7.62–7.67 (m, 2H), 7.78 (s, 2H), 7.81–7.86 (m, 2H), 9.31 (s, 1H); ^{13}C NMR (100 MHz, DMSO-d_6) δ: 31.0, 34.6, 120.0, 120.2, 124.2, 126.7, 130.8, 134.0, 136.9, 141.3, 144.3, 151.8; HRMS (ESI) $[M+H]^+$: m/z Calcd for ($C_{16}H_{19}N_4O_2S_2$) 363.0949. Found 363.0952.

*5-[1-(4-Methoxyphenyl)-1H-1,2,3-triazol-4-yl]thiophene-2-sulfonamide (**9**):*

Compound **9** was prepared according to the general procedure from **4** (0.30 g, 1.60 mmol), 1-azido-4-methoxybenzene[36] (0.24 g, 1.60 mmol), $CuSO_4{\cdot}5H_2O$ (0.51 g, 2.04 mmol), sodium ascorbate (1.27 g, 6.41 mmol) and AcOH (1.83 mL, 32.04 mmol) as a light brown solid (0.37 g, 69%). Mp 258-259 °C. IR (KBr, cm^{-1}) ν_{max}: 3337 (NH), 3233 (NH), 1340 (S=O), 1151 (S=O); ^{1}H NMR (400 MHz, DMSO-d_6) δ: 3.85 (s, 3H), 7.15–7.20 (m, 2H), 7.49 (d, J = 3.9 Hz, 1H), 7.59 (d, J = 3.9 Hz, 1H), 7.77 (br s, 2H), 7.81–7.86 (m, 2H), 9.25 (s, 1H); ^{13}C NMR (100 MHz, DMSO-d_6) δ: 55.6, 115.0, 120.3, 122.0, 124.1, 129.7, 130.8, 137.0, 141.2, 144.3, 159.6; HRMS (ESI) $[M+H]^+$: m/z Calcd for ($C_{13}H_{13}N_4O_3S_2$) 337.0429. Found 337.0435.

*5-[1-(Naphthalen-1-yl)-1H-1,2,3-triazol-4-yl]thiophene-2-sulfonamide (**10**):*

Compound **10** was prepared according to the general procedure from **4** (0.20 g, 1.07 mmol), 1-azidonaphthalene[39] (0.18 g, 1.07 mmol), $CuSO_4{\cdot}5H_2O$ (0.34 g, 1.36 mmol), sodium ascorbate (0.85 g, 4.27 mmol) and AcOH (1.22 mL, 21.36 mmol) as a brown solid (0.34 g, 89%). Mp 228–229 °C. IR (KBr, cm^{-1}) ν_{max}: 3307 (NH), 1346 (S=O), 1153 (S=O); ^{1}H NMR (400 MHz, DMSO-d_6) δ: 7.55 (d, J = 3.9 Hz, 1H), 7.57–7.60 (m, 1H), 7.61 (d, J = 3.9 Hz, 1H), 7.63–7.76 (m, 3H), 7.80 (s, 2H), 7.84 (dd, J = 7.3, 1.2 Hz, 1H), 8.14–8.17 (m, 1H), 8.22–8.26 (m, 1H), 9.22 (s, 1H); ^{13}C NMR (100 MHz, DMSO-d_6) δ: 122.0, 124.1, 124.3, 124.7, 125.5, 127.3, 127.8, 128.3, 128.4, 130.7, 130.9, 132.9, 133.7, 137.0, 140.9, 144.4; HRMS (ESI) $[M+H]^+$: m/z Calcd for ($C_{16}H_{13}N_4O_2S_2$) 357.0480. Found 357.0488.

*5-{1-[4-(Trifluoromethyl)phenyl]-1H-1,2,3-triazol-4-yl}thiophene-2-sulfonamide (**11**):*

Compound **11** was prepared according to the general procedure from **4** (0.20 g, 1.07 mmol), 1-azido-4-(trifluoromethyl)benzene[40] (0.20 g, 1.07 mmol), $CuSO_4{\cdot}5H_2O$ (0.34 g, 1.36 mmol), sodium ascorbate (0.85 g, 4.27 mmol) and AcOH (1.22 mL, 21.36 mmol) as a light brown solid (0.28 g, 70%). Mp 252–253 °C. IR (KBr, cm^{-1}) ν_{max}: 3320 (NH), 1340 (S=O), 1152 (S=O); ^{1}H NMR (400 MHz, DMSO-d_6, δ): 7.53 (d, J = 3.8 Hz, 1H), 7.61 (d, J = 3.8 Hz, 1H), 7.80 (s, 2H), 8.02–8.07 (m, 2H), 8.17–8.23 (m, 2H), 9.51 (s, 1H); ^{13}C NMR (100 MHz, DMSO-d_6) δ: 120.5, 120.7, 123.8 (q, J = 273 Hz), 124.5, 127.4 (q, J = 3.8 Hz), 129.0 (q, J = 33.0 Hz), 130.9, 136.4, 139.1, 141.7, 144.7; HRMS (ESI) $[M+H]^+$: m/z Calcd for ($C_{13}H_{10}F_3N_4O_2S_2$) 375.0197. Found 375.0250.

*5-[1-(3-Bromophenyl)-1H-1,2,3-triazol-4-yl]thiophene-2-sulfonamide (**12**):*

Compound **12** was prepared according to the general procedure from **4** (0.30 g, 1.60 mmol), 1-azido-3-bromobenzene[41] (0.32 g, 1.60 mmol), $CuSO_4{\cdot}5H_2O$ (0.51 g, 2.04 mmol), sodium ascorbate

(1.27 g, 6.41 mmol) and AcOH (1.83 mL, 32.04 mmol) as a yellowish solid (0.33 g, 54%). Mp 246–247 °C. IR (KBr, cm^{-1}) ν_{max}: 3304 (NH), 1342 (S=O), 1152 (S=O); ^1H NMR (400 MHz, DMSO-d_6) δ: 7.49 (d, J = 3.9 Hz, 1H), 7.57–7.63 (m, 2H), 7.72–7.76 (m, 1H), 7.79 (br s, 2H), 7.97–8.01 (m, 1H), 8.18–18.21 (m, 1H), 9.43 (s, 1H); ^{13}C NMR (100 MHz, DMSO-d_6) δ: 119.2, 120.5, 122.5, 122.8, 124.3, 130.9, 131.8, 131.9, 136.5, 137.4, 141.5, 144.6; HRMS (ESI) $[M+H]^+$: m/z Calcd for ($C_{12}H_{10}BrN_4O_2S_2$) 384.9429. Found 384.9454.

*5-[1-(3-Cyanophenyl)-1H-1,2,3-triazol-4-yl]thiophene-2-sulfonamide (**13**):*

Compound **13** was prepared according to the general procedure from **4** (0.20 g, 1.07 mmol), 3-azidobenzonitrile[37] (0.15 g, 1.07 mmol), $CuSO_4{\cdot}5H_2O$ (0.34 g, 1.36 mmol), sodium ascorbate (0.85 g, 4.27 mmol) and AcOH (1.22 mL, 21.36 mmol) as a yellow solid (0.32 g, 92%). Mp 243–244 °C. IR (KBr, cm^{-1}) ν_{max}: 3331 (NH), 3232 (NH), 2235 (C≡N), 1336 (S=O), 1157 (S=O); ^1H NMR (400 MHz, DMSO-d_6) δ: 7.50 (d, J = 3.9 Hz, 1H), 6.61 (d, J = 3.9 Hz, 1H), 7.80 (s, 2H), 7.86 (app t, J = 8.2 Hz, 1H), 8.00–8.04 (m, 1H), 8.32 (ddd, J = 8.2, 2.4, 1.2 Hz, 1H), 8.46–8.48 (m, 1H), 9.45 (s, 1H); ^{13}C NMR (100 MHz, DMSO-d_6) δ: 112.9, 117.8, 120.6, 123.7, 124.5, 124.9, 130.9, 131.4, 132.7, 136.4, 136.8, 141.6, 144.7; HRMS (ESI) $[M+H]^+$: m/z Calcd for ($C_{13}H_{10}N_5O_2S_2$) 332.0276. Found 332.0335.

*5-[1-(3,4-Dichlorophenyl)-1H-1,2,3-triazol-4-yl]thiophene-2-sulfonamide (**14**):*

Compound **14** was prepared according to the general procedure from **4** (0.20 g, 1.07 mmol), 4-azido-1,2-dichlorobenzene[37] (0.20 g, 1.07 mmol), $CuSO_4{\cdot}5H_2O$ (0.34 g, 1.36 mmol), sodium ascorbate (0.85 g, 4.27 mmol) and AcOH (1.22 mL, 21.36 mmol) as a white solid (0.34 g, 85%). Mp 260–261 °C. IR (KBr, cm^{-1}) ν_{max}: 3325 (NH), 3218 (NH), 1343 (S=O), 1155 (S=O); ^1H NMR (400 MHz, DMSO-d_6) δ: 7.49 (d, J = 3.9 Hz, 1H), 7.60 (d, J = 3.9 Hz, 1H), 7.79 (s, 2H), 7.93 (d, J = 8.7 Hz, 1H), 7.99 (dd, J = 8.7, 2.4 Hz, 1H), 8.29 (d, J = 2.4 Hz, 1H), 9.44 (s, 1H); ^{13}C NMR (100 MHz, DMSO-d_6) δ: 120.3, 120.6, 122.0, 124.4, 130.9, 131.4, 131.9, 132.4, 135.8, 136.4, 141.6, 144.7; HRMS (ESI) $[M+H]^+$: m/z Calcd for ($C_{12}H_9Cl_2N_4O_2S_2$) 374.9544. Found 374.9597.

*5-[1-(3-Chloro-4-fluorophenyl)-1H-1,2,3-triazol-4-yl]thiophene-2-sulfonamide (**15**):*

Compound **15** was prepared according to the general procedure from **4** (0.20 g, 1.07 mmol), 4-azido-2-chloro-1-fluorobenzene[42] (0.18 g, 1.07 mmol), $CuSO_4{\cdot}5H_2O$ (0.34 g, 1.36 mmol), sodium ascorbate (0.85 g, 4.27 mmol) and AcOH (1.22 mL, 21.36 mmol) as a light yellow solid (0.34 g, 89%). Mp 240–241 °C. IR (KBr, cm^{-1}) ν_{max}: 3314 (NH), 1340 (S=O), 1152 (S=O); ^1H NMR (400 MHz, DMSO-d_6) δ: 7.48 (d, J = 3.9 Hz, 1H), 7.60 (d, J = 3.9 Hz, 1H), 7.72 (app t, J = 9.0 Hz, 1H), 7.79 (s, 2H), 7.99 (ddd, J = 9.0, 4.3, 2.7 Hz, 1H), 8.24 (dd, J = 6.3, 2.7 Hz, 1H), 9.38 (s, 1H); ^{13}C NMR (100 MHz, DMSO-d_6) δ: 118.3 (d, J = 22.8 Hz), 120.7, 120.9 (d, J = 19.3 Hz), 121.2 (d, J = 7.9 Hz), 122.7, 124.4, 130.9, 133.3 (d, J = 3.1 Hz), 136.5, 141.5, 144.6, 157.1 (d, J = 249 Hz); HRMS (ESI) $[M+H]^+$: m/z Calcd for ($C_{12}H_9ClFN_4O_2S_2$) 358.9839. Found 358.9866.

*5-[1-(3-Chloro-4-methoxyphenyl)-1H-1,2,3-triazol-4-yl]thiophene-2-sulfonamide (**16**):*

Compound **16** was prepared according to the general procedure from **4** (0.10 g, 0.53 mmol), 4-azido-2-chloro-1-methoxybenzene[43] (0.10 g, 0.53 mmol), $CuSO_4{\cdot}5H_2O$ (0.17 g, 0.68 mmol), sodium ascorbate (0.42 g, 2.14 mmol) and AcOH (0.61 mL, 10.68 mmol) as a light brown solid (0.20 g, 90%). Mp 262–263 °C. IR (KBr, cm^{-1}) ν_{max}: 3332 (NH), 1336 (S=O), 1156 (S=O); ^1H NMR (400 MHz, DMSO-d_6) δ: 3.95 (s, 3H), 7.39 (d, J = 9.0 Hz, 1H), 7.47 (d, J = 3.9 Hz, 1H), 7.59 (d, J = 3.9 Hz, 1H), 7.78 (s, 2H), 7.90 (dd, J = 9.0, 2.7 Hz, 1H), 8.05 (d, J = 2.7 Hz, 1H), 9.31 (s, 1H); ^{13}C NMR (100 MHz, DMSO-d_6) δ: 56.7, 113.6, 120.4, 120.5, 121.9, 122.0, 124.2, 129.8, 130.9, 136.8, 141.3, 144.4, 154.9; HRMS (ESI) $[M+H]^+$: m/z Calcd for ($C_{13}H_{12}ClN_4O_3S_2$) 371.0039. Found 371.0047.

*5-[1-(4-Iodophenyl)-1H-1,2,3-triazol-4-yl]thiophene-2-sulfonamide (**17**):*

Compound **17** was prepared according to the general procedure from **4** (0.10 g, 0.53 mmol), 1-azido-4-iodobenzene[35,36] (0.13 g, 0.53 mmol), $CuSO_4{\cdot}5H_2O$ (0.17 g, 0.68 mmol), sodium ascorbate (0.42 g, 2.14 mmol) and AcOH (0.61 mL, 10.68 mmol) as a light brown solid (0.20 g, 90%). Mp 274–275 °C. IR (KBr, cm^{-1}) ν_{max}: 3349 (NH), 3246 (NH), 1342 (S=O), 1150 (S=O); ^1H NMR (400 MHz, DMSO-d_6) δ: 7.50 (d, J = 3.9 Hz, 1H), 7.59 (d, J = 3.9 Hz, 1H), 7.74–7.77 (m, 2H), 7.78 (s, 2H), 7.99–8.03 (m, 2H), 9.37 (s, 1H); ^{13}C NMR (100 MHz, DMSO-d_6) δ: 94.9, 120.2, 122.1, 124.4, 130.9, 136.0, 136.6, 138.8, 141.6, 144.5; HRMS (ESI) $[M+H]^+$: m/z Calcd for ($C_{12}H_{10}IN_4O_2S_2$) 432.9290. Found 432.9306.

*5-{1-[2-Fluoro-4-(methylsulfonyl)phenyl]-1H-1,2,3-triazol-4-yl}thiophene-2-sulfonamide (**18**):*

Compound **18** was prepared according to the general procedure from **4** (0.10 g, 0.53 mmol), 1-azido-2-fluoro-4-(methylsulfonyl)benzene (0.12 g, 0.53 mmol) prepared: To a solution of 2-fluoro-4-(methylsulfonyl)aniline (1.00 g, 5.28 mmol) in mixture of H_2O (6.7 mL) and conc. HCl (3.3 mL) aqueous 4 M $NaNO_2$ (1.72 mL, 6.87 mmol) dropwise was added at 0 °C. The mixture was stirred at 0 °C for 10 min before aqueous 4 M NaN_3 (1.59 mL, 6.36 mmol) dropwise was added at 0 °C and stirring was continued at the same temperature for 1 h. H_2O (15 mL) was added and the product was extracted with Et_2O (2 × 25 mL). The organic phase was washed with H_2O (25 mL) and dried over Na_2SO_4. Solvent evaporation afforded 1-azido-2-fluoro-4-(methylsulfonyl)benzene (0.89 g, 78%) as orange solid.

IR (KBr, cm^{-1}) ν_{max}: 2142 (N_3), 2101 (N_3), 1318 (S=O), 1148 (S=O); ^1H NMR (400 MHz, DMSO-d_6) δ: 3.26 (s, 3H), 7.58 (app t, J = 8.3 Hz, 1H), 7.77 (ddd, J = 8.3, 2.0, 0.8 Hz, 1H), 7.88 (dd, J = 10.6, 2.0 Hz, 1H); ^{13}C NMR (100 MHz, DMSO-d_6) δ: 43.3, 115.7 (d, J = 21.9 Hz), 122.3 (d, J = 1.6 Hz), 124.3 (d, J = 3.6 Hz), 133.1 (d, J = 0.9 Hz), 137.7 (d, J = 3.9 Hz), 153.0 (d, J = 252 Hz).), $CuSO_4{\cdot}5H_2O$ (0.17 g, 0.68 mmol), sodium ascorbate (0.42 g, 2.14 mmol) and AcOH (0.61 mL, 10.68 mmol) as a light brown solid (0.15 g, 72%). Mp 279–280 °C. IR (KBr, cm^{-1}) ν_{max}: 3343 (NH), 3261 (NH), 1349 (S=O), 1298 (S=O), 1164 (S=O), 1133 (S=O); ^1H NMR (400 MHz, DMSO-d_6) δ: 7.59–7.62 (m, 2H), 7.80 (s, 2H), 8.01–8.05 (m, 1H), 8.20–8.28 (m, 2H), 9.27 (d, J = 2.3 Hz, 1H); ^{13}C NMR (100 MHz, DMSO-d_6) δ: 43.1, 116.7 (d, J = 22.9 Hz), 123.3 (d, J = 5.5 Hz), 124.4 (d, J = 3.5 Hz), 125.0, 126.6, 128.3 (d, J = 10.8 Hz), 130.9, 136.1, 141.5, 142.9 (d, J = 6.2 Hz), 144.8, 153.1 (d, J = 257 Hz); HRMS (ESI) $[M+H]^+$: m/z Calcd for ($C_{13}H_{12}FN_4O_4S_3$) 403.0005. Found 402.9996.

*5-{1-[4-Cyano-3-(trifluoromethyl)phenyl]-1H-1,2,3-triazol-4-yl}thiophene-2-sulfonamide (**19**):*

Compound **19** was prepared according to the general procedure from **4** (0.20 g, 1.07 mmol), 4-azido-2-(trifluoromethyl)benzonitrile (0.23 g, 1.07 mmol) prepared: To a solution of 4-amino-2-(trifluormetyl)benzonitrile (1.00 g, 5.37 mmol) in mixture of H_2O (6.7 mL) and conc. HCl (3.3 mL) aq 4 M $NaNO_2$ (1.75 mL, 6.98 mmol) dropwise was added at 0 °C. The mixture was stirred at 0 °C for 10 min before aq 4 M NaN_3 (1.61 mL, 6.44 mmol) dropwise was added at 0 °C and stirring was continued at the same temperature for 1 h. H_2O (15 mL) was added and the product was extracted with Et_2O (2 × 25 mL). The organic phase was washed with H_2O (25 mL), dried over Na_2SO_4. Solvent evaporation afforded 4-azido-2-(trifluoromethyl)benzonitrile (0.71 g, 62%) as light brown solid. IR (KBr, cm^{-1}) ν_{max}: 2229 (C≡N), 2133 (N_3); ^1H NMR (400 MHz, DMSO-d_6) δ: 7.61–7.66 (m, 2H), 8.17 (d, J = 8.2 Hz, 1H); ^{13}C NMR (100 MHz, DMSO-d_6) δ: 103.7 (q, J = 2.2 Hz), 115.4, 118.3 (q, J = 4.8 Hz), 122.1 (q, J = 274 Hz), 123.7, 132.5 (q, Jv32.7 Hz), 137.0, 145.8.), $CuSO_4{\cdot}5H_2O$ (0.34 g, 1.36 mmol), sodium ascorbate

(0.85 g, 4.27 mmol) and AcOH (1.22 mL, 21.36 mmol) as a yellow solid (0.31 g, 73%). Mp 254–255 °C. IR (KBr, cm^{-1}) ν_{max}: 3368 (NH), 3276 (NH), 2230 (CN), 1340 (S=O), 1138 (S=O); ^1H NMR (400 MHz, DMSO-d_6) δ: 7.52 (d, J = 3.9 Hz, 1H), 7.62 (d, J = 3.9 Hz, 1H), 7.81 (s, 2H), 8.45–8.56 (m, 3H), 9.65 (s, 1H); ^{13}C NMR (100 MHz, DMSO-d_6) δ: 108.2, 115.0, 118.5 (q, J = 4.9 Hz), 120.9, 122.0 (q, J = 274 Hz), 124.1, 124.7, 131.0, 132.7 (q, J = 32.7 Hz), 136.0, 137.6, 139.4, 142.0, 145.0; HRMS (ESI) $[M+H]^+$: m/z Calcd for ($C_{14}H_9F_3N_5O_2S_2$) 400.0150. Found 400.0161.

4.2. Protein production and purification

hCA I, hCA II, hCA IX and hCA XII were produced and purified as described earlier by our groups.[8,9,11]

4.3. CA inhibition assay

An Applied Photophysics stopped-flow instrument has been used for assaying the CA catalysed CO_2 hydration activity.[31] Phenol red (at a concentration of 0.2 mM) has been used as indicator, working at the absorbance maximum of 557 nm, with 20 mM Hepes (pH 7.5) as buffer, and 20 mM Na_2SO_4 (for maintaining constant the ionic strength), following the initial rates of the CA-catalyzed CO_2 hydration reaction for a period of 10–100 s. The CO_2 concentrations ranged from 1.7 to 17 mM for the determination of the kinetic parameters and inhibition constants. For each inhibitor at least six traces of the initial 5–10% of the reaction have been used for determining the initial velocity. The uncatalyzed rates were determined in the same manner and subtracted from the total observed rates. Stock solutions of inhibitor (0.1 mM) were prepared in distilled-deionized water and dilutions up to 0.01 nM were done thereafter with the assay buffer. Inhibitor and enzyme solutions were preincubated together for 15 min at room temperature prior to assay, in order to allow for the formation of the E–I complex. The inhibition constants were obtained by non-linear least-squares methods using PRISM 3, as reported earlier,[8] and represent the mean from at least three different determinations. All CA isofoms were recombinant ones obtained in-house as reported earlier.[8,9,11]

4.4. Crystallization and data collection

Protein was concentrated to 10.8 mg/ml in 20 mM tris–HCl pH 8.0 using 10 kDa cutoff Amicon concentrator. Crystallization was done by sitting drop technique in 96-well MRC plates (Molecular Dimensions). 1 μl of protein was mixed with 1 μl of bottom solution, (1.5 M Na citrate, 80 mM tris–HCl pH 9.0) and 0.2 μl of 100 mM inhibitor in 100% DMSO. The obtained crystals were flash-frozen in liquid nitrogen. Data were collected at beamline I911-3, MAX-lab synchrotron, Lund, Sweden.

4.5. Structure determination

Images were processed by MOSFLM[44] and scaled by SCALA.[45] The structure was refined by REFMAC[46] using unliganded CA II mutant (PDB code 3DC3)[9] as an initial model. The parameter files for sulfonamides 10 and 13 were generated by LIBCHECK.[47] The ligand was fitted in electron density in COOT (Emsley and Cowtan 2004),[48] followed by further REFMAC runs. Data scaling, refinement, and validation statistics are listed in Table 1. Atomic coordinates and structure factors were deposited in PDB with accession code 4bf1 and 4bf6.

Acknowledgment

This work was financed by two FP7 EU grant (METOXIA and DYNANO).

References and notes

1. a Aggarwal, M.; Kondeti, B.; McKenna, R. *Bioorg. Med. Chem.* **2013**, *21*, 1526; b Aggarwal, M.; McKenna, R. *Expert Opin. Ther. Pat.* **2012**, *22*, 903; c Supuran, C. T.; Scozzafava, A.; Casini, A. *Med. Res. Rev.* **2003**, *23*, 146; (d) Pastorekova, S.; Parkkila, S.; Pastorek, J.; Supuran, C. T. *J. Enzyme Inhib. Med. Chem.* **2004**, *19*, 199; e Jain, A.; Whitesides, G. M.; Alexander, R. S.; Christianson, D. W. *J. Med. Chem.* **1994**, *37*, 2100; f Baranauskiene, L.; Hilvo, M.; Matuliene, J.; Golovenko, D.; Manakova, E.; Dudutiene, V.; Michailoviene, V.; Torresan, J.; Jachno, J.; Parkkila, S.; Maresca, A.; Supuran, C. T.; Grazulis, S.; Matulis, D. *J. Enzyme Inhib. Med. Chem.* **2010**, *25*, 863.
2. a Supuran, C. T. *Nat. Rev. Drug Disc.* **2008**, *7*, 168; b Supuran, C. T. *Front. Pharmacol.* **2011**, *2*, 34; c Supuran, C. T. *J. Enzyme Inhib. Med. Chem.* **2012**, *27*, 759.
3. a Alterio, V.; Di Fiore, A.; D'Ambrosio, K.; Supuran, C. T.; De Simone, G. *Chem. Rev.* **2012**, *112*, 4421; b Capasso, C.; De Luca, V.; Carginale, V.; Cannio, R.; Rossi, M. *J. Enzyme Inhib. Med. Chem.* **2012**, *27*, 892.
4. a Alber, B. E.; Ferry, J. G. *Proc. Natl. Acad. Sci. USA* **1994**, *91*, 6909; b Kisker, C.; Schindelin, H.; Alber, B. E.; Ferry, J. G.; Rees, D. C. *EMBO J.* **1996**, *15*, 2323; c Zimmerman, S. A.; Tomb, J. F.; Ferry, J. G. J. *Bacteriology* **2010**, *192*, 1353.
5. a Ferry, J. G. *Bioorg. Med. Chem.* **2013**, *21*, 1392; b Tripp, B. C.; Bell, C. B., 3rd; Cruz, F.; Krebs, C.; Ferry, J. G. *J. Biol. Chem.* **2004**, *279*, 6683.
6. a Viparelli, F.; Monti, S. M.; De Simone, G.; Innocenti, A.; Scozzafava, A.; Xu, Y.; Morel, F. M. M.; Supuran, C. T. *Bioorg. Med. Chem. Lett.* **2010**, *20*, 4745; b Alterio, V.; Langella, E.; Viparelli, F.; Vullo, D.; Ascione, G.; Dathan, N. A.; Morel, F. M. M.; Supuran, C. T.; De Simone, G.; Monti, S. M. *Biochimie* **2012**, *94*, 1232.
7. Briganti, F.; Mangani, S.; Orioli, P.; Scozzafava, A.; Vernaglione, G.; Supuran, C. T. *Biochemistry* **1997**, *36*, 10384.
8. a Carta, F.; Temperini, C.; Innocenti, A.; Scozzafava, A.; Kaila, K.; Supuran, C. T. *J. Med. Chem.* **2010**, *53*, 5511; b Davis, R. A.; Hofmann, A.; Osman, A.; Hall, R. A.; Mühlschlegel, F. A.; Vullo, D.; Innocenti, A.; Supuran, C. T.; Poulsen, S. A. *J. Med. Chem.* **2011**, *54*, 1682; c Kazancıoğlu, E. A.; Güney, M.; Şentürk, M.; Supuran, C. T. *J. Enzyme Inhib. Med. Chem.* **2012**, *27*, 880.
9. Tars, K.; Vullo, D.; Kazaks, A.; Leitans, J.; Lends, A.; Grandane, A.; Zalubovskis, R.; Scozzafava, A.; Supuran, C. T. *J. Med. Chem.* **2013**, *56*, 293.
10. a Innocenti, A.; Vullo, D.; Scozzafava, A.; Supuran, C. T. *Bioorg. Med. Chem. Lett.* **2008**, *18*, 1583; b Innocenti, A.; Vullo, D.; Scozzafava, A.; Supuran, C. T. *Bioorg. Med. Chem.* **2008**, *16*, 7424; c Davis, R. A.; Innocenti, A.; Poulsen, S. A.; Supuran, C. T. *Bioorg. Med. Chem.* **2010**, *18*, 14.
11. a Maresca, A.; Temperini, C.; Vu, H.; Pham, N. B.; Poulsen, S. A.; Scozzafava, A.; Quinn, R. J.; Supuran, C. T. *J. Am. Chem. Soc.* **2009**, *131*, 3057; b Maresca, A.; Temperini, C.; Pochet, L.; Masereel, B.; Scozzafava, A.; Supuran, C. T. *J. Med. Chem.* **2010**, *53*, 335.
12. a Maresca, A.; Scozzafava, A.; Supuran, C. T. *Bioorg. Med. Chem. Lett.* **2010**, *20*, 7255; b Touisni, N.; Maresca, A.; McDonald, P. C.; Lou, Y.; Scozzafava, A.; Dedhar, S.; Winum, J. Y.; Supuran, C. T. *J. Med. Chem.* **2011**, *54*, 8271; c Bonneau, A.; Maresca, A.; Winum, J. Y.; Supuran, C. T. *J. Enzyme Inhib. Med. Chem.* **2013**, *28*, 397.
13. a Carta, F.; Maresca, A.; Scozzafava, A.; Supuran, C. T. *Bioorg. Med. Chem.* **2012**, *20*, 2266; b Davis, R. A.; Vullo, D.; Maresca, A.; Supuran, C. T.; Poulsen, S. A. *Bioorg. Med. Chem.* **2013**, *21*, 1539.
14. a Vullo, D.; Luca, V. D.; Scozzafava, A.; Carginale, V.; Rossi, M.; Supuran, C. T.; Capasso, C. *Bioorg. Med. Chem.* **2013**, *21*, 1534; b Winum, J. Y.; Maresca, A.; Carta, F.; Scozzafava, A.; Supuran, C. T. *Chem. Commun. (Camb.)* **2012**, *48*, 8177.
15. a Di Fiore, A.; Maresca, A.; Alterio, V.; Supuran, C. T.; De Simone, G. *Chem. Commun. (Camb.)* **2011**, *47*, 11636; b Scozzafava, A.; Carta, F.; Supuran, C. T. *Expert Opin. Ther. Pat.* **2013**, *23*, 203; c Carta, F.; Scozzafava, A.; Supuran, C. T. *Expert Opin. Ther. Pat.* **2012**, *22*, 747.
16. a Carta, F.; Aggarwal, M.; Maresca, A.; Scozzafava, A.; McKenna, R.; Supuran, C. T. *Chem. Commun. (Camb.)* **2012**, *48*, 1868; b Maresca, A.; Carta, F.; Vullo, D.; Supuran, C. T. *J. Enzyme Inhib. Med. Chem.* **2013**, *28*, 407; c Monti, S. M.; Maresca, A.; Carta, F.; De Simone, G.; Mühlschlegel, F. A.; Scozzafava, A.; Supuran, C. T. *Bioorg. Med. Chem. Lett.* **2012**, *22*, 859; d Carta, F.; Aggarwal, M.; Maresca, A.; Scozzafava, A.; McKenna, R.; Masini, E.; Supuran, C. T. *J. Med. Chem.* **2012**, *55*, 1721.
17. Carta, F.; Akdemir, A.; Scozzafava, A.; Masini, E.; Supuran, C. T. *J. Med. Chem* **2013**, *56*, 4691.
18. Di Fiore, A.; Maresca, A.; Supuran, C. T.; De Simone, G. *Chem. Commun. (Camb.)* **2012**, *48*, 8838.
19. a Parkkila, S.; Vullo, D.; Maresca, A.; Carta, F.; Scozzafava, A.; Supuran, C. T. *Chem. Commun. (Camb.)* **2012**, *48*, 3551; b De Simone, G.; Supuran, C. T. *J. Inorg. Biochem.* **2012**, *111*, 117.
20. a Masini, E.; Carta, F.; Scozzafava, A.; Supuran, C. T. *Expert Opin. Ther. Pat.* **2013**, *23*, 705; b Supuran, C. T. *Expert Opin. Ther. Pat.* **2013**, *23*, 677.
21. Carta, F.; Supuran, C. T. *Expert Opin. Ther. Pat.* **2013**, *23*, 681.
22. a Arechederra, R. L.; Waheed, A.; Sly, W. S.; Supuran, C. T.; Minteer, S. D. *Bioorg. Med. Chem.* **2013**, *21*, 1544; b Supuran, C. T. *Expert Opin. Ther. Pat.* **2003**, *13*, 1545; c Supuran, C. T. *Expert Opin. Emergency Drugs* **2012**, *17*, 11; d Scozzafava, A.; Supuran, C. T.; Carta, F. *Expert Opin. Ther. Pat.* **2013**, *23*, 725.
23. a Neri, D.; Supuran, C. T. *Nat. Rev. Drug Disc.* **2011**, *10*, 767; b Thiry, A.; Dogné, J. M.; Masereel, B.; Supuran, C. T. *Trends Pharmacol. Sci.* **2006**, *27*, 566–573; c Alterio, V.; Hilvo, M.; Di Fiore, A.; Supuran, C. T.; Pan, P.; Parkkila, S.; Scaloni, A.; Pastorek, J.; Pastorekova, S.; Pedone, C.; Scozzafava, A.; Monti, S. M.; De Simone, G. *Proc. Natl. Acad. Sci. USA* **2009**, *106*, 16233; d Monti, S. M.; Supuran, C. T.; De Simone, G. *Expert Opin. Ther. Pat.* **2013**, *23*, 737.

24. Capasso, C.; Supuran, C. T. *Expert Opin. Ther. Pat.* **2013**, *23*, 693.
25. Shepard, K. L.; Graham, S. L.; Hudcosky, R. J.; Michelson, S. R.; Scholz, T. H.; Schwam, H.; Smith, A. M.; Sondey, J. M.; Strohmaier, K. M.; Smith, R. L.; Sugrue, M. F. *J. Med. Chem.* **1991**, *34*, 3098.
26. Supuran, C. T.; Scozzafava, A.; Casini, A. Development of Sulfonamide Carbonic Anhydrase Inhibitors (CAIs). In *Carbonic Anhydrase – Its Inhibitors and Activators*; Supuran, C. T., Scozzafava, A., Conway, J., Eds.; CRC Press: Boca Raton (FL), 2004; pp 67–147.
27. Meldal, M.; Tornøe, C. W. *Chem. Rev.* **2008**, *108*, 2952.
28. Shao, C.; Wang, X.; Xu, J.; Zhao, J.; Zhang, Q.; Hu, Y. *J. Org. Chem.* **2010**, *75*, 7002.
29. a Menabuoni, L.; Scozzafava, A.; Mincione, F.; Briganti, F.; Mincione, G.; Supuran, C. T. *J. Enzyme Inhib. Med. Chem.* **1999**, *14*, 457; b Scozzafava, A.; Menabuoni, L.; Mincione, F.; Briganti, F.; Mincione, G.; Supuran, C. T. *J. Med. Chem.* **1999**, *42*, 2641.
30. a Pacchiano, F.; Aggarwal, M.; Avvaru, B. S.; Robbins, A. H.; Scozzafava, A.; McKenna, R.; Supuran, C. T. *Chem. Commun. (Camb.)* **2010**, *46*, 8371; b D'Ambrosio, K.; Smaine, F. Z.; Carta, F.; De Simone, G.; Winum, J. Y.; Supuran, C. T. *J. Med. Chem.* **2012**, *55*, 6776; c Carta, F.; Garaj, V.; Maresca, A.; Wagner, J.; Avvaru, B. S.; Robbins, A. H.; Scozzafava, A.; McKenna, R.; Supuran, C. T. *Bioorg. Med. Chem.* **2011**, *19*, 3105; d Biswas, S.; Aggarwal, M.; Guzel, O.; Scozzafava, A.; McKenna, R.; Supuran, C. T. *Bioorg. Med. Chem.* **2011**, *19*, 3732.
31. Khalifah, R. G. J. *Biol. Chem.* **1971**, *246*, 2561.
32. (a) De Simone, G.; Alterio, V.; Supuran, C. T. *Expert Opin. Drug Discov* **2013**, *8*, 793; (b) Aggarwal, M.; Boone, C. D.; Kondeti, B.; McKenna, R. *J. Enzyme Inhib. Med. Chem.* **2013**, *28*, 267; (c) Fisher, S. Z.; Aggarwal, M.; Kovalevsky, A. Y.; Silverman, D. N.; McKenna, R. *J. Am. Chem. Soc.* **2012**, *134*, 14726.
33. (a) Sippel, K. H.; Robbins, A. H.; Domsic, J.; Genis, C.; Agbandje-McKenna, M.; McKenna, R. *Acta Crystallogr., Sect. F* **2009**, *65*, 992; b Aggarwal, M.; Boone, C. D.; Kondeti, B.; Tu, C.; Silverman, D. N.; McKenna, R. *Acta Crystallogr., Sect. D* **2013**, *69*, 860.
34. Gatti McArthur, S.; Goetschi, E.; Palmer, W. S.; Wichmann, J.; Woltering, T. J.; WO Patent 099972 A1, 2006.
35. Faucher, N.; Ambroise, Y.; Cintrat, J.-C.; Doris, E.; Pillon, F.; Rousseau, B. *J. Org. Chem.* **2002**, *67*, 932.
36. Barral, K.; Moorhouse, A. D.; Moses, J. E. *Org. Lett.* **2007**, *9*, 1809.
37. Boechat, N.; Ferreira, V. F.; Ferreira, S. B.; de Lourdes, G.; Ferreira, M.; De C da Silva, F.; Bastos, M. M.; dos S Costa, M.; Lourenco, M. C. S.; Pinto, A. C.; Krettli, A. U.; Aguiar, A. C.; Teixeira, B. M.; da Silva, N. V.; Martins, P. R. C.; Bezerra, F. A. F. M.; Camilo, A. L. S.; da Silva, G. P.; Costa, C. C. P *J. Med. Chem.* **2011**, *54*, 5988.
38. Lee, S.; Hua, Y.; Park, H.; Flood, A. H. *Org. Lett.* **2010**, *12*, 2100.
39. Kitamura, M.; Yano, M.; Tashiro, N.; Miyagawa, S.; Sando, M.; Okauchi, T. *Eur. J. Org. Chem.* **2011**, 458.
40. Hu, H.; Zhang, A.; Ding, L.; Lei, X.; Zhang, L. *Molecules* **2008**, *13*, 556.
41. Knepper, K.; Vanderheiden, S.; Brasa, S. *Eur. J. Org. Chem.* **2006**, *1886*.
42. Garzya, V.; Watson, S. T. WO Patent 115486 A1, 2009.
43. Rieber, N.; Böhm, H. J. *Heterocycl. Chem.* **1981**, *18*, 1.
44. Leslie, A. G. W. *Newslett. Protein Crystallogr.* **1992**, *28*, 15.
45. Evans, P. R. *Newslett. Protein Crystallogr.* **1997**, *33*, 22–24.
46. Murshudov, G. N.; Vagin, A. A. *Acta Crystallogr., Sect. D* **1997**, *53*, 240.
47. Vagin, A. A.; Murshudov, G. N. *J. Appl. Crystallogr.* **1998**, *31*, 98–112.
48. Emsley, P.; Cowtan, K. *Acta Crystallogr., Sect. D* **2004**, *60*, 2126.

3.2. X-ray crystallography-promoted drug design of carbonic anhydrase inhibitors

It has been known previously that saccharin has properties of carbonic anhydrase inhibitor (Köhler et al., 2007). Saccharin proved to be much more selective to some of the mammalian CA isoforms than most of the medically used sulfonamide inhibitors. In later studies binding modes of saccharin-sulfonamide derivatives were tested. It was discovered that by addition of a sulfonamide group to the saccharine moiety it is energetically more favorable for the compound to bind to the Zn^{2+} ion via its sulfonamide moiety (Alterio et al., 2015b). Further saccharin-sulfonamide derivates were synthesized and three of them tested by crystallographic studies on hCA II. Atomic resolution crystal structures were achieved with clearly visible electron density for the ligand. The results were totally unpredicted – isothiazole cycle in the saccharin moiety was hydrolyzed and compounds were bound to the enzyme in a previously undescribed way. Unforeseen hCA II-ligand 3D structures inspired synthesis of novel CA inhibitors – open ring saccharine derivatives.

Further analysis of the compound suggested that all three of the tested compounds bind to the enzyme in a similar manner. Compounds formed hydrogen bonds with residues Asn67, Gln92 and interacted with residues Phe131, Val135, Leu198, Pro202 and Leu204.

This study is an example of how X-ray crystallography can promote drug design. All of the further saccharin-sulfonamide derivates were synthesized, inspired by these X-ray structures.

Crystal structures are deposited on PDB with access codes: 5AMD, 5AMG and 5AML.

ChemComm

COMMUNICATION

View Article Online
View Journal | View Issue

Cite this: Chem. Commun., 2015, 51, 7108

Received 4th March 2015,
Accepted 20th March 2015

DOI: 10.1039/c5cc01854d

www.rsc.org/chemcomm

X-ray crystallography-promoted drug design of carbonic anhydrase inhibitors†

Jekaterina Ivanova,‡[a] Janis Leitans,‡[b] Muhammet Tanc,‡[cd] Andris Kazaks,[b] Raivis Zalubovskis,*[a] Claudiu T. Supuran*[cd] and Kaspars Tars[be]

1-*N*-Alkylated-6-sulfamoyl saccharin derivatives were prepared and assayed as carbonic anhydrase inhibitors (CAIs). During X-ray crystallographic experiments an unexpected hydrolysis of the isothiazole ring was evidenced which allowed us to prepare highly potent enzyme inhibitors with selectivity for some isoforms with medical applications.

The artificial sweetener saccharin (**SAC**) (Fig. 1) was previously reported as an efficient inhibitor of several isoforms of the human metalloenzymes carbonic anhydrases (CAs, EC 4.2.1.1) with promising selectivity towards the cancer associated isoforms hCA IX and hCA XII,[1] both of which have been recently validated as drug targets for anti-cancer therapy or imaging of hypoxic tumors.[2] It should be noted that CAs are efficiently but indiscriminately inhibited by most sulfonamides such as acetazolamide (**AAZ**) but hCA IX selective inhibitors, such as SLC-0111, are also known, this compound being in Phase I clinical trials for the treatment of patients with advanced solid, metastatic tumors overexpressing CA IX/XII.[3]

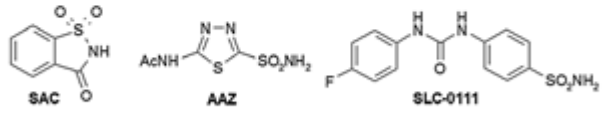

Fig. 1 Chemical structures of known CAIs.

Despite promising achievements in selective inhibition of hCA IX and hCA XII there is still a demand for more effective and selective inhibitors of various CA isoforms, such as CA II, VA, VB, IX, *etc.*[2]

The mechanism of CA inhibition by **SAC** is rather different compared to that of primary sulfonamides, the most investigated class of CA inhibitors (CAIs) including those used clinically (**AAZ**). Even though in both cases the binding to the Zn ion within the active site of CA takes place by the deprotonated nitrogen of the sulfonamide group, the **SAC** binding significantly differs from that of primary sulfonamides. The presence of the acyl group incorporated into the isothiazole ring and the absence of a proton on the nitrogen exhibit a rather different binding pattern of **SAC** to the enzyme compared to primary sulfonamides.[2]

Such different interactions directly reflect the inhibition profile of **SAC**, which efficiently inhibits only the cytosolic isoform hCA VII and the tumor associated one hCA IX compared to primary sulfonamides such as **AAZ**, which is a highly efficient inhibitor of 14 out of the 15 hCAs known to date.[1,2] For this purpose **SAC** was extensively used as a lead molecule for obtaining novel CAIs ultimately.[4–6] For example, we synthesized 6-sulfamoylsaccharin **1** and its 1-substituted derivatives **2** (Scheme 1)[4] where the opportunity to investigate competition of binding of the primary and secondary sulfonamide to the enzyme (in the case of **1**) emerged.[7]

Indeed, recently we reported the high resolution X-ray crystal structure of the adduct of hCA II with **1**, which proved that only the primary sulfonamide participates in the interaction with the metal ion.[7] Thus a series of *N*-substituted saccharin derivatives **2a–2i** appeared to be of interest for being prepared by reacting **1** with alkyl/aralkyl bromides in DMF (Scheme 1, see the ESI† for details). We investigated the inhibitory properties of these compounds and their binding to the enzyme by means of kinetic experiments and X-ray crystallography.

In order to visualize the binding mode of saccharin sulfonamide derivatives **2** to hCA II, we solved the high resolution

[a] *Latvian Institute of Organic Synthesis, Aizkraukles 21, LV-1006 Riga, Latvia. E-mail: raivis@osi.lv; Fax: +371-67550338; Tel: +371-67014826*
[b] *Biomedical Research and Study Center, Ratsupites 1, LV-1067 Riga, Latvia*
[c] *Università degli Studi di Firenze, NEUROFARBA Department, Section of Pharmaceutical Chemistry, Via Ugo Schiff 6, 50019 Sesto Fiorentino, Florence, Italy. E-mail: claudiu.supuran@unifi.it; Fax: +39-055-4573385; Tel: +39-055-4573005*
[d] *Università degli Studi di Firenze, Polo Scientifico, Laboratorio di Chimica Bioinorganica, Rm. 188, Via dellaLastruccia 3, 50019 Sesto Fiorentino, Florence, Italy*
[e] *University of Latvia, Faculty of Biology, Department of Molecular Biology, Kronvalda bulv. 4, LV-1010 Riga, Latvia*

† Electronic supplementary information (ESI) available: A detailed description of the synthesis and characterization of compounds **1–4**, as well as the enzyme inhibitory assays. See DOI: 10.1039/c5cc01854d

‡ These authors contributed equally to this study.

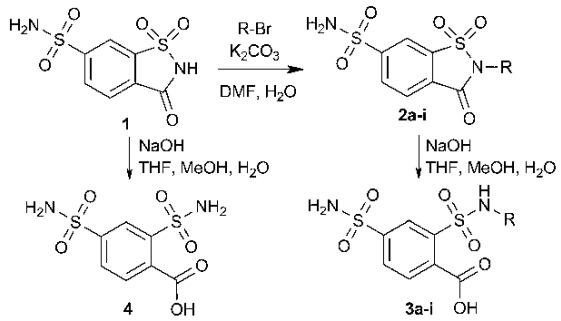

Scheme 1 Synthesis of 1-*N*-substituted 6-sulfamoylsaccharins **2** and their hydrolysis products **3** and **4**.

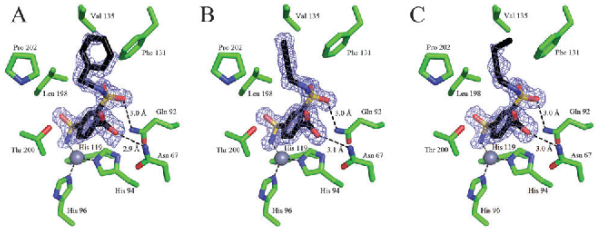

Fig. 2 Comparison of binding modes of compounds **2i**, **2e** and **2d** within the hCA II active site. Compound **2i**/**3i** is shown in panel A, **2e**/**3e** is shown in panel B and **2d**/**3d** is shown in panel C. The zinc ion is the gray sphere and its coordinating residues (His94, 96 and 119) are shown in green. Residues 67, 92, 131, 135, 198, 200 and 202 participating in hydrogen bonding, hydrophobic and van der Waals contacts with inhibitors are also indicated. For the sake of clarity, $F_o - F_c$ OMIT electron density is shown only for ligands and contoured at 3σ. The figure was prepared by using Pymol (DeLano ThePyMOL Molecular Graphics System San Carlos, CA, USA, DeLano Scientific).

crystal structures of hCA II in complex with compounds **2i**, **2e** and **2d** reported here. The electron density was interpretable for all inhibitors (Fig. 2) and surprisingly revealed that the isothiazole ring was open in all of them. Even though the isothiazole ring opening occurs most probably by alkaline hydrolysis due to the relatively high pH (of 9.0) in the crystallization buffer it unexpectedly and clearly revealed a new possibility of designing CAIs. One should mention that initially we explored the possibility that the enzyme itself hydrolyzed the amide bond from derivatives **2**, but this did not occur (data not provided). Indeed, although the CAs have esterase and thioesterase activity,[8,9] they do not possess peptidase activity. Notably all three compounds were bound in a very similar fashion, coordinating to the zinc ion with their primary sulfonamide, whereas oxygens of carboxyl and sulfone groups made H-bonds with the Asn67 and Gln92 side chains. The R moieties occupied a hydrophobic pocket, formed by the side chains of residues Phe131, Val135, Leu198, Leu204 and Pro202 (Fig. 2).

The observed binding mode of all three compounds is substantially different from that previously reported for unsubstituted saccharin (PDB code 2Q38),[1] or derivative **1**,[7] when the two inhibitors were not hydrolysed. Thus, the binding observed for compounds **3**, obtained by hydrolysis of derivatives **2** reported here, is indeed very different compared to other saccharin based CAIs reported so far[4–7] (Fig. 3). Inspired by these crystallographic results

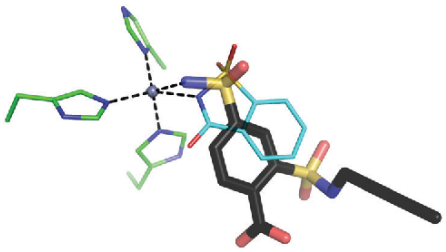

Fig. 3 Different binding modes of **SAC** (grey carbons, thin sticks) and *N*-substituted 'open' saccharin **3e** (black carbons, thick sticks). Both compounds are coordinating active site Zn ions (grey sphere), but **3e** is bound to the metal ion by its primary sulfonamide whereas **SAC** by the secondary, acylated sulfonamide.

we thereafter prepared all the corresponding open forms of the 6-sulfamoyl saccharins **1** and **2**, obtaining the bissulfamoyl carboxylic acids **3** and **4** (Scheme 1), under alkaline hydrolytic conditions. Even though we expected that these carboxylic acids **3** and **4** might undergo a ring closure under neutral or acidic conditions, we did not observe the isothiazole ring closure even by storing compounds **3** and **4** for a prolonged period at ambient temperatures.

All compounds obtained were subjected to CA inhibition studies summarized in Table 1.

Four hCA isoforms were included in this study: two cytosolic ones hCA I and hCA II, and two tumor-associated transmembrane isoforms hCA IX and hCA XII, all of which are drug targets for various applications of their inhibitors.[2,3] Data of Table 1 show the following interesting findings.

Against the slow cytosolic isoform hCA I the activity range of compounds **1**–**4** was between 2.6 and 451 nM. Almost all compounds showed a better inhibition compared to the non-selective compound **AAZ**. Only compound **4** showed low inhibition against this isoform, whereas derivatives **1**, **2a** and **3g** had a comparable inhibition profile to that of **AAZ**. However the most interesting observation was that in pairs of closed/open ring derivatives **1**/**4** and **2**/**3**, the net reduction of the inhibitory activity for the open forms **4** and **3** (1.7 to up to 43 times) compared to the corresponding closed form ones **1** and **2** occurred. The most significant reduction of activity, by two orders of magnitude, was observed for compounds **3e** and **3g**, which were 27 and 43 times, respectively, less inhibitory compared to the corresponding benzisothiazoles **2e** and **2g**. The only exceptions to this rule were the pairs **2a**/**3a** and **2h**/**3h**, for which the closed form was less inhibitory than the open ones (Table 1).

For the rapid isoform hCA II a similar inhibition pattern was observed as for hCA I discussed above. All compounds except **4** showed an excellent, better inhibitory activity than **AAZ**, with K_is in the range of 0.2–8.4 nM. A similar reduction of the inhibitory activity of the open *versus* the closed forms was also observed with most compounds, but already many of the closed ones were low nanomolar hCA II inhibitors and thus, this reduction seems to be less relevant for this isoform than for hCA I. The nature of the R group also influenced the inhibition pattern of these derivatives significantly. Thus, an increase of the aliphatic chain from C2 to C4 led to an increase of the hCA II

Table 1 CA inhibition data of isoforms hCA I, II, IX and XII with saccharin derivatives **1–2** and the corresponding open forms **3–4** reported in this communication, by a CO_2 hydrase stopped-flow assay[12]

		K_i (nM)			
Compound	R	hCA I	hCA II	hCA IX	hCA XII
1	—	251	8.4	337	52.9
2a	Et	257	1.0	452	7.2
2b	*n*Pr	49	0.6	278	5.9
2c	*n*Bu	4.8	0.6	51.2	5.7
2d	nC_5H_{11}	4.3	3.5	380	5.2
2e	$CH_2CHCHMe$	4.6	0.4	271	9.5
2f	Bn	2.6	0.4	51.8	5.8
2g	$CH_2C_6H_4(4\text{-}NO_2)$	4.9	0.2	52.9	7.9
2h	$CH_2C_6H_4(4\text{-}Br)$	57.8	0.8	321	14.3
2i	CH_2CH_2Ph	9.1	0.4	378	6.7
3a	Et	66.2	1.7	92.8	77.7
3b	*n*Pr	81.4	0.2	89.5	63.6
3c	*n*Bu	41.4	1.1	130	58.7
3d	nC_5H_{11}	29.9	6.0	333	68.3
3e	$CH_2CHCHMe$	125	0.7	78.1	67.8
3f	Bn	64.0	1.5	67.4	50.5
3g	$CH_2C_6H_4(4\text{-}NO_2)$	213	2.2	73.6	195
3h	$CH_2C_6H_4(4\text{-}Br)$	38.7	0.3	70.5	27.0
3i	CH_2CH_2Ph	59.0	2.8	71.6	48.6
4	—	451	31.7	42.1	63.3
AAZ[a]	—	250	12	25	5.7

[a] Acetazolamide (**AAZ**) was used as a standard inhibitor for all CAs investigated in this communication.

inhibitory properties but a further increase to C5 was detrimental for the inhibitory activity (compare **2d** to **2a–c**, Table 1). However, unsaturated or aralkyl chains (as in **2e–2i**) led again to highly effective, subnanomolar CAIs, for all the substitution patterns of compounds **2e–2i**, *i.e.*, benzyl, 4-substituted benzyl moieties or phenethyl.

An opposite inhibition pattern was observed in the case of the tumor-associated transmembrane isoform hCA IX with compounds **2–4** reported here. Even though none of the compounds was superior to **AAZ**, the inhibitory activity increased going from the closed to the open forms for the compound pair **1**/**4** and most of the pairs **2**/**3**. As shown in Table 1, the highest increase, more than 4 times, was observed for compounds **3a**, **3h**, **3i** and **4** with K_is in the range of 42.1–92.9 nM, which are effective inhibitors of this tumor-associated isoform.

For the second transmembrane isoform, hCA XII, the inhibition pattern was similar to those of the cytosolic isoforms hCA I and hCA II discussed above. All closed forms except **1** and **2h** exhibited comparable inhibitory activity with **AAZ**, whereas the open forms **3a–3f**, **3h–4** were around one order of magnitude less inhibitory compared to **AAZ**. Overall, many low nanomolar hCA XII inhibitors were detected such as for instance **2a–2i**, which had inhibition constants ranging between 5.2 and 14.3 nM, in the same range as the classical sulfonamide inhibitor **AAZ**.

The most interesting finding of this communication is however the fact that our drug design has been guided by the crystallographic work, which evidenced a hydrolytic process taking place during the crystallization experiments. Unexpectedly, the hydrolysis afforded compounds possessing a free COOH moiety in addition to the primary and secondary sulfamoyl moieties. This type of sulfonamide was in fact not synthesized so far using other synthetic procedures, and as shown above, they possess notable inhibitory properties, with a profile quite different from that of the structurally related, closed form (or the primary sulfonamide **AAZ**). In fact all sulfonamides **3a–3i** were highly effective, CA II-selective inhibitors, and this type of profile is very rare or even absent among the many sulfonamide CAIs reported so far.[10] Furthermore, the crystallographic experiments (Fig. 2 and 3) also showed that the R moiety present in these compounds may adopt a variety of orientations within the CA II active site, which may explain their very high affinity for this isoform and the relatively lower ones for other isoforms such as hCA I, IX and XII (Table 1). As hCA II is the main target for designing anti-glaucoma CAIs (in clinical use for decades but with many side effects due to inhibition of other isoforms),[11] these findings may lead to the design of water-soluble (due to the presence of the COOH moiety, which may form sodium salts), highly effective and selective hCA II inhibitors belonging to a novel chemical space.

In conclusion we report here new CAIs obtained by a 'side reaction' which occurred during an X-ray crystallographic study of sulfonamide–CA adducts. We have demonstrated the high potential of the newly obtained compounds (open/closed forms of 1-*N*-substituted saccharins or the unsymmetrically substituted bissulfamoyl benzoic acids), possessing an improved selectivity towards some CA isoforms with medical applications. Considering the chemical simplicity and good water solubility of the newly obtained CAIs, their scaffold may find applications in the development of new types of CAIs, probably by modulating the nature of the moieties substituting in position 1 the saccharin derivatives (the R moiety). Indeed, in this communication we explored few substitution patterns which are aliphatic, alkenyl and aralkyl groups. By extending the type and nature of these moieties, which as shown in the crystal structures, interact with amino acid residues critical for the binding of inhibitors, compounds with improved potency and selectivity may presumably be obtained.

This research was in part financed by two FP7 EU projects (InnovaBalt and Dynano).

Notes and references

1 K. Köhler, A. Hillebrecht, J. Schulze Wischeler, A. Innocenti, A. Heine, C. T. Supuran and G. Klebe, *Angew. Chem., Int. Ed. Engl.*, 2007, **46**, 7697.
2 (*a*) V. Alterio, A. Di Fiore, K. D'Ambrosio, C. T. Supuran and G. De Simone, *Chem. Rev.*, 2012, **112**, 4421; (*b*) C. T. Supuran, *Nat. Rev. Drug Discovery*, 2008, **7**, 168.
3 (*a*) See more at ClinicalTrails.gov: Safety Study of SLC-0111 in Subjects With Advanced Solid Tumours-ClinicalTrials_gov.mht; (*b*) F. Pacchiano, F. Carta, P. C. McDonald, Y. Lou, D. Vullo, A. Scozzafava, S. Dedhar and C. T. Supuran, *J. Med. Chem.*, 2011, **54**, 1896; (*c*) C. T. Supuran, *J. Enzyme Inhib. Med. Chem.*, 2012, **27**, 759; (*d*) C. T. Supuran, *J. Enzyme Inhib. Med. Chem.*, 2013, **28**, 229.
4 E. M. Ivanova, E. Y. Simin, I. V. Vozny, P. Trapencieris and R. Žalubovskis, *Chem. Heterocycl. Compd.*, 2012, **47**, 1561.
5 M. D'Ascenzio, S. Carradori, C. De Monte, D. Secci, M. Ceruso and C. T. Supuran, *Bioorg. Med. Chem.*, 2014, **22**, 1821.
6 (*a*) J. Moeker, T. S. Peat, L. F. Bornaghi, D. Vullo, C. T. Supuran and S. A. Poulsen, *J. Med. Chem.*, 2014, **57**, 3522; (*b*) B. P. Mahon, A. M. Hendon, J. M. Driscoll, G. M. Rankin, S. A. Poulsen, C. T. Supuran and R. McKenna, *Bioorg. Med. Chem.*, 2015, **23**, 849.
7 V. Alterio, M. Tanc, J. Ivanova, R. Zalubovskis, I. Vozny, S. M. Monti, A. Di Fiore, G. De Simone and C. T. Supuran, *Org. Biomol. Chem.*, 2015, **13**, 4064.

8 (*a*) Y. Pocker and J. T. Stone, *J. Am. Chem. Soc.*, 1965, **87**, 5497; (*b*) A. Innocenti, A. Scozzafava, S. Parkkila, L. Puccetti, G. De Simone and C. T. Supuran, *Bioorg. Med. Chem. Lett.*, 2008, **18**, 226; (*c*) H. Çavdar, D. Ekinci, O. Talaz, N. Saraçoğlu, M. Şentürk and C. T. Supuran, *J. Enzyme Inhib. Med. Chem.*, 2012, **27**, 148; (*d*) E. A. Kazancıoğlu, M. Güney, M. Şentürk and C. T. Supuran, *J. Enzyme Inhib. Med. Chem.*, 2012, **27**, 880.
9 M. Tanc, F. Carta, A. Scozzafava and C. T. Supuran, *ACS Med. Chem. Lett.*, 2015, **6**, 292.
10 (*a*) F. Pacchiano, M. Aggarwal, B. S. Avvaru, A. H. Robbins, A. Scozzafava, R. McKenna and C. T. Supuran, *Chem. Commun.*, 2010, **46**, 8371; (*b*) A. Di Fiore, A. Maresca, V. Alterio, C. T. Supuran and G. De Simone, *Chem. Commun.*, 2011, **47**, 11636; (*c*) S. Parkkila, D. Vullo, A. Maresca, F. Carta, A. Scozzafava and C. T. Supuran, *Chem. Commun.*, 2012, **48**, 3551; (*d*) J. Y. Winum, A. Maresca, F. Carta, A. Scozzafava and C. T. Supuran, *Chem. Commun.*, 2012, **48**, 8177; (*e*) B. Métayer, A. Mingot, D. Vullo, C. T. Supuran and S. Thibaudeau, *Chem. Commun.*, 2013, **49**, 6015.
11 (*a*) A. Maresca, F. Carta, D. Vullo and C. T. Supuran, *J. Enzyme Inhib. Med. Chem.*, 2013, **28**, 407; (*b*) S. M. Monti, A. Maresca, F. Carta, G. De Simone, F. A. Mühlschlegel, A. Scozzafava and C. T. Supuran, *Bioorg. Med. Chem. Lett.*, 2012, **22**, 859; (*c*) F. Carta, M. Aggarwal, A. Maresca, A. Scozzafava, R. McKenna, E. Masini and C. T. Supuran, *J. Med. Chem.*, 2012, **55**, 1721.
12 R. J. Khalifah, *J. Biol. Chem.*, 1971, **246**, 2561.

3.3. Efficient Expression and Crystallization System of Cancer-Associated Carbonic Anhydrase Isoform IX

There is a limited number of semi-selective CA IX inhibitors described in literature. One of the reasons is the poor structural background of hCA IX-ligand interactions. Up until 2015 there was only one hCA IX crystal structure available in the PDB (Alterio et al., 2009). Limited number of available structural data for hCA IX can be explained by inefficient expression and purification systems. Also, the described crystallization conditions in literature could not be easily reproduced.

We decided to develop hCA IX protein production and purification protocol suitable for X-ray crystallography studies. hCA IX gene was genetically fused with MBP and N-terminal 6x His tag. Further, hCA IX gene was incorporated in *Pichia pastoris* by transfer plasmid vector. After selection of the most promising clones (in terms of protein production) the expression temperature was optimized to 24° C. Initially hCA IX-MBP was purified with a metal ion affinity column, followed by digestion with TEV protease. Additional purification using gel filtration column and ion exchange column was necessary to obtain 90+ % pure protein. Obtained hCA IX was crystallized using JCSG+ screen from Molecular Dimensions with following optimization. Three high resolution structures of hCA IX complexes with thiophene-2-sulfonamide derivatives were solved at resolutions ranging from 1.82 Å to 2.05 Å. Compounds were bound within the active site of hCA IX without additional polar contacts apart from the standard sulfonamide-Zn^{2+}/Thr199 interactions, meaning that the compound binding mode was stabilized solely by hydrophobic and van der Waals contacts.

The observed electron density for all three compounds was good and interpretable throughout the whole ligand. Within the active site of hCA IX these compounds were bound in a similar way and their tail moieties were oriented towards the region which differs most between α-CA isoforms ("hot spot") (Alterio et al., 2009). The compounds made interactions with residues Gln92, Val131, Leu135, Leu198, Thr200 and Pro202 (CA II numbering).

Notable differences were observed comparing binding modes between hCA II and hCA IX. By analyzing the binding modes, we concluded that ligand tail moieties could not bind in the same way in hCA II as in hCA IX due to potential clash with Phe131 (CA II numbering).

These results open wider possibilities for structure-based hCA IX targeted drug design in order to develop more selective compounds suitable for medical use.

Crystal structures are deposited in PDB with access codes: 5FL4, 5FL5, 5FL6.

Journal of Medicinal Chemistry

Article

pubs.acs.org/jmc

Efficient Expression and Crystallization System of Cancer-Associated Carbonic Anhydrase Isoform IX

Janis Leitans,[†,#] Andris Kazaks,[†,#] Agnese Balode,[‡] Jekaterina Ivanova,[‡] Raivis Zalubovskis,[‡] Claudiu T. Supuran,[§,∥] and Kaspars Tars[*,†,⊥]

[†]Biomedical Research and Study Center, Ratsupites 1, LV-1067, Riga, Latvia

[‡]Latvian Institute of Organic Synthesis, Aizkraukles 21, LV-1006, Riga, Latvia

[§]NEUROFARBA Department, Section of Pharmaceutical Chemistry, Università degli Studi di Firenze, Via Ugo Schiff 6, 50019 Sesto Fiorentino, Florence, Italy

[∥]Laboratorio di Chimica Bioinorganica, Polo Scientifico, Università degli Studi di Firenze, Rm. 188, Via dellaLastruccia 3, 50019 Sesto Fiorentino, Florence, Italy

[⊥]Faculty of Biology, Department of Molecular Biology, University of Latvia, Jelgavas 1, LV-1004, Riga, Latvia

Supporting Information

ABSTRACT: Human carbonic anhydrase IX (CA IX) is overexpressed in a number of solid tumors and is considered to be a marker for cellular hypoxia that it is not produced in most normal tissues. CA IX contributes to the acidification of the extracellular matrix, which, in turn, favors tumor growth and metastasis. Therefore, CA IX is considered to be a promising anti-cancer drug target. However, the ability to specifically target CA IX is challenging due to the fact that the human genome encodes 15 different carbonic anhydrase isoforms that have a high degree of homology. Furthermore, structure-based drug design of CA IX inhibitors so far has been largely unsuccessful due to technical difficulties regarding the expression and crystallization of the enzyme. Currently, only one baculovirus-produced CA IX structure in complex with a nonspecific CA inhibitor, acetazolamide, is available in Protein Data Bank. We have developed an efficient system for the production of the catalytic domain of CA IX in methylotrophic yeast *Pichia pastoris*. The produced protein can be easily crystallized in the presence of inhibitors, as we have demonstrated for several 2-thiophene-sulfonamide compounds. We have also observed significant differences in the binding mode of chemically identical compounds to CA IX and CA II, which can be further exploited in the design of CA IX-specific inhibitors

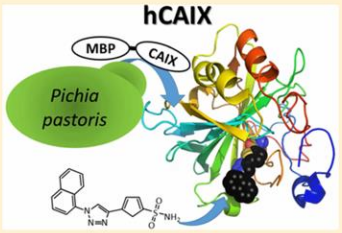

INTRODUCTION

Carbonic anhydrases (CAs, EC 4.2.1.1) catalyze the rapid interconversion of carbon dioxide and water into bicarbonate, a reaction that, in mammals, is important in a variety of biological processes, including maintaining the acid−base balance and transporting carbon dioxide.[1] Carbonic anhydrase IX (CA IX) is a membrane protein, containing a proteoglycan-like domain, thought to be important in cell adhesion, a catalytic domain, a transmembrane domain, responsible for anchoring of enzyme in the membrane, and an intracellular tail. CA IX is expressed in a limited number of normal tissues; however, it is overexpressed in many solid tumors and is considered to be one of the best markers for cellular hypoxia.[2] CA IX contributes to the acidification of the extracellular matrix, which, in turn, favors tumor growth and metastasis.[3] Consequently, CA IX is considered to be an attractive anti-cancer drug target.[4] However, the human genome encodes 15 carbonic anhydrases (CAs) that have a considerable degree of homology; therefore, the ability to specifically target a particular CA is challenging.[2]

Currently, there are a limited number of CA IX-selective inhibitors reported in the literature, with their predominant core structures being coumarins, sulfocoumarins, and ureido-benzenesulfonamides (Figure 1).[5−12] It is worth mentioning that the ureido-benzenesulfonamide compound SLC-0111 has entered Phase I clinical trials for the treatment of advanced solid, metastatic tumors overexpressing CA IX/XII.[13]

Information about the three-dimensional structure of an enzyme in complex with an inhibitor is invaluable in drug

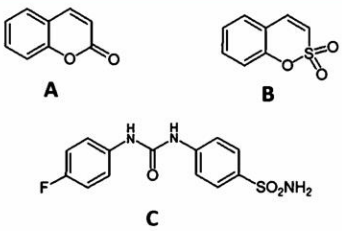

Figure 1. Some of the known inhibitors of CA: (A) coumarin, (B) sulfocoumarin, and (C) ureidobenzenesulfonamide SLC-0111 (in Phase I clinical trials).

Received: September 2, 2015

DOI: 10.1021/acs.jmedchem.5b01343
J. Med. Chem. XXXX, XXX, XXX−XXX

design. In fact, the first unequivocal example of structure-based drug design is dorzolamide, an efficient CA inhibitor, used in the treatment of glaucoma. However, structure-based drug design of CA IX inhibitors has been hampered by difficulties in the expression and crystallization of the enzyme; to date, only one CA IX structure in complex with the non-isoform-specific inhibitor acetazolamide (Figure 1) is available in Protein Data Bank (PDB code 3IAI)[14]

Here, we report an efficient system for the production of the catalytic domain of CA IX in yeast and the crystal structure of the obtained enzyme in complex with 2-thiophene-sulfonamide derivatives, which act as highly efficient inhibitors.

RESULTS AND DISCUSSION

Cloning, Expression, and Purification of CA IX Catalytic Domain. cDNA of the catalytic domain (CAT) of CA IX, comprising residues 137−391, was fused in-frame with a 6×His-tagged maltose binding protein (MBP) gene and inserted into a yeast (*Pichia pastoris*) expression transfer plasmid vector, as shown in Figure 2. Two point mutations

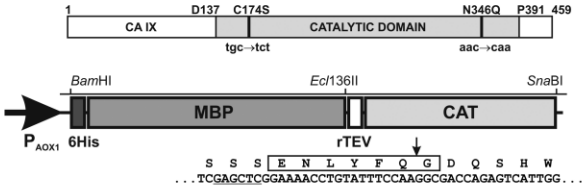

Figure 2. Mutagenesis and cloning of the CA IX CAT gene. Upper panel: schematic presentation of CA IX protein. CAT domain, flanked by residues D137 and P391, and mutated residues C174 and N346 are shown. Lower panel: design of the MBP−CAT fusion gene, with a more detailed picture of the gene fusion region depicted below. The rTEV amino acid recognition sequence introduced between genes is shown in the box, and its cleavage site is indicated by an arrow. The *Ecl*136II restriction site used for to create the gene fusion is underlined.

were introduced within the CAT-encoding sequence, namely, C174 → S and N346 → Q, to avoid possible aggregation and glycosylation of the recombinant protein, respectively.

Ten individual clones obtained under G418 selection at a concentration of 2.5 mg/mL were cultivated under standard expression conditions, and one of them was selected as the most promising clone in terms of its production level (data not shown). To optimize the synthesis, we analyzed the influence of temperature on production of the target protein. It was observed that cultivation temperatures below 30 °C and down to 24 °C led to increased production of soluble MBP−CAT protein (Figure 3A). Further decreasing the temperature down to 20 °C reduced the amount of soluble protein (data not shown). Thus, cultivation of cells for preparative purposes was performed at 24 °C.

The initial capture of the target protein from cell supernatant was performed by Ni-affinity chromatography (Figure 3B, lane 1). Eluted MBP−CAT protein was then efficiently cleaved by rTEV protease in the presence of imidazole (Figure 3B, lane 2). The next purification step was size-exclusion chromatography. Although this approach did not result in the separation of MBP and CAT proteins, a significant portion of the impurities was removed (Figure 3B, lanes 3−5, and Figure 3D). Our attempts to separate MBP and CAT by either a Ni- or MBP-affinity column failed, as both proteins co-migrated in the same eluate fractions (data not shown). Further experiments revealed that separation can be accomplished on a MonoQ anion-exchange column in the presence of 100 mM NaCl. Under these conditions, MBP passed through the column, whereas CAT remained attached and eluted with ∼200 mM NaCl (Figure 3B, lane 6, Figure 3C, and Figure 3E). The final product yielded ∼0.15 mg per 1 g of wet cells, with a purity suitable for crystallization.

Protein X-ray Crystallography. To determine the binding mechanisms of compounds **1**−**3** (Figure 4) within the active site of CA IX (compounds **1**−**3** were previously reported in a recent publication[15] as very active at CA II, with K_i values in the nanomolar range (Table 1), and the binding mechanism of compound **2** was tested on cytosolic CA II), we solved X-ray crystal structures of CA IX in complex with these compounds at resolutions of 2.05 Å (compound **1**), 1.82 Å (compound **2**), and 1.95 Å (compound **3**). Currently, there is only one CA IX structure available in Protein Data Bank (PDB code 3IAI[14]), and all three of our described structures have noticeably better resolution. The statistics for the refinement and data collection are shown in Table 2. The obtained electron density revealed that CA IX's structure is essentially identical to that previously published, although the expression system used was changed from a baculovirus-insect cell expression system to *P. pastoris*. As in all CA−sulfonamide complexes, the deprotonated sulfonamide moiety of this compound is coordinated to the Zn^{2+} ion and a hydrogen bond is formed between the sulfonamide's NH moiety and the OH of Thr200. Apart from these interactions, compounds **1**−**3** are not involved in other polar contacts with CA IX, as was also the case in the CA II−**2** complex.[15] Thus, ligand binding within the CA IX active site is achieved mostly by van der Waals and hydrophobic interactions, involving amino acid residues Gln92, Val130, Leu134, Leu199, Thr201, and Pro203 (Figure 5). In the CA IX−**1** complex, the ligand's electron density was good, except for the methyl group of the methoxyphenyl moiety (Figure 5A). For all three compounds, a glycerol molecule is clearly visible in the electron density map that is bound within the active site of CA IX in a nearly identical position as that observed in the previous CA IX structure.[14] Presumably, the glycerol molecule was bound during the cryoprotection of the crystals and, therefore, it should not affect the binding and positioning of the sulfonamide inhibitor. The electron density of the ligand in the CA IX−**2** complex was good for most of the molecule, except for the naphthyl moiety, where it was weaker, but it was still interpretable (Figure 5B). In the CA IX−**3** complex, the electron density was good for all of the ligand (Figure 5C). All three compounds bind very similarly within the CA IX active site, and it is notable that their binding mechanism is very similar to that of acetazolamide in complex with CA IX[14] despite the fact that they are missing the hydrogen bond between the thiadiazole moiety and Thr201 (Figure 6). Interestingly, the binding mode of compound **2** between the CA IX and II isoforms is noticeably different (Figure 7). In the CA IX−**2** complex, the ligand is positioned toward the hydrophobic half of the CA IX active site and interacts with residues Gln92, Val130, Leu134, Leu199, Thr201, and Pro203, whereas in CA II−**2**, the naphthyl moiety of the ligand fits in a hydrophobic pocket and interacts with residues Phe131, Val135, Leu204, and Pro202. It should be noted that the ligand in CA II−**2** cannot be bound in the same way as that in CA IX−**2** due to a clash with residue Phe131 (Figure 5). Importantly, in complexes CA IX−**1**, CA IX−**2**, and

DOI: 10.1021/acs.jmedchem.5b01343
J. Med. Chem. XXXX, XXX, XXX−XXX

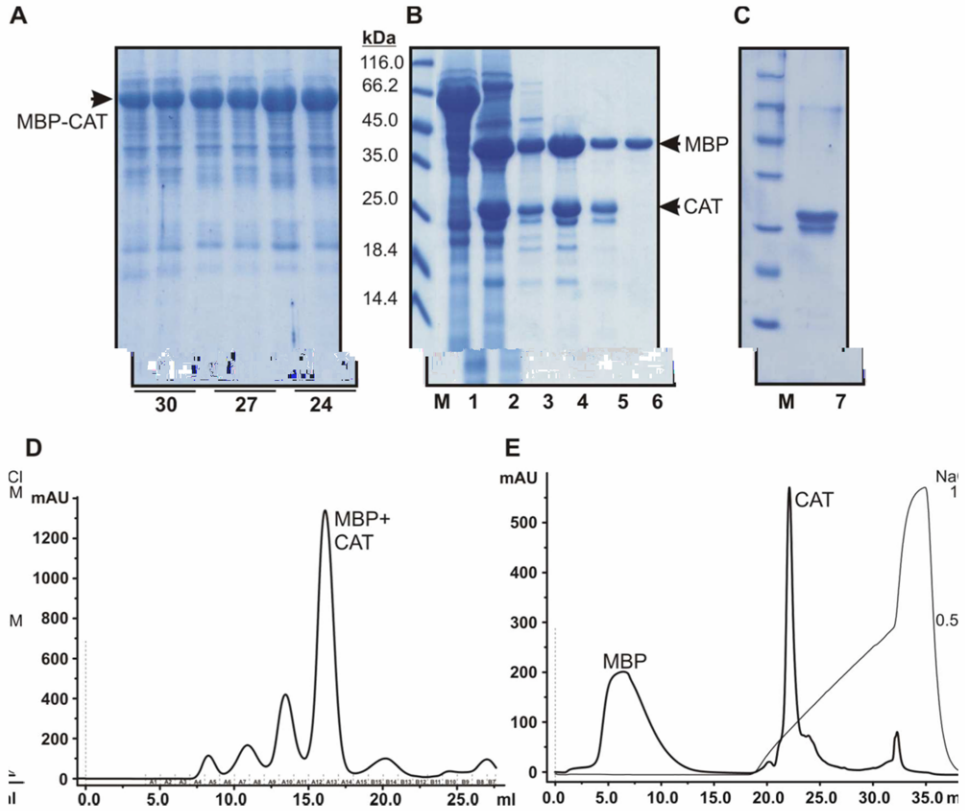

Figure 3. Purification of the CAT of CA IX. (A) Optimization of the cultivation temperature. Two individual colonies from the selected producer clone were cultivated in parallel at the indicated temperature. (B, C) Individual purification steps. Lanes 1 and 2, protein eluate from Ni-affinity column before and after rTEV cleavage, respectively; lanes 3−5, peak fractions from Superdex column; lanes 6 and 7, nonbound and bound material on the MonoQ column, respectively; M, protein molecular mass marker. (D, E) Superdex and MonoQ chromatography profiles, respectively.

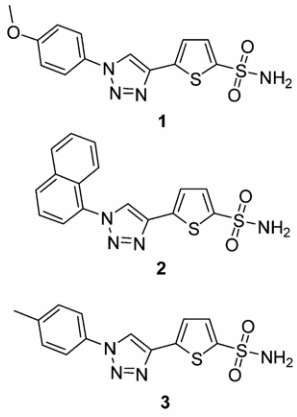

Figure 4. CA inhibitors used in this study.

CA IX−**3**, the tails of all ligands are positioned at the CA IX active site region, which differs the most among CA isoforms, i.e., the region comprising residues 127−137, described previously as a hot spot for structure-based drug design.[14]

■ CONCLUSIONS

Our results can be used for the rational design of novel CAIs and provide broad possibilities to improve isoform-selective inhibitors for tumor-associated CA IX, a validated anti-tumor/anti-metastatic drug target. The *P. pastoris* based expression and purification system will probably provide an efficient pipeline for determining crystal structures with a variety of CA IX inhibitors.

Regarding the solved structures, of particular importance is the different binding mode of compound **2** to CA II and CA IX and the fact that all bound compounds are positioned in a CA IX active site region that differs both in its structure and sequence among the other CA isoforms.

Table 1. CA Inhibition Data[15]

		K_i (nM)		
entry	compound	CA I	CA II	CA IX
1	**1**	746	6.3	6.4
2	**2**	750	2.4	101
3	**3**	526	3.5	43.6
4	AAZ[a]	250	12	25

[a]AAZ, acetazolamide, a nonselective CA inhibitor. AAZ inhibition data are presented for comparison.

■ EXPERIMENTAL SECTION

Cloning and Expression. A synthetic gene encoding full-length human CA IX (GenBank DQ892208) was purchased from IDT (Germany). All further manipulations were performed only with the catalytic domain of CA IX (CAT; residues 137−391). Point mutations were introduced by PCR mutagenesis and verified by sequencing. The

DOI: 10.1021/acs.jmedchem.5b01343
J. Med. Chem. XXXX, XXX, XXX−XXX

Table 2. Data Processing, Refinement, and Validation Statistics for the CA IX−1, CA IX−2, and CA II−3 Complexes

structure	CA IX−1	CA IX−2	CA IX−3
space group	H3	H3	H3
cell dimensions			
a (Å)	152.4	152.3	153.2
c (Å)	170.6	172.1	170.8
resolution (Å)	38−2.05	62−1.82	48−1.95
highest resolution shell (Å)	2.05−2.16	1.82−1.92	1.95−2.06
no. of reflections	92 662	133 470	108 977
no. of reflections in test set	4640	6944	5344
completeness (%)	100.0 (100.0[a])	100.0 (100.0[a])	100.0 (100.0[a])
R_{merge}	0.13 (0.68[a])	0.06 (0.49[a])	0.15 (0.58[a])
$\langle I/\sigma I \rangle$	8.2 (2.0[a])	9.9 (2.0[a])	5.2 (2.0[a])
average multiplicity	3.8 (3.8[a])	2.9 (2.5[a])	2.9 (2.9[a])
R-factor	0.16 (0.16[a])	0.19 (0.32[a])	0.17 (0.26[a])
R_{free}	0.20 (0.20[a])	0.22 (0.33[a])	0.20 (0.28[a])
average B factor (Å^2)	26.4	31.8	23.7
average B factor for inhibitor (Å^2)	34.1	36.8	34.2
⟨B⟩ from Wilson plot (Å^2)	19.4	20.9	23.6
no. of protein atoms	7706	7768	7710
no. of inhibitor atoms	88	96	84
no. of solvent molecules	902	1050	1146
rms deviations from ideal values			
bond lengths (Å)	0.01	0.01	0.01
bond angles (deg)	1.75	1.72	1.70
outliers in Ramachandran plot (%)	0.10	0.20	0.00

[a]Values in parentheses are for the high-resolution bin.

modified CAT gene was fused in-frame with a 6×His-tagged maltose binding protein (MBP) gene by PCR. The MBP−CAT expression cassette was then cloned under the control of the *AOX1* promoter in the pPIC3.5K vector (Invitrogen) between the *Bam*HI and *Sna*BI restriction sites, resulting in the pPICMalECAIX vector.

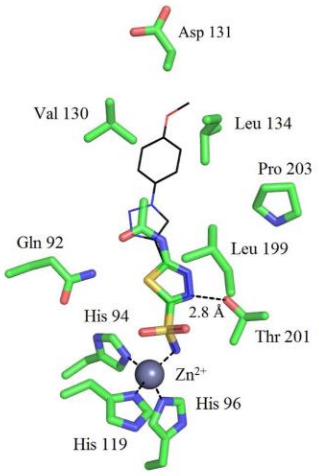

Figure 6. Comparison of binding modes of compound **1** (thin lines with black carbons) and CA inhibitor acetazolamide (PDB code 3IAI; thick lines with green carbons) within the active site of CA IX. The zinc ion is shown as a gray sphere, and its coordinating histidines (His94, 96, and 119) are shown in green. Residues 92, 130, 134, 199, 201, 203, and 131, participating in hydrogen bonding, hydrophobic, and van der Waals contacts with the inhibitors, are indicated. The figure was prepared using PyMOL.

After sequencing, the pPICMalECAIX plasmid was linearized with *Pme*I in the *AOX1* promoter region and used for transformation of the *P. pastoris* GS115 *his4* strain by electroporation. Mut$^+$His$^+$ transformants were isolated on agar plates containing minimal medium (1.34% yeast nitrogen base, 2% glucose, 4 × 10^{-5}% biotin, 2% agar). For selection of clones with multiple integration units, transformants were replica-plated onto agar plates containing yeast extract peptone dextrose (YEPD) medium containing increased concentrations of the G418 antibiotic (1.8−2.5 mg/mL). Selected clones were cultivated at 30 °C on a shaker in 0.5 L Erlenmeyer flasks containing 100 mL of buffered complex glycerol medium (BMGY) for 20−24 h until OD_{590} reached 6−8. Then, and each subsequent day, 100% methanol was added to a final concentration of 1%, and cells were harvested 3 days

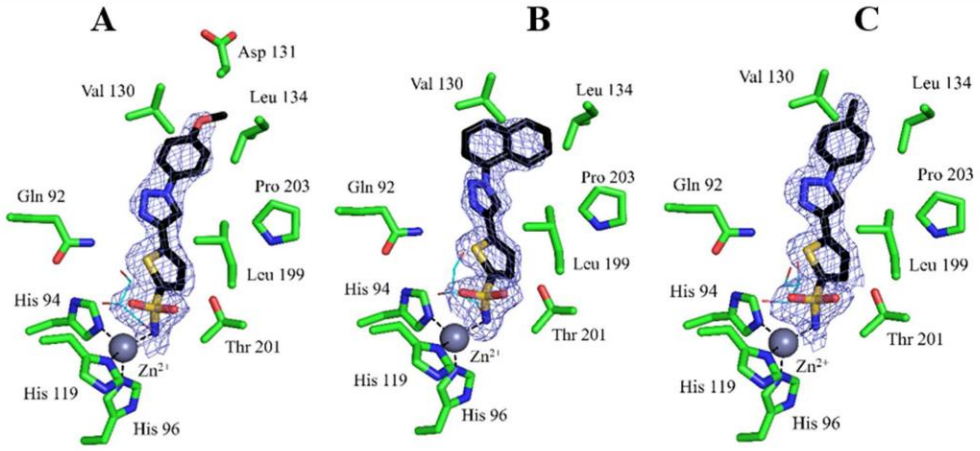

Figure 5. Comparison of the binding modes of compounds (A) **1**, (B) **2**, and (C) **3** within the active site of CA IX. The zinc ion is shown as a gray sphere, and its coordinating histidines (His94, 96, and 119) are shown in green. Residues 92, 130, 134, 199, 201, 203, and 131, participating in hydrophobic and van der Waals contacts with the inhibitors, are indicated. A glycerol molecule bound to the enzyme is shown as a thin stick model with sky blue carbon atoms. For clarity, $F_o - F_c$ omit electron density is shown only for the ligand and is contoured at 3σ. The figure was prepared using PyMOL (San Carlos, CA, USA).

DOI: 10.1021/acs.jmedchem.5b01343
J. Med. Chem. XXXX, XXX, XXX−XXX

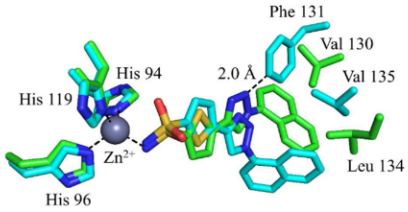

Figure 7. Comparison of binding mode of compound **2** within the active site of CA IX (carbons are green) and CA II (PDB code 4BF1; carbons are light blue). The zinc ion is shown as a gray sphere, and its coordinating histidines (His94, 96, and 119) are shown in green for CA IX and light blue for CA II. Residues 130, 131, 134, 135, participating in hydrophobic and van der Waals contacts with the inhibitor, are indicated. It should be noted that compound **2** in CA IX is placed in a region that differs significantly between these two isoforms. The figure was prepared using PyMOL.

after induction. The level of soluble CAT production was determined by disrupting 1 g of yeast cells by 425−600 μ glass beads (Sigma) in 10 mL of lysis buffer LB (20 mM Tris-HCl, pH 8.0, 300 mM NaCl) by vortexing 10 times for 0.5 min. The supernatant was incubated with 50 μL of Ni-agarose beads (Qiagen) for 1 h on a rotatory shaker. Ni-beads were then washed with LB containing 20 mM imidazole, and agarose-bound material was analyzed in PAGE.

Protein Purification. The cells were resuspended in LB, at a proportion of 5 mL of buffer per 1 g of wet cells, and disrupted with a French press (three cycles, 20 000 psi). The soluble fraction was separated by centrifugation for 30 min at 15 500*g* and manually (with syringe) passed through a 1 mL HisTrap FF crude column (GE Healthcare). The column was washed with 5 mL of LB and subsequently with 2 mL of LB containing 20 mM imidazole. Column-bound proteins were eluted with 2 mL of LB containing 300 mM imidazole. Eluted protein was cleaved with rTEV protease in the presence of 1 mM DTT overnight at 4 °C. After cleavage, the protein mixture in 1 mL portions was loaded on a Superdex 200 10/300 GL column connected to an ÄKTA chromatography system (Amersham Biosciences). The column was pre-equilibrated with 20 mM Tris-HCl, pH 8.0, 200 mM NaCl and run at 0.5 mL/min. Peak fractions were pooled, diluted twice with 20 mM TrisHCl, pH 8.0, and applied to a MonoQ TM column pre-equilibrated with 20 mM Tris-HCl, pH 8.0, 100 mM NaCl. Column-bound proteins were eluted by a linear salt gradient (0.1−0.5 M NaCl in 15 mL) at 1 mL/min. All purification steps were monitored by SDS-PAGE, with a 4% stacking and 15% separating gel, according to standard protocols. To visualize protein bands, the gels were stained with Coomassie brilliant blue G-250.

Crystallization and Data Collection. Protein was concentrated to 10 mg/mL in 20 mM Tris-HCl, pH 8.0, using a 10 kDa cutoff Amicon concentrator. Crystallization was performed using the sitting drop technique in 96-well MRC plates (MolecularDimensions). To determine the structure of the CA IX−**1** complex, 1 μL of protein was mixed with 1 μL of bottom solution, which contained 0.2 M lithium sulfate, 1.26 M ammonium sulfate, and 0.1 M Tris-HCl, pH 8.5. To determine the structures of the CA IX−**2** and CA IX−**3** complexes, the bottom solution contained 1.0 M diammonium hydrogen phosphate, 0.1 M sodium acetate, pH 4.5. To fully grown crystals was added 2 μL of mother liquor buffer containing 5 mM of the respective compound, and the crystals were left to soak for 5 days. The crystals were flash frozen in liquid nitrogen in mother liquor supplemented with 30% glycerol.

Data were collected at beamline I911-3, MAX-lab synchrotron, Lund, Sweden.

Structure Determination. Images were processed by MOSFLM[16] and scaled by SCALA.[17] The CA IX−**1**, CA IX−**2**, and CA IX−**3** structures were solved by molecular replacement in MOLREP[18] using the CA IX structure with PDB ID 3IAI as a search model. The parameter files for inhibitors were generated by LIBCHECK.[19] The electron density fits for the ligands were carried out in COOT,[20] followed by refinement in REFMAC.[21] Water molecules were picked automatically in COOT and inspected manually. Data scaling, refinement, and validation statistics are listed in Table 2.

■ ASSOCIATED CONTENT

Supporting Information

The Supporting Information is available free of charge on the ACS Publications website at DOI: 10.1021/acs.jmedchem.5b01343.

SMILES notation and K_i values for CA I−IV (CSV)

Accession Codes

The atomic coordinates and experimental structure factors for the crystals have been deposited in the Protein Data Bank under accession codes 5FL5 for CA IX−**1**, 5FL4 for CA IX−**2**, and 5FL6 for CA IX−**3**

■ AUTHOR INFORMATION

Corresponding Author

*Phone: +37127076237. Fax: +37167442407. E-mail: kaspars@biomed.lu.lv.

Author Contributions

[#]J.L. and A.K. contributed equally to this work.

Notes

The authors declare no competing financial interest.

■ ACKNOWLEDGMENTS

We thank staff at MAX lab synchrotron for their support during data collection. This work was supported by a Biostruct-X grant BIOSTRUCTX_7869.

■ REFERENCES

(1) Supuran, C. T. Carbonic anhydrases–an overview. *Curr. Pharm. Des.* **2008**, *14*, 603−14.

(2) Alterio, V.; Di Fiore, A.; D'Ambrosio, K.; Supuran, C. T.; De Simone, G. Multiple binding modes of inhibitors to carbonic anhydrases: how to design specific drugs targeting 15 different isoforms? *Chem. Rev.* **2012**, *112*, 4421−68.

(3) Chiche, J.; Ilc, K.; Brahimi-Horn, M. C.; Pouyssegur, J. Membrane-bound carbonic anhydrases are key pH regulators controlling tumor growth and cell migration. *Adv. Enzyme Regul.* **2010**, *50*, 20−33.

(4) Monti, S. M.; Supuran, C. T.; De Simone, G. Carbonic anhydrase IX as a target for designing novel anticancer drugs. *Curr. Med. Chem.* **2012**, *19*, 821−30.

(5) Maresca, A.; Temperini, C.; Vu, H.; Pham, N. B.; Poulsen, S. A.; Scozzafava, A.; Quinn, R. J.; Supuran, C. T. Non-zinc mediated inhibition of carbonic anhydrases: coumarins are a new class of suicide inhibitors. *J. Am. Chem. Soc.* **2009**, *131*, 3057−62.

(6) Maresca, A.; Temperini, C.; Pochet, L.; Masereel, B.; Scozzafava, A.; Supuran, C. T. Deciphering the mechanism of carbonic anhydrase inhibition with coumarins and thiocoumarins. *J. Med. Chem.* **2010**, *53*, 335−44.

(7) Tars, K.; Vullo, D.; Kazaks, A.; Leitans, J.; Lends, A.; Grandane, A.; Zalubovskis, R.; Scozzafava, A.; Supuran, C. T. Sulfocoumarins (1,2-benzoxathiine-2,2-dioxides): a class of potent and isoform-selective inhibitors of tumor-associated carbonic anhydrases. *J. Med. Chem.* **2013**, *56*, 293−300.

(8) Grandane, A.; Tanc, M.; Zalubovskis, R.; Supuran, C. T. Synthesis of 6-tetrazolyl-substituted sulfocoumarins acting as highly potent and selective inhibitors of the tumor-associated carbonic anhydrase isoforms IX and XII. *Bioorg. Med. Chem.* **2014**, *22*, 1522−8.

(9) Grandane, A.; Tanc, M.; Zalubovskis, R.; Supuran, C. T. 6-Triazolyl-substituted sulfocoumarins are potent, selective inhibitors of

DOI: 10.1021/acs.jmedchem.5b01343
J. Med. Chem. XXXX, XXX, XXX−XXX

the tumor-associated carbonic anhydrases IX and XII. *Bioorg. Med. Chem. Lett.* **2014**, *24*, 1256−60.
(10) Grandane, A.; Tanc, M.; Zalubovskis, R.; Supuran, C. T. Synthesis of 6-aryl-substituted sulfocoumarins and investigation of their carbonic anhydrase inhibitory action. *Bioorg. Med. Chem.* **2015**, *23*, 1430−6.
(11) Grandane, A.; Tanc, M.; Di Cesare Mannelli, L.; Carta, F.; Ghelardini, C.; Zalubovskis, R.; Supuran, C. T. 6-Substituted Sulfocoumarins Are Selective Carbonic Anhdydrase IX and XII Inhibitors with Significant Cytotoxicity against Colorectal Cancer Cells. *J. Med. Chem.* **2015**, *58*, 3975−83.
(12) Pacchiano, F.; Carta, F.; McDonald, P. C.; Lou, Y.; Vullo, D.; Scozzafava, A.; Dedhar, S.; Supuran, C. T. Ureido-substituted benzenesulfonamides potently inhibit carbonic anhydrase IX and show antimetastatic activity in a model of breast cancer metastasis. *J. Med. Chem.* **2011**, *54*, 1896−902.
(13) Supuran, C. T.; Winum, J. Y. Designing carbonic anhydrase inhibitors for the treatment of breast cancer. *Expert Opin. Drug Discovery* **2015**, *10*, 591−7.
(14) Alterio, V.; Hilvo, M.; Di Fiore, A.; Supuran, C. T.; Pan, P.; Parkkila, S.; Scaloni, A.; Pastorek, J.; Pastorekova, S.; Pedone, C.; Scozzafava, A.; Monti, S. M.; De Simone, G. Crystal structure of the catalytic domain of the tumor-associated human carbonic anhydrase IX. *Proc. Natl. Acad. Sci. U. S. A.* **2009**, *106*, 16233−8.
(15) Leitans, J.; Sprudza, A.; Tanc, M.; Vozny, I.; Zalubovskis, R.; Tars, K.; Supuran, C. T. 5-Substituted-(1,2,3-triazol-4-yl)thiophene-2-sulfonamides strongly inhibit human carbonic anhydrases I, II, IX and XII: solution and X-ray crystallographic studies. *Bioorg. Med. Chem.* **2013**, *21*, 5130−8.
(16) Leslie, A. G. W. Recent changes to the MOSFLM package for processing film and image plate data. *Joint CCP4+ ESF-EAMCB Newsletter on Protein Crystallography* **1992**, *26*.
(17) Evans, P. R. Scala. *Joint CCP4+ ESF-EAMCB Newsletter on Protein Crystallography* **1997**, *33*, 22−24.
(18) Vagin, A.; Teplyakov, A. MOLREP: an Automated Program for Molecular Replacement. *J. Appl. Crystallogr.* **1997**, *30*, 1022−1025.
(19) Vagin, A. A.; Murshudov, G. N.; Strokopytov, B. V. BLANC: the program suite for protein crystallography. *J. Appl. Crystallogr.* **1998**, *31*, 98−112.
(20) Emsley, P.; Cowtan, K. Coot: model-building tools for molecular graphics. *Acta Crystallogr., Sect. D: Biol. Crystallogr.* **2004**, *60*, 2126−32.
(21) Murshudov, G. N.; Vagin, A. A.; Dodson, E. J. Refinement of macromolecular structures by the maximum-likelihood method. *Acta Crystallogr., Sect. D: Biol. Crystallogr.* **1997**, *53*, 240−55.

DOI: 10.1021/acs.jmedchem.5b01343
J. Med. Chem. XXXX, XXX, XXX−XXX

3.4. Novel fluorinated carbonic anhydrase IX inhibitors reduce hypoxia-induced acidification and clonogenic survival of cancer cells

Using the previously described hCA IX expression, purification and crystallization system, multiple fluorinated benzene-sulfonamides were co-crystallized with the enzyme. Judging from the available kinetic data the tested sulfonamides had a remarkable increase in selectivity to hCA IX. The resolutions of obtained crystal structures were in a range from 1.75 Å to 2.47 Å with clearly interpretable electron densities for the ligands. The sulfonamide part and trifluorobenzene cycle part of the ligand fitted in the conservative region of hCA IX almost invariably compared to literature (Dudutiene et al., 2015). For all the tested compounds the cycloalkane moiety was oriented to the hydrophobic part of the enzyme active site while relatively more polar tail moiety with terminal hydroxyl group was oriented towards polar part of the hCA active site.

The impressive selectivity against hCA II can be explained by occupation of the most diverse region of hCA by the bulky 12-carbon ring and potential collision with residue Phe131 in the case of compound VR16-09.

Comparing to an un-liganded hCA IX structure, the determined crystal structures clearly displayed shifts in positions of conserved residues Gln67 and Gln92. This was the first time when it was observed that the ligand could interfere with the active site pocket conformation of hCA IX.

Crystal structures are deposited on PDB with access codes: 6G98, 6G9U, 6FE0, 6FE1, 6FE2.

www.oncotarget.com Oncotarget, 2018, Vol. 9, (No. 42), pp: 26800-26816

Research Paper

Novel fluorinated carbonic anhydrase IX inhibitors reduce hypoxia-induced acidification and clonogenic survival of cancer cells

Justina Kazokaitė[1,2], Raymon Niemans[2], Virginija Dudutienė[1], Holger M. Becker[3], Jānis Leitāns[4], Asta Zubrienė[1], Lina Baranauskienė[1], Gabor Gondi[5,6], Reinhard Zeidler[5,6], Jurgita Matulienė[1], Kaspars Tārs[1], Ala Yaromina[2], Philippe Lambin[2], Ludwig J. Dubois[2,*] and Daumantas Matulis[1,*]

[1]Department of Biothermodynamics and Drug Design, Institute of Biotechnology, Vilnius University, Vilnius, Lithuania

[2]Department of Radiotherapy (The M-Lab Group), GROW – School for Oncology and Developmental Biology, Maastricht Comprehensive Cancer Centre, Maastricht University Medical Centre, Maastricht, The Netherlands

[3]Department of Physiological Chemistry, University of Veterinary Medicine Hannover, Hannover, Germany

[4]Latvian Biomedical Research and Study Center, Riga, Latvia

[5]Department of Gene Vectors, Helmholtz Center for Environmental Health, Munich, Germany

[6]Department of Otorhinolaryngology, Klinikum der Universität München, Munich, Germany

[*]These authors are contributed equally to this work

Correspondence to: *Daumantas Matulis,* ***email:*** *matulis@ibt.lt, daumantas.matulis@bti.vu.lt*

Keywords: *cancer; hypoxia; drug design; sulfonamide; carbonic anhydrase IX*

Received: *April 12, 2018* ***Accepted:*** *May 14, 2018* ***Published:*** *June 01, 2018*

ABSTRACT

Human carbonic anhydrase (CA) IX has emerged as a promising anticancer target and a diagnostic biomarker for solid hypoxic tumors. Novel fluorinated CA IX inhibitors exhibited up to 50 pM affinity towards the recombinant human CA IX, selectivity over other CAs, and direct binding to Zn(II) in the active site of CA IX inducing novel conformational changes as determined by X-ray crystallography. Mass spectrometric gas-analysis confirmed the CA IX-based mechanism of the inhibitors in a CRISPR/Cas9-mediated CA IX knockout in HeLa cells. Hypoxia-induced extracellular acidification was significantly reduced in HeLa, H460, MDA-MB-231, and A549 cells exposed to the compounds, with the IC_{50} values up to 1.29 nM. A decreased clonogenic survival was observed when hypoxic H460 3D spheroids were incubated with our lead compound. These novel compounds are therefore promising agents for CA IX-specific therapy.

INTRODUCTION

Tumor hypoxia promotes invasiveness and is associated with resistance to chemotherapeutics and radiation and thus poor prognosis [1–5]. Human carbonic anhydrase IX (CA IX) shows limited expression in normal tissues [6] and is significantly up-regulated by hypoxia-inducible factor 1α (HIF-1α) [7] or other alternative microenvironmental factors [8–12] in a variety of tumors. CA IX is crucial for cancer cell survival because bicarbonate and protons, produced upon CA IX-catalyzed reversible hydration of CO_2, are necessary to maintain the cellular pH balance: bicarbonate is transported into the cell to neutralize intracellular acid, while protons increase extracellular acidification [13–16]. CA IX also stimulates cell spreading and epithelial-mesenchymal transition [17, 18]. Therefore, CA IX has been proposed to be a promising tumor hypoxia biomarker for diagnostic and targeted drug delivery applications [19].

Sulfonamides are classical CA inhibitors, where the deprotonated sulfonamide group is required for displacement of the catalytic Zn^{2+}-bound water

molecule to bind directly with Zn^{2+} in the active site to inhibit CA [20, 21]. Therefore, the binding affinity can be enhanced using inhibitors with the lowered pK_a of the sulfonamide group [21, 22]. Introduction of fluorine atoms that lower the pK_a due to their electron-withdrawing capabilities is one of the choices due to unique features, such as high electronegativity, small size, low atomic weight, and contribution to increased lipophilicity. Fluorine is found in ~20% of current pharmaceuticals and this trend is increasing [23]. Krishnamurthy and colleagues investigated fluorinated benzensulfonamides and concluded that fluorine is the best choice for electron-withdrawing substituents [21]. We expanded this strategy and created new routes for functionalization of pentafluorobenzensulfonamides [24, 25] including *para*-, *ortho*-, and *meta*- substituted fluorinated benzensulfonamides. The bulky hydrophobic groups at *ortho* or *meta* positions are necessary for the favorable hydrophobic contacts with the amino acids of CA IX binding pocket [26]. Here we present novel the *ortho*-substituted fluorinated benzenesulfonamides VR16-09 and VR16-10 (Table 1, Scheme 1) in combination with the previously chemically and biophysically characterized *meta* and *ortho*-substituted fluorinated inhibitors VD11-4-2 and VD12-09 [26]. We hypothesized that these benzenesulfonamides will exhibit high affinity and strong selectivity towards recombinant CA IX and will possess significant functional effects in cancer cell lines on reducing hypoxia-induced acidosis as well as hypoxia-dependent clonogenic survival, providing efficacious opportunity to target CA IX-expressing cells.

RESULTS AND DISCUSSION

Binding and inhibition of recombinant CA isoforms

The affinities of VR16-09 and VR16-10 to 12 catalytically active recombinant CA isoforms were determined by the fluorescent thermal-shift assay (FTSA) and compared with previously published [26] inhibitors VD11-4-2 and VD12-09 (Table 1). The K_i values against CA IX and CA XII were also measured by the stopped-flow inhibition assay (SFA) of the CO_2 hydration CA enzymatic activity (Table 1). FTSA revealed that VR16-09 bound CA IX significantly (K_d = 0.16 nM) stronger than other CA isoforms (K_ds > 200 μM) (Table 1, Figure 1A–1C). VR16-09 with the bulky aminocyclododecyl group exhibited greater selectivity towards CA IX as compared with VR16-10, VD12-09, and VD11-4-2 bearing aminocyclooctyl groups. SFA did not allow the determination of K_i < ~2 nM against CA IX, because the concentration of CA IX was 10 nM, thus limiting the determination of IC_{50} at 5 nM. Therefore, the K_ds determined by the FTSA should be used rather than SFA. Nevertheless, SFA confirmed that VR16-09 and VR16-10 efficiently inhibited the CA IX activity (Figure 1D–1F). These compounds are advantageous compared to SLC-0111 that has entered the clinical trials ($K_{i(CA\ IX)}$ = 45 nM, $K_{i(CA\ XII)}$ = 4.5 nM and only 20-fold selectivity over CA II, thus would possibly exhibit larger adverse effects [27, 28]). In contrast, selectivity of VR16-09 for CA IX over CA I and CA II is more than one million-fold.

Crystal structures of inhibitors bound to recombinant CA IX

The structures of the CA IX catalytic domain in complex with VR16-09 (PDB ID: 6G98), VR16-10 (PDB ID: 6G9U), VD12-09 (PDB ID: 6FE0) and VD11-4-2 (PDB ID: 6FE1) were determined by X-ray crystallography at resolutions ranging from 1.75 Å to 2.47 Å (Figure 2, Supplementary Table 1). The sulfonamide moiety and trifluorobenzene cycle of all observed ligands fit in the conserved region of the CA IX active site, the cycloalkane tail moieties were guided towards the hydrophobic part of the active site and moieties with terminal hydroxyl group were located in the hydrophilic part of the active site. The sulfonamide amino group formed a coordination bond with Zn(II), as observed in many other CA-sulfonamide complexes. All ligands were positioned very similarly within the active site of CA IX, except with some differences occurring in the case of VD11-4-2 (Figure 2). VD11-4-2 also formed two additional hydrogen bonds with Asn62 and Gln92, which might explain its stronger affinity for CA IX as compared to other analyzed compounds. All four crystal structures showed that some conformational changes have occurred in the CA IX active site pocket as compared to other known CA IX structures [29, 30]. In order to fully understand conformational changes occurring in those cases, we also determined apo (ligand free) CA IX structure at 1.87 Å resolution (PDB ID: 6FE2). In case of VR16-09, the cyclododecyl moiety altered rotamer of Gln92, which in turn changed the conformation of Gln67 (Figure 2).

CA IX-dependent functional activities of inhibitors in cancer cells

Compounds were evaluated for their biological functional activities in a panel of human cancer cell lines. CA IX expression was increased in hypoxic (0.2% O_2) A549 (lung), AsPC-1 (pancreatic), MDA-MB-231 (breast), H460 (lung), and HeLa (cervical) cancer cells, whereas CA XII expression was similar under normoxia and hypoxia (Supplementary Figures 1, 2). We evaluated the potency of the compounds to inhibit the CA catalytic activity in hypoxic MDA-MB-231 cells by determining the rate of the CO_2/HCO_3^- hydration/dehydration reaction via ^{18}O depletion from $^{13}C^{18}O_2$, measured by mass-spectrometric (MS) gas analysis. Addition of cell

Table 1: The dissociation constants (K_ds) of VR16-09, VR16-10, VD11-4-2, and VD12-09 for 12 recombinant catalytic domains of human active CA isoforms as determined by FTSA at pH 7.0 (37° C)

	K_d (K_i), nM			
	VR16-09 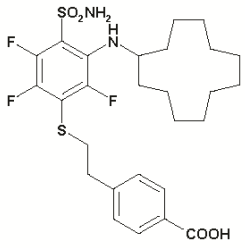	VR16-10 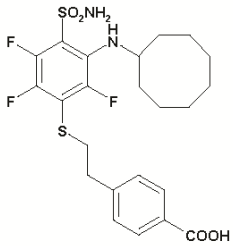	VD11-4-2* 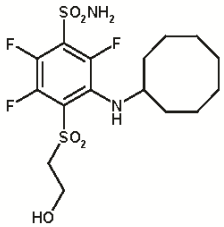	VD12-09* 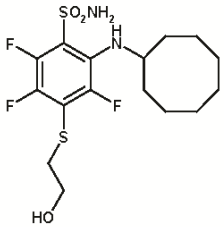
CA isoform				
CA I	≥200 000	5000	710	50 000
CA II	≥200 000	1000	60	1 300
CA III	≥200 000	≥200 000	40 000	≥200 000
CA IV	≥200 000	1820	25	1 700
CA VA	≥200 000	5000	2 500	3 300
CA VB	45000	100	5.6	210
CA VI	≥200 000	26300	95	4 300
CA VII	37 000	100	9.8	330
CA IX	**0.16** (<1)	**0.20** (<1)	**0.05**	**1.1**
CA XII	710 (100)	370	3.3	330
CA XIII	20	40	3.6	140
CA XIV	170	170	1.6	170

The K_i values determined by SFA (pH 7.5, 25° C) are shown in the parentheses. Uncertainties of FTSA and SFA measurements do not exceed 2-fold.

*K_d values of VD11-4-2 and VD12-09 towards CA isoforms have been already published [26].

suspension resulted in an acceleration of the reaction, indicating CA catalytic activity in MDA-MB-231 cells (Figure 3A). Pre-incubation of the cell suspension with VR16-09, VD11-4-2, or VD12-09 resulted in a dose-dependent decrease in CA activity (Figure 3B–3D). To verify the CA IX specificity, hypoxic HeLa cells, in which CA IX was knocked out (KO) (Supplementary Figure 3), were exposed to VR16-09, VD11-4-2 and VD12-09 at concentrations of near maximum inhibition of extracellular CA activity in hypoxic MDA-MB-231 cells. In both HeLa CA IX KO lines, VR16-09 (300 nM), VD11-4-2 (300 nM), or VD12-09 (30 μM) did not alter CA activity (Figure 3E), although considerable CA activity remained, indicating activity of other CA isoforms. In HeLa wild-type (WT) cells, CA activity decreased ($P < 0.01$) to 30–40%, values that did not significantly differ from the two HeLa CA IX KO cell lines. Thus, VR16-09, VD11-4-2, and VD12-09 specifically target CA IX, while other CAs remain unaffected. Previously Frost and colleagues reported a K_i value of 85.3 nM against extracellular CA for the fluorescent sulfonamide Cpd 5c in intact hypoxic MDA-MB-231 cells using the same ^{18}O exchange assay [31]. Extracellular CA activity of MDA-MB-231 cells was also significantly reduced by 1 μM acetazolamide [32]. The inhibitors VR16-09 and VD11-4-2 exhibited higher effect towards CA IX expressed in cellular models than previously reported compounds likely due to higher affinity.

The functional activity of inhibitors was further confirmed by measuring the rise in extracellular pH directly inside a hypoxic chamber [33]. VR16-09, VD11-4-2, and VD12-09 significantly ($p < 0.05$) reduced hypoxia-induced acidification of HeLa cells in a dose-dependent manner, while the effect on cells exposed to normoxia was negligible (Figure 4A). This functional activity was the most pronounced for VR16-09 at 50 μM, which significantly reduced hypoxia-induced acidosis of 4 investigated cell lines (Figure 4A, 4B). VD11-4-2 also significantly reduced ($p < 0.05$) hypoxic acidification of HeLa, H460, MDA-MB-231, and A549 cells (Figure 4A, 4C). A 4-fold lower concentration of sodium bicarbonate in the medium was used for A549 to determine the functional effects of the compounds due to relatively low levels of hypoxia-induced CA IX

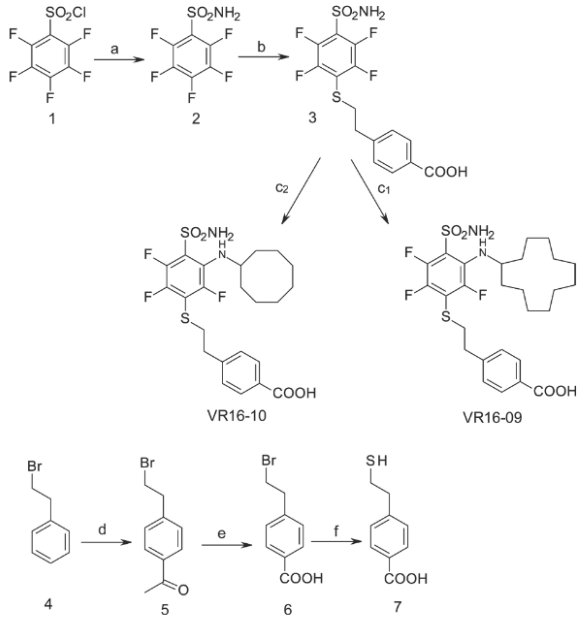

Scheme 1: Synthesis scheme of VR16-09 and VR16-10. Reagents and conditions: (a) NH_3 aq, THF, –10° C; (b) **7**, Et_3N, MeOH, r.t. 24 h, then conc. HCl; (c_1) cyclododecylamine, Et_3N, DMSO, 70° C, 36 h, then H_2O, HCl; (c_2) cyclooctylamine, Et_3N, DMSO, 70° C, 24 h, then H_2O, HCl; (d) CH_3COCl, $AlCl_3$, CH_2Cl_2, 0° C – +2° C, then conc. HCl; (e) NaOH, H_2O, dioxane, Br_2, 0° C – +2° C, then conc. HCl, (f) NH_2CSNH_2, H_2O, reflux 3 h, then NaOH 1 h reflux, then 2M HCl.

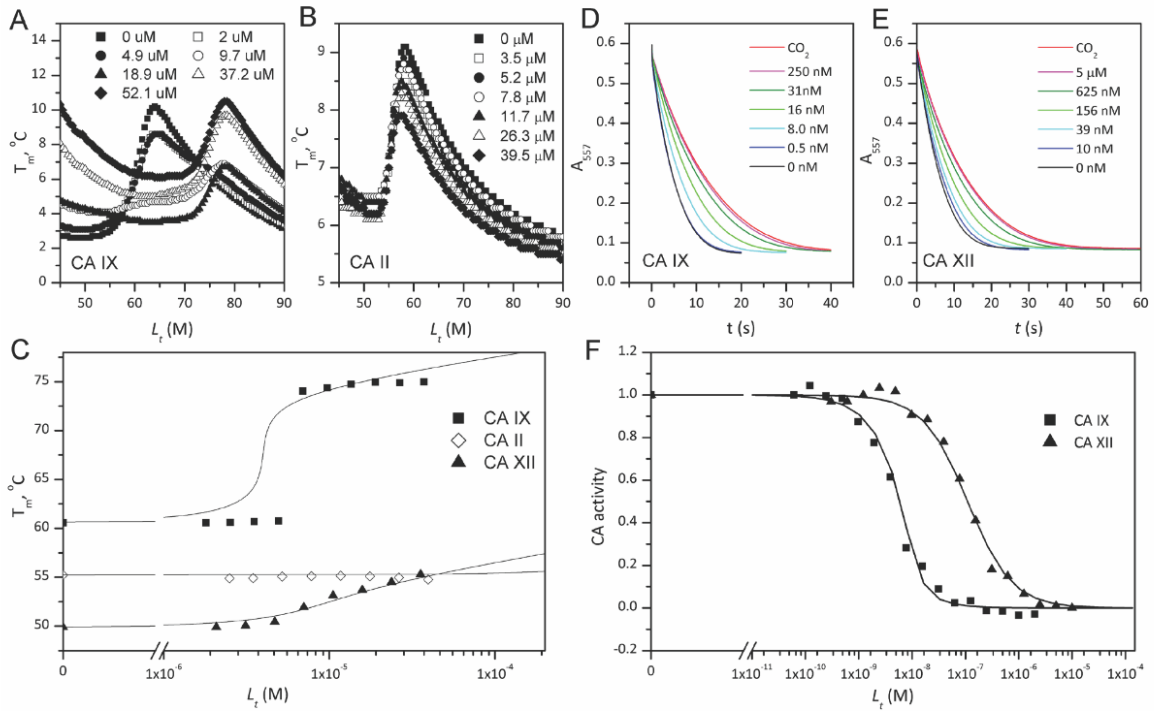

Figure 1: The binding affinity by FTSA (panels **A–C**) and inhibition by SFA (panels **D–F**) of VR16-09 towards human recombinant CAs. Thermal melting curves of 8 µM CA IX (A) and 5 µM CA II (B) determined by ANS fluorescence in the presence of various VR16-09 concentrations. (C) Melting temperatures (T_m) of CA IX (■), CA II (◊) and CA XII (▲) as a function of added compound concentration. The lines were regressed according to [60]. Absorbance decrease due to enzymatic acidification of the medium by CA IX (D) or CA XII (E) for various VR16-09 concentrations. (F) Fraction inhibition of CA IX (■) or CA XII (▲) as a function of the total VR16-09 concentration. The lines are fit according to the Morrison equation [50].

(Supplementary Figure 1). VD12-09 exhibited functional activity in HeLa cells (Figure 4A). The smallest, albeit significant ($p < 0.05$), impact on extracellular acidification was found for VR16-10 (Supplementary Figure 4). Interestingly, inhibitors VR16-09 and VR16-10 differ structurally by the size of the hydrophobic ring at *ortho* position. Thus, a 12-carbon ring of VR16-09 was found to be more favorable than an 8-carbon ring of VR16-10 because ~3-fold higher functional effects of VR16-09 on the reduction of hypoxia-induced acidification of H460 cells were observed, even though their affinities towards recombinant CA IX were similar (K_is of 0.16 and 0.20 nM, respectively). Functional activities of several CA IX-targeting agents, such as fluorescent sulfonamide [33] and nitroimidazole-based inhibitors [34, 35] have been previously reported using the same method in HeLa cells, where a dose-dependent reduction in hypoxia-induced extracellular acidification was observed. Results of the current study indicate that the inhibitors investigated here are more efficacious in decreasing extracellular acidification than previously described compounds because of their significant functionality at lower concentrations (5–50 μM), highlighting the potential for CA IX-targeting therapy.

Interestingly, hypoxia-induced acidosis of AsPC-1 cells increased after exposure to VR16-09 or VD11-4-2 (Figure 4B, 4C), related to the unique expression of monocarboxylate transporter 1 (MCT1) under both normoxic and hypoxic conditions in these cells (Supplementary Figure 5A). Recently, CA IX was

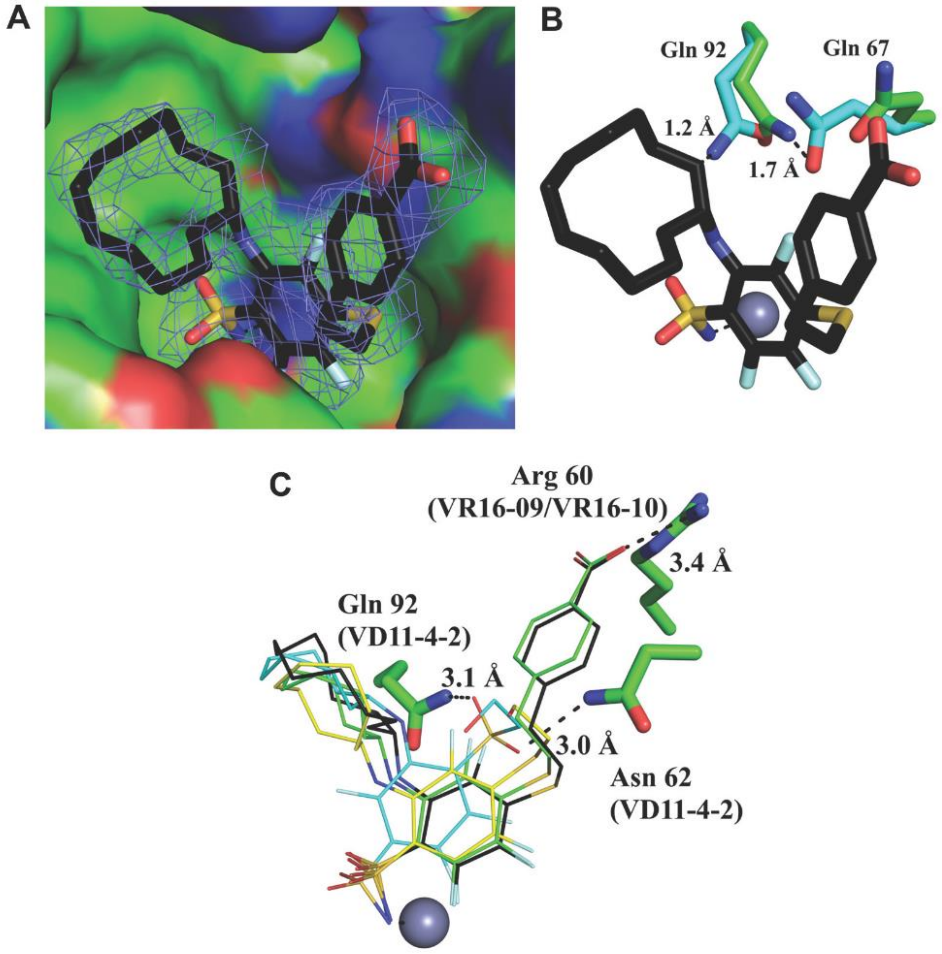

Figure 2: Crystal structure of VR16-09 (panel **A**, PDB ID: 6G98) bound in the active site of human recombinant CA IX. The $F_o - F_c$ omit map is contoured at 3σ. (Panel **B**) shows that VR16-09 fitted in apo-CA IX structure (PDB ID: 6FE2), demonstrating collision points with residues indicating too short inter-atomic distances if conformational changes had not occurred. Protein and ligand carbons are shown in green and black, respectively, and apo-CA IX residues are shown in light blue. Atom colors are: oxygen (red), nitrogen (blue), fluorine (light blue), and sulfur (yellow). (Panel **C**) shows comparison of binding modes for compounds VR16-09 (black carbons), VR16-10 (green carbons), VD12-09 (yellow carbons), and VD11-4-2 (light blue carbons). The zinc ion is shown as a gray sphere and residues participating in hydrogen bonds or charged interactions are also specified for the respective inhibitors. The figure was prepared using Pymol [61].

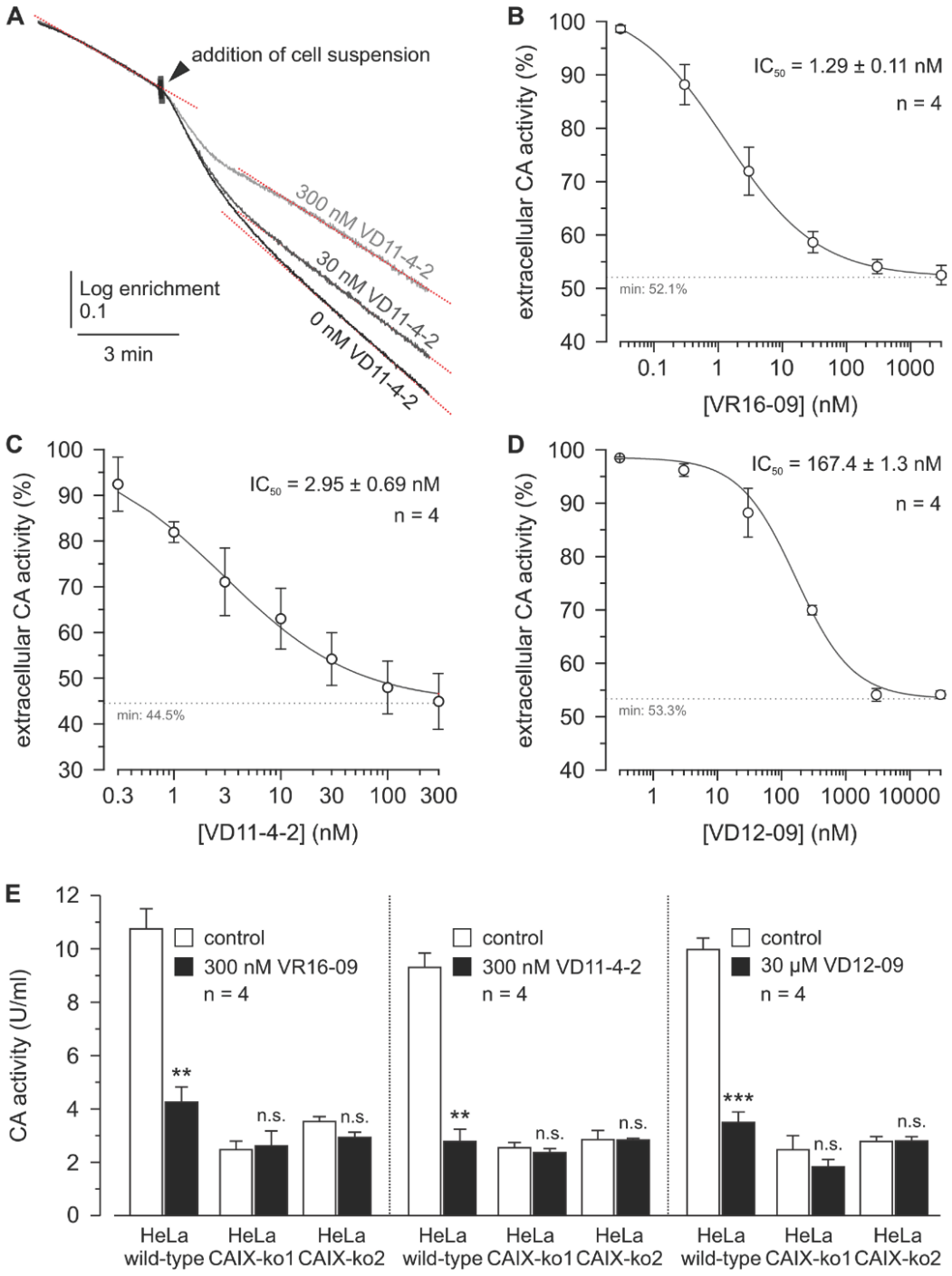

Figure 3: IC_{50} determination of VR16-09, VD11-4-2, and VD12-09 in hypoxic MDA-MB-231 cells and CA IX-dependent mode of action for inhibitors in hypoxic HeLa CA IX KO cells. (**A**) Original recordings of the log enrichment of MDA-MB-231 cells pre-incubated with VD11-4-2 for up to 3 h. The beginning of each trace shows the rate of degradation of the ^{18}O-labeled substrate in the non-catalyzed reaction. (**B**–**D**) – Relative CA activity in MDA-MB-231 cells, incubated under hypoxia (1% O_2) for 3 days. Cells were pre-incubated with VR16-09 (B), VD11-4-2 (C), or VD12-09 (D) for up to 3 h. CA activity was determined by MS gas-analysis from the increase in the rate of log enrichment after addition of cell suspension. CA activity in the presence of inhibitor was normalized to the activity in the absence of inhibitor. (**E**) CA activity in HeLa-WT and HeLa-CA IX-KO cells, before (white bars) and after addition of VR16-09, VD11-4-2 or VD12-09 (black bars). Average + SD of 4 independent experiments per cell line are shown. Asterisks indicate significant difference between CA activity before and after addition of inhibitor ($^{**}p < 0.01$, $^{***}p < 0.001$, n.s.: not significant).

proposed to be a 'H^+-distributing antenna' for MCT1 to facilitate rapid extrusion of lactate and H^+ from the cell [36]. Even though the catalytic activity of CA IX was inhibited in AsPC-1 by compounds, the rise of acidification might be caused by MCT1 which is further non-catalytically stimulated by CA IX. In contrast, MCT4 was expressed in all tested cell lines and was up-regulated in response to hypoxia (Supplementary Figure 5B), in line with previously confirmed HIF-1α-dependent mechanism of MCT4 expression in cancer cells [37].

Inhibitor-induced cytotoxicity

Cytotoxicity of tested compounds was higher in normoxic than hypoxic cell monolayers, as determined by cell viability assay using alamarBlue® after treatment for 48

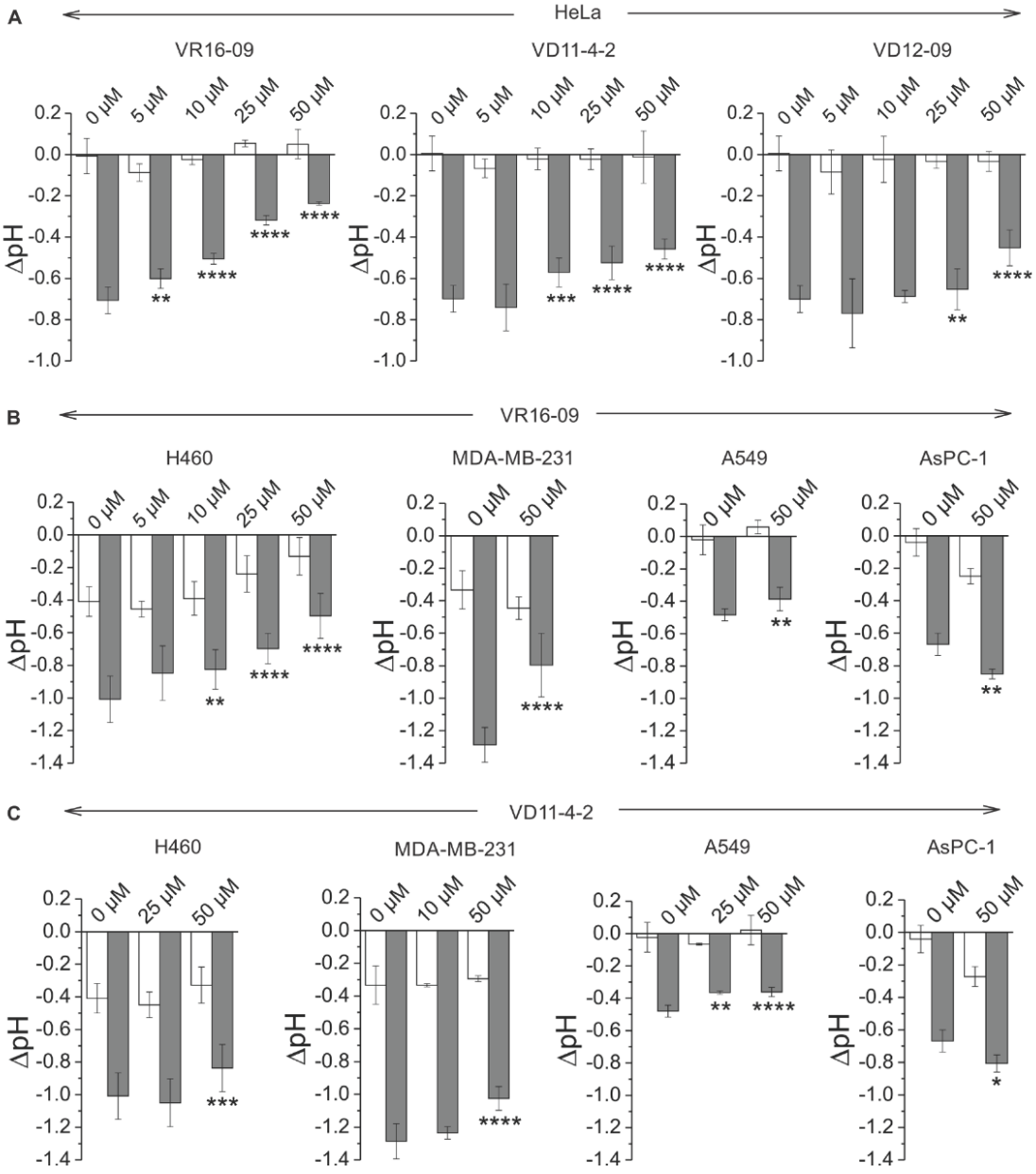

Figure 4: (**A**) Changes in extracellular acidification of HeLa cells after the treatment with VR16-09, VD11-4-2 or VD12-09 for 72 h under normoxia (21% O_2; white bars) or hypoxia (0.2% O_2; grey bars). (**B–C**) Effect of VR16-09 (B) and VD11-4-2 (C) on the hypoxia-induced extracellular acidification of H460, MDA-MB-231, A549, and AsPC-1 after the exposure for 72 h. Average ± SD of at least 3 independent experiments is shown. Asterisks indicate significant difference between medium pH of cells exposed to DMSO and cells treated with various doses of inhibitor under hypoxic conditions ($^{*}p < 0.05$; $^{**}p < 0.01$, $^{***}p < 0.001$, $^{****}p < 0.0001$).

h or 72 h (Supplementary Figure 6A, 6B, Supplementary Table 2). Inhibitors were less effective in reducing viability of hypoxic CA IX-expressing cells than normoxic cells without or with significantly lower CA IX expression. Sensitivity of HeLa and H460 cells to VR16-10 was the lowest and is in line with the lowest VR16-10 functional activity measured by extracellular pH assay. Therefore, VR16-10 was not investigated further. Similarly, compounds were more effective in reducing clonogenic survival in normoxic compared to hypoxic monolayer HeLa cells (Supplementary Figure 6C). Our results correlate with previously published cytotoxicity profiles of benzenesulfonamides, including SLC-0111 [38], sulfamate S4 [39], and dual-target compounds bearing various CA IX-targeting moieties combined with different anti-cancer drugs [40], which showed more effective cell kill in normoxia than hypoxia. We hypothesize that higher cytotoxicity of inhibitors in normoxic cells as compared with hypoxic cells could be due to the affinity of investigated compounds towards CA XII, expressed in all cell lines investigated here and shown to be up-regulated to compensate the CA IX knockdown [41]. Thus, new cellular models with both CA IX and CA XII KO would be crucial to determine the link between functional activity of compounds and CA IX or CA XII-dependent cellular mechanisms.

Hypoxia-dependent effect on spheroid clonogenic survival

To confirm the CA IX-dependent efficacy of the compounds, H460 spheroids were employed. Immunofluorescence analysis confirmed overlap between CA IX expression and pimonidazole (PIMO)-positive hypoxia in sections of H460 spheroids grown for 11 days, whereas neither CA IX nor hypoxia were found in spheroids grown for 7 days (Figure 5A). Therefore, non-hypoxic (4 days) and hypoxic (11 days) H460 spheroids were exposed to VR16-09 using an effective dose based on extracellular pH assays (Figure 4A, 4B) for 24 h and afterwards plated for clonogenic survival. In contrast to 2D cell viability and clonogenic survival assays, a hypoxia-dependent effect on clonogenic survival of VR16-09 was

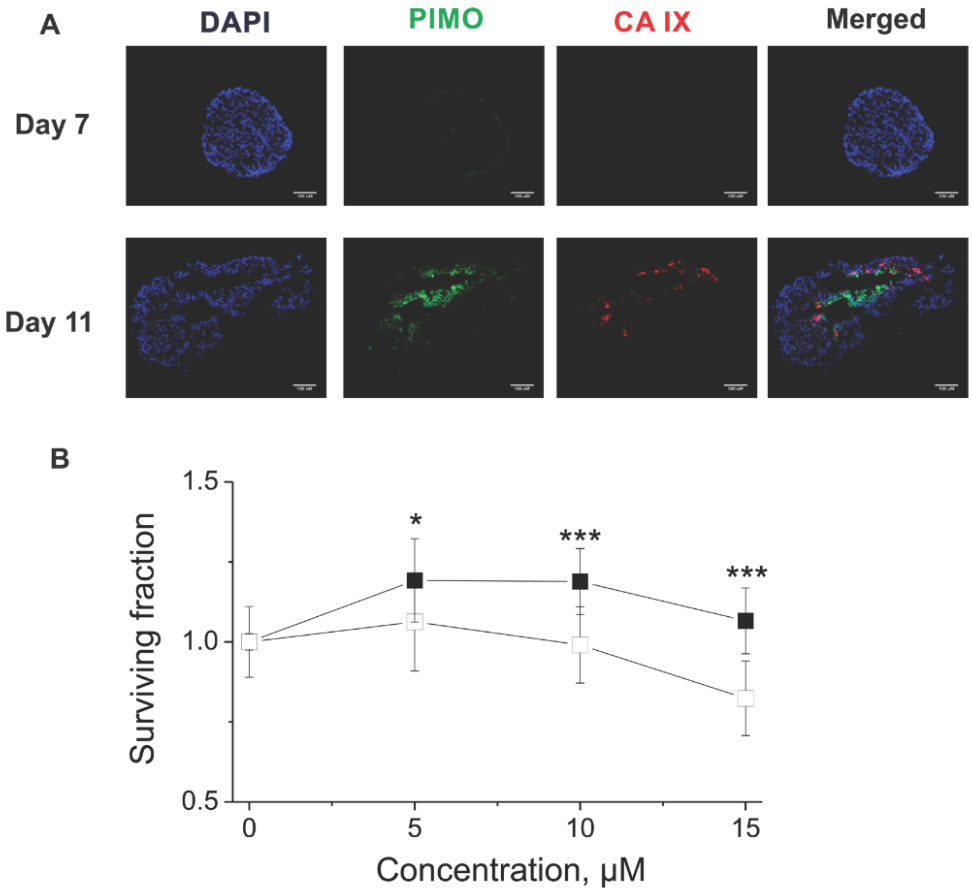

Figure 5: (**A**) Immunofluorescence images of H460 spheroids stained for DAPI (blue), PIMO (green) and CA IX (red). The scale bar indicates 100 μM. (**B**) Survival of clonogenic cells derived from non-hypoxic (■) and hypoxic (□) H460 spheroids exposed to VR16-09 for 24 h on day 4 or day 11, respectively. Asterisks indicate statistically significant differences between the surviving fractions of clonogenic cells derived from normoxic or hypoxic spheroids after exposure to the same dose ($^{*}p < 0.05$, $^{***}p < 0.001$).

found in H460 spheroids (Figure 5B). The 3D cell models reflect important properties of *in vivo* tumors such as interactions between cells, oxygen gradients, penetration of drugs, response and resistance, and production/deposition of extracellular matrix, which are absent in rapidly and uncontrollably growing 2D cells [42–44]. Our study confirms the importance of using *in vitro* 3D cellular models for screening of CA IX-targeting inhibitors.

MATERIALS AND METHODS

Chemistry

VR16-09 and VR16-10 were synthesized following a similar route as described in our previous research [24]. Pentafluorobenzenesulfonyl chloride (1, Acros Organics) was converted to pentafluorobenzenesulfonamide (2) via amination with aqueous ammonia (scheme 1) by our improved method [25]. On the basis of our previous investigations, sulfonamide 2 undergoes aromatic nucleophilic substitution reactions with sulfur-centered nucleophiles readily and forms exclusively the *para*-substituted products. High reactivity of polyfluorinated compounds leads to the formation of monosubstituted or even further substituted compounds. The subsequent *ortho*-substitution occurs in the case of 4-substituted-2,3,5,6-tetrafluobenzenesulfonamides, bearing non-oxidized sulfur-centered substitutes at *para* position. Similarly, sulfonamide 2 was treated with 4-(2-mercaptoethyl)benzoic acid (7) to furnish *para*-substituted compound 3 and subsequent aromatic nucleophilic substitution reactions with cyclododecylamine and cyclooctylamine in DMSO in the presence of Et_3N yielded desirable compounds VR16-09 and VR16-10. Since suitable sulfur-centered nucleophile 7 was not commercially available, it was synthesized using literature methods. Starting from commercially available (2-bromoethyl)benzene (4, Acros Organics), Friedel-Crafts acylation with acetyl chloride proceeded in high yield. Acylation was accomplished as described in literature [45], except for changing highly toxic solvent carbon disulfide to more acceptable dichloromethane. Conversion of methyl ketone 5 into benzoic acid 6 was carried out via haloform reaction by the method of Foreman and McElvain [46]. Finally, benzoic acid 6 was treated with thiourea in refluxing water to generate intermediate salt, which was partitioned by adding sodium hydroxide solution as described by Takano [47].

Compound characterization

All starting materials and reagents were commercial products. They were used without further purification. Melting points of the compounds were determined in open capillaries on a Thermo Scientific 9100 Series and are uncorrected. ^1H and ^{13}C NMR spectra were recorded on a Bruker spectrometer (400 and 100 MHz, respectively) in DMSO-d_6 using residual DMSO signals (2.52 ppm and 40.21 ppm for ^1H and ^{13}C NMR spectra, respectively) as internal standard. ^{19}F NMR spectra were recorded on a Bruker spectrometer (376 MHz) with $CFCl_3$ as an internal standard. Proton, carbon and fluorine chemical shifts were expressed in parts per million (ppm) in the indicated solvent. Multiplicity was defined as s (singlet), d (doublet), t (triplet), q (quartet), dd (a doublet of doublets), ddd (a doublet of doublet of doublets), m (multiplet), br s (broad singlet). TLC was performed with silica gel 60 F_{254} aluminum plates (Merck) and visualized with UV light. Column chromatography was performed using silica gel 60 (0.040–0.063 mm, Merck). High-resolution mass spectra (HRMS) were recorded on a Dual-ESI Q-TOF 6520 mass spectrometer (Agilent Technologies). The purity of final compounds was verified by HPLC to be >95% using the Agilent 1290 Infinity instrument with a Poroshell 120 SB-C18 (2.1 mm × 100 mm, 2.7 μm) reversed-phase column.

Pentafluorobenzenesulfonamide (2)

The solution of pentafluorobenzenesulfonyl chloride (1) (1.00 g, 3.75 mmol) and THF (60 mL) was cooled to ~ –10° C and aqueous ammonia (~1.20 mL, 25 %) was added dropwise while stirring until the solution was at pH ~7. After stirring for an additional 1 h, the solvent was removed under reduced pressure and the white solid was washed with cold H_2O. Recrystallization was accomplished from H_2O. Yield: 0.84 g (90 %), mp 156–157° C close to the value in the literature, mp 156° C [48]. ^1H NMR (400 MHz, DMSO-d_6): 8.48 (2H, s, SO_2NH_2). ^{19}F NMR (376 MHz, DMSO-d_6): –139.5 (2F, dd, ^1J = 19 Hz, ^2J = 6 Hz), –149.39 (1F, t, J = 22 Hz), –161.03 (2F, t, J = 20 Hz).

4-(2-{[4-(Aminosulfonyl)-2,3,5,6-tetrafluorophenyl]thio}ethyl)benzoic acid (3)

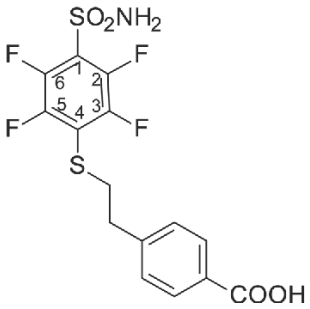

The mixture of pentafluorobenzenesulfonamide (2) (2.00 g, 8.09 mmol), 4-(2-mercaptoethyl)benzoic acid (7) (1.77 g, 9.71 mmol), Et_3N (2.50 mL, 17.9 mmol), and MeOH (20 mL) was stirred at ambient temperature for 24 h. The solution was acidified to pH = 5 with conc. HCl and

MeOH was removed under reduced pressure. The white solid was washed with water and dried. Recrystallization was accomplished from EtOH. Yield: 2.42 g (73 %), mp 235–236° C. ^{1}H NMR (DMSO-d_6, 400 MHz) δ 12.87 (1H, br s, COOH), 8.40 (2H, s, SO_2NH_2), 7.85 (2H, d, J = 8.1 Hz, ArH), 7.36 (2H, d, J = 8.1 Hz, ArH), 3.36 (2H, t, J = 7.3 Hz, S$\underline{CH_2}$CH$_2$), 2.95 (2H, t, J = 7.3 Hz, SCH$_2\underline{CH_2}$). ^{13}C NMR (DMSO-d_6, 100 MHz) δ 167.57 (CO), 146.85 (C3, C5, dd, ^1J (^{19}F-^{13}C) = 244.2 Hz, ^2J (^{19}F-^{13}C) = 17.1 Hz), 142.99 (C2, C6, dd, ^1J (^{19}F-^{13}C) = 254.0 Hz, ^2J (^{19}F-^{13}C) = 17.1 Hz), 144.79 (Ar), 129.78 (Ar), 129.53 (Ar), 129.28 (Ar), 122.92 (C4, t, J (^{19}F-^{13}C) = 15.3 Hz), 118.64 (C1, t, J (^{19}F-^{13}C) = 20.4 Hz), 35.91 (SCH$_2\underline{CH_2}$), 34.79 (S$\underline{CH_2}$CH$_2$). ^{19}F NMR (DMSO-d_6, 376 MHz) δ: –133.0 (2F, dd, ^1J = 24.3 Hz, ^2J = 9.9 Hz), –139.1 (2F, dd, ^1J = 24.2 Hz, ^2J = 9.9 Hz). HRMS for $C_{15}H_{11}F_4NO_4S_2$ [(M-H)$^-$]: calcd. 407.9993, found 407.9986.

4-(2-{[4-(Aminosulfonyl)-3-(cyclododecylamino)-2,5,6-tetrafluorophenyl]thio}ethyl)benzoic acid (VR16-09)

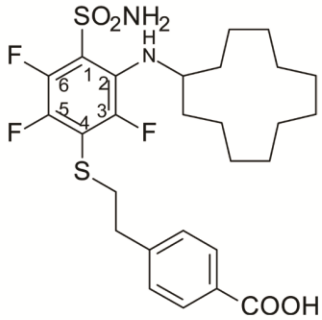

The mixture of 4-(2-{[4-(aminosulfonyl)-2,3,5,6-tetrafluorophenyl]thio}ethyl)benzoic acid (3) (0.40 g, 0.98 mmol), cyclododecylamine (0.286 g, 1.56 mmol), Et_3N (0.34 mL, 2.44 mmol), and DMSO (6 mL) was stirred at 70° C for 36 h. The solution was cooled to room temperature, diluted with water (20 mL) and acidified to pH = 5 with 2 M HCl. The white solid was filtered, washed with water and dried. Recrystallization was accomplished from EtOH:H_2O (2:1). Yield: 0.36 g (64 %), mp 169–170° C. ^{1}H NMR (DMSO-d_6, 400 MHz) δ 12.86 (1H, br s, COOH), 8.13 (2H, s, SO_2NH_2), 7.85 (2H, d, J = 8.1 Hz, ArH), 7.33 (2H, d, J = 8.1 Hz, ArH), 6.19 (1H, d, J = 9.2 Hz, NH), 3.69 (1H, br s (unresolved m), CH of cyclododecane), 3.28 (2H, t, J = 7.3 Hz, S$\underline{CH_2}$CH$_2$), 2.91 (2H, t, J = 7.3 Hz, SCH$_2\underline{CH_2}$), 1.8-1.1 (22H, m, cyclododecane). ^{13}C NMR (DMSO-d_6, 100 MHz) δ 167.63 (CO), 148.18 (C3, d, J (^{19}F-^{13}C) = 244 Hz), 144.84 (C6, ddd, ^1J (^{19}F-^{13}C) = 249.6 Hz, ^2J (^{19}F-^{13}C) = 15.6 Hz), ^3J (^{19}F-^{13}C) = 3.6 Hz), 144.86 (Ar), 141.62 (C5, ddd, ^1J (^{19}F-^{13}C) = 236.5 Hz, ^2J (^{19}F-^{13}C) = 15.3 Hz, ^3J (^{19}F-^{13}C) = 4.6 Hz), 132.81 (C2, d, J (^{19}F-^{13}C) = 15.1Hz), 129.78 (Ar), 129.57 (Ar), 129.14 (Ar), 119.53 (C1, dd, ^1J (^{19}F-^{13}C) = 11.9 Hz, ^2J (^{19}F-^{13}C) = 4.5 Hz), 117.52 (C4, dd, ^1J (^{19}F-^{13}C) = 23.8 Hz, ^2J (^{19}F-^{13}C) = 19.1 Hz), 52.68 (CH of cyclododecane, d, J = 10.6 Hz), 35.85 (SCH$_2\underline{CH_2}$), 34.73 (S$\underline{CH_2}$CH$_2$), 30.95 (cyclododecane), 24.10 (cyclododecane), 23.75 (cyclododecane), 23.40 (cyclododecane), 23.23 (cyclododecane), 21.28 (cyclo dodecane). ^{19}F (DMSO-d_6, 376 MHz) δ –120.6 (C3-F, d, J = 11.3 Hz), –137.0 (C5-F, dd, ^1J = 27 Hz, ^2J = 11.5 Hz), –145.1 (C6-F, dd, ^1J = 27 Hz, ^2J = 2.5 Hz). HRMS for $C_{27}H_{35}F_3N_2O_4S_2$ [(M-H)$^-$]: calcd. 571.1918, found 571.1924.

4-(2-{[4-(Aminosulfonyl)-3-(cyclooctylamino)-2,5,6-tetrafluorophenyl]thio}ethyl)benzoic acid (VR16-10)

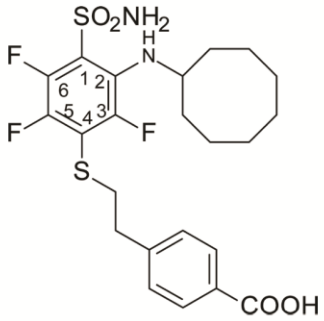

The mixture of 4-(2-{[4-(aminosulfonyl)-2,3,5,6-tetrafluorophenyl]thio}ethyl)benzoic acid (3) (0.40 g, 0.98 mmol), cyclooctylamine (0.214 mL, 1.56 mmol), Et_3N (0.34 mL, 2.44 mmol), and DMSO (6 mL) was stirred at 70° C for 24 h. The solution was cooled to room temperature, diluted with water (20 mL) and acidified to pH = 5 with 2 M HCl. The white solid was filtered, washed with water and dried. Recrystallization was accomplished from EtOH:H_2O (2:1). Yield: 0.32 g (64 %), mp 166–168° C. ^{1}H NMR (DMSO-d_6, 400 MHz) δ 12.87 (1H, br s, COOH), 8.11 (2H, s, SO_2NH_2), 7.85 (2H, d, J = 8.1 Hz, ArH), 7.33 (2H, d, J = 8.1 Hz, ArH), 6.33 (1H, d, J = 8.7 Hz, NH), 3.71 (1H, br s (unresolved m), CH of cyclooctane), 3.30 (2H, t, J = 7.3 Hz, S$\underline{CH_2}$CH$_2$), 2.91 (2H, t, J = 7.3 Hz, SCH$_2\underline{CH_2}$), 1.9-1.4 (14H, m, cyclooctane). ^{13}C NMR (DMSO-d_6, 100 MHz) δ 167.64 (CO), 148.16 (C3, d, J (^{19}F-^{13}C) = 242.7 Hz), 144.84 (C6, ddd, ^1J (^{19}F-^{13}C) = 249.7 Hz, ^2J (^{19}F-^{13}C) = 15.7 Hz, ^3J (^{19}F-^{13}C) = 3.8 Hz), 144.9 (Ar), 141.62 (C5, ddd, ^1J (^{19}F-^{13}C) = 236.0 Hz, ^2J (^{19}F-^{13}C) = 15.1 Hz, ^3J (^{19}F-^{13}C) = 4.4 Hz), 132.21 (C2, d, J (^{19}F-^{13}C) =14.1 Hz), 129.81 (Ar), 129.53 (Ar), 129.21 (Ar), 119.41 (C1, dd, ^1J (^{19}F-^{13}C) = 11.5 Hz, ^2J (^{19}F-^{13}C) = 4.9 Hz), 117.51 (C4, dd, ^1J (^{19}F-^{13}C) = 23.7 Hz, ^2J (^{19}F-^{13}C) = 18.5 Hz), 55.66 (CH of cyclooctane, d, J = 11.4 Hz), 35.86 (SCH$_2\underline{CH_2}$), 34.63 (S$\underline{CH_2}$CH$_2$), 32.62 (cyclooctane), 27.29 (cyclooctane), 25.94 (cyclooctane), 25.53 (cyclooctane), 23.38 (cyclooctane). ^{19}F NMR (DMSO-d_6, 376MHz) δ –120.81 (C3-F, dd, ^1J = 11.4 Hz, ^2J = 3.1 Hz), –137.1 (C5-F, dd, ^1J = 27.0 Hz, ^2J = 11.5

Hz), –145.2 (C6-F, dd, ^1J = 26.9 Hz, ^2J = 3.0 Hz). HRMS for $C_{23}H_{27}F_3N_2O_4S_2$ [(M-H)$^-$]: calcd. 515.1292, found 515.1284.

1-[4-(2-Bromoethyl)phenyl]ethanone (5)

A mixture of $AlCl_3$ (2.91 g, 21.82 mmol), acetyl chloride (1.71 mL, 24.05 mmol) and CH_2Cl_2 (50 mL) was stirred at 0° C – +5° C until $AlCl_3$ dissolved. Solution of (2-bromoethyl)benzene (4) (2.00 mL, 14.64 mmol) in acetyl chloride (3.4 mL) was then added dropwise at 0° C – +2° C. The resulting mixture was stirred at 0° C – +2° C for 1h and then poured into a mixture of concentrated HCl (20 mL) and ice (200 mL). This mixture was extracted with CH_2Cl_2 (30 mL × 3). The combined organic extracts were washed with 1N NaOH, water and brine, dried over Na_2SO_4 and concentrated under reduced pressure. The resultant residue was subjected to flash chromatography (silica gel, hexane/EtOAc, 9:1) to afford compound 5 (2.83 g, 85 %) as an oil. ^{1}H NMR (400 MHz, DMSO-d_6) δ 7.94 (2H, d, J = 8.2 Hz, ArH), 7.33 (2H, d, J = 8.2 Hz, ArH), 3.61 (2H, t, J = 7.3 Hz, CH_2), 3.24 (2H, t, J = 7.3 Hz, CH_2), 2.60 (3H, s, $COCH_3$).

4-(2-Bromoethyl)benzoic acid (6)

A solution of sodium hydroxide (4.16 g, 104 mmol) in H_2O/dioxane (50 mL/40 mL) was prepared in three-necked, round bottomed flask fitted with a thermometer and a dropping funnel. The solution was cooled to 0° C in an ice-salt bath, and bromine (2.04 mL, 39.6 mmol) was slowly added with stirring at 0° C – +7° C. 1-[4-(2-Bromoethyl)phenyl]ethanone (5) (3.00 g, 13.2 mmol) was then added dropwise to sodium hypobromite solution at 0° C – +2° C. The resulting mixture was stirred at 0° C – +5° C for 1.5 h and then acidified with concentrated HCl. The precipitated acid was filtered, washed with water and dried. Recrystallization was accomplished from toluene. Yield: 2.50 g (83 %), mp 207–208° C, close to the value in the literature mp 205–207° C [46]. ^{1}H NMR (400 MHz, DMSO-d_6) δ 12.91 (1H, br s, COOH), 7.89 (2H, d, J = 8.3 Hz, ArH), 7.41 (2H, d, J = 8.4 Hz, ArH), 3.78 (2H, t, J = 7.1 Hz, CH_2), 3.21 (2H, t, J = 7.1 Hz, CH_2).

4-(2-Mercaptoethyl)benzoic acid (7)

The mixture of 4-(2-bromoethyl)benzoic acid (6) (2.00 g, 8.73 mmol), thiourea (0.80 g, 10.43 mmol), H_2O (20 mL) was refluxed for 3 h. The solution was cooled to room temperature and 10 % (w/v) aqueous NaOH (18 mL) was added and the mixture was refluxed again for 1h. The solution was then cooled to room temperature, acidified to pH = 5 with 2 M HCl and filtered. The white solid was washed with water and dried. Recrystallization was accomplished from EtOH. Yield: 1.47 g (92 %), mp 157–159° C, close to the value in the literature mp 156–158° C [47]. ^{1}H NMR (400 MHz, DMSO-d_6) δ 12.85 (1H, br s, COOH), 7.88 (2H, d, J = 8.2 Hz, ArH), 7.36 (2H, d, J = 8.2 Hz, ArH), 2.92 (2H, t, J = 7.4 Hz, CH_2), 2.77 (2H, q, J = 6.8 Hz, CH_2), 2.30 (1H, t, J = 7.7 Hz, SH).

CA inhibition assay

The enzymatic activity of carbonic anhydrase isoforms and their inhibition was determined by the stopped-flow CO_2 hydration assay where the formed acid was followed by the absorbance change of a pH indicator. The Applied Photophysics SX.18MV-R stopped-flow spectrometer was used to measure the absorbance change of Phenol-Red pH indicator at 557 nm [49]. Saturated CO_2 solution was prepared by bubbling the CO_2 gas in MilliQ water at 25° C for 1 h. Experiments were performed at 25° C using 25 mM Hepes buffer containing 50 mM NaCl (pH 7.5), 0–10 μM compound with the final 0.4% (v/v) DMSO concentration. The final enzyme concentration was 10 nM for CA IX and 20 nM for CA XII. Raw curves of absorbance change were analyzed using Origin 8.1 (OriginLab Corporation) and the slope values were used to evaluate the rates of CO_2 hydration. Spontaneous CO_2 hydration rate was used as a zero value, while the CA catalyzed reaction rate - as a maximum value. The K_d values were determined using the Morrison equation [50]:

$$\text{CA act.}(\%) = \left(1 - \frac{([CA]+[I]+K_d) - \sqrt{([CA]+[I]+K_d)^2 - 4[CA][I]}}{2[CA]}\right)100\%$$

Fluorescent thermal shift assay

The binding affinity of synthesized compounds to recombinant human CAs was measured by the fluorescent thermal shift assay (FTSA) where the thermal stabilization of the protein by the compound was determined by following the fluorescence dependence on temperature at various added compound concentrations. The melting temperature (T_m) of CA was measured using the Corbett Rotor-Gene 6000 instrument (QIAGEN Rotor-Gene Q, excitation at 365 ± 20 nm, emission detection at 460 ± 15 nm). The protein was heated from 25 to 99° C at a rate of 1° C/min and the fluorescence change of the solvatochromic dye 8-anilino-1-naphthalene sulfonate (ANS) was followed. The samples consisted of 5–10 μM CA, 0–200 μM ligand, 50 μM ANS, and 50 mM sodium phosphate buffer containing 100 mM NaCl at pH 7.0, with the final DMSO concentration of 2% (v/v). Protein unfolding profiles and the melting temperatures were determined at each ligand concentration while recording extrinsic fluorescence of ANS. Data analysis was performed as previously described [51]. All experiments were repeated at least twice.

CA IX purification, crystallization and X-ray crystallography data collection

Protein was prepared and crystalized as described previously [30]. Data were collected at beamline BL14.1, Helmholtz-Zentrum Berlin, in Berlin, Germany. Images were processed by MOSFLM [52] and reflections scaled by SCALA [53]. The structure was determined by molecular replacement in MOLREP [54]. The ligand parameter files were generated by LIBCHECK [55]. Ligand modeling and manual refinement of the structure were done in COOT, followed by refinement in REFMAC. Data processing, refinement, and validation statistics are shown in Supplementary Table 1.

Cell culture

Human cervical (HeLa), lung (H460, A549), breast (MDA-MB-231), and pancreatic (AsPC-1) cancer cells were cultured in Dulbecco's Modified Eagle's Medium (DMEM, Lonza) supplemented with 10% fetal bovine serum (FBS, Lonza). Cells were exposed to hypoxic conditions in the hypoxic chamber (MACS VA500 microaerophilic workstation, Don Whitley Scientific, UK) with 0.2% O_2, 5% CO_2 and residual N_2. Simultaneously, normoxic cells were grown in the humidified incubator with 21% O_2, 5% CO_2 at 37° C.

Generating HeLa CA IX knockout cells

HeLa CA IX knockout (KO) clones were established as described elsewhere [56]. HeLa cells were routinely cultured in DMEM (Lonza) supplemented with 10% FBS (Lonza) and transfected with a vector containing a CA IX-CRISPR guide RNA (CACCGGGGAATCCTCCTGCATCCG) using linear polyethylenimine (P-PEI, Polysciences Inc.). 24 h after transfection, selection with puromycin was started and maintained for 48 h, after which monoclones were picked and routinely cultured. After exposure to hypoxia (0.2%, 24 h), an initial screening for CA IX expression was performed by Western blotting (Supplementary Figure 3), followed by genetic confirmation of CA IX KO in clones that showed no CA IX expression. This was done by single allele sequencing using the TOPO® TA Cloning® Kit (Invitrogen) according to the manufacturer's protocol. KO-causing mutations in the *CA9* gene were confirmed in two alleles per clone.

Determination of CA catalytic activity in cancer cells via gas-analysis mass spectrometry

Catalytic activity of CA in hypoxic MDA-MB-231 and HeLa cancer cells was determined by monitoring the ^{18}O depletion of doubly labeled $^{13}C^{18}O_2$ through several hydration and dehydration steps of CO_2 and HCO_3^- at 24° C [57, 58]. The reaction sequence of ^{18}O loss from $^{13}C^{18}O^{18}O$ (m/z = 49) over the intermediate product $^{13}C^{18}O^{16}O$ (m/z = 47) and the end product $^{13}C^{16}O^{16}O$ (m/z = 45) was monitored with a quadrupole mass spectrometer (OmniStar GSD 320; Pfeiffer Vacuum, Asslar, Germany). The relative ^{18}O enrichment was calculated from the measured 45, 47, and 49 m/z abundance as a function of time according to: log enrichment = log (49×100/(49+47+45)). For the calculation of CA activity, the rate of ^{18}O depletion was obtained from the linear slope of the log enrichment over the time, using OriginPro 8.6 (OriginLab Corporation). The rate was compared with the corresponding rate of the non-catalyzed reaction. Enzyme activity in units (U) was calculated from these two values as defined by Badger and Price [59]. From this definition, one unit corresponds to 100% stimulation of the non-catalyzed ^{18}O depletion of doubly labeled $^{13}C^{18}O_2$. MDA-MB-231 cells were cultured in Gibco Leibovitz-L15 medium (Life Technologies GmbH, Darmstadt, Germany), supplemented with 10% fetal calf serum, 5 mM glucose and 1% penicillin/streptomycin, pH 7.4. HeLa cells were cultured in RPMI-1640 Medium (Sigma Aldrich, Schnelldorf, Germany), supplemented with 10% fetal calf serum and 1% penicillin / streptomycin. Both cell lines were cultured under hypoxia (1% O_2) for 3 days prior to measurements. Cells were trypsinized, washed and resuspended in HEPES-buffered saline (143 mM NaCl, 5 mM KCl, 2 mM $CaCl_2$, 1 mM $MgSO_4$, 1 mM Na_2HPO_4, 10 mM HEPES, pH 7.2). For determination of IC_{50} values, 2 cell culture plates (58 cm^2), grown to 80% confluency, were used for every single measurement. To ensure an equal amount of cells within one set of measurements, cells from several plates were pooled and then aliquoted according to the number of tested inhibitor concentrations. For the determination of IC_{50}, the cell suspensions were incubated in the corresponding concentration of inhibitor for up to 3 h. For every measurement, the non-catalyzed reaction was determined for 6 min in the presence of inhibitor, before cell suspension was added to the measuring cuvette and the catalyzed reaction was determined for 8 min. CA activity in the presence of inhibitor was normalized to the activity in the absence of inhibitor. IC_{50} values were determined by Hill equation using OriginPro 8.6. To investigate specificity of the inhibitors in HeLa WT and HeLa CA IX KO cells, the non-catalyzed reaction was determined for 6 min in the absence of inhibitor, before a suspension of 5 × 10^6 cells was added to the measuring cuvette. After the catalyzed reaction was determined for 6 min, the inhibitor was added to the cuvette and the reaction was determined for another 6 min.

Extracellular acidification (pH) assay

HeLa, H460, MDA-MB-231, and AsPC-1 cells were cultured in DMEM (Lonza) supplemented with 10% FBS (Lonza), whereas A549 cells were grown in-house made analogous medium differing only by a lower amount of

sodium bicarbonate (final concentration 10 mM). Cell densities for each cell line were optimized to get ~100% confluence at the end of experiment under normoxic and hypoxic (0.2% O_2) conditions upon vehicle (0.05% DMSO) treatment. Such conditions were necessary to obtain the highest possible level of CA IX-dependent extracellular acidification. Cells were plated in 6 cm dishes and allowed to attach overnight in normoxia. The next day cells were exposed to 5–50 μM doses of each inhibitor or DMSO for 72 h in parallel under normoxic or hypoxic conditions and pH of the culture medium was measured at the end of each experiment as previously reported [33]. Results are shown as a difference between the pH of medium in the control plate (without seeded cells) and the pH of medium in the targeted plate (cells exposed to the compound or vehicle).

Cell viability assay

Cytotoxicity of inhibitors was determined by the alamarBlue® cell viability assay (Life Technologies). Cell densities for HeLa, H460, MDA-MB-231, A549, and AsPC1 were optimized to get ~80% confluence at the end of experiment under normoxic and hypoxic (0.2% O_2) conditions upon vehicle (0.25% DMSO) treatment. Briefly, cells were seeded in 96-well plates and allowed to attach overnight in normoxia. On the next day, cells were exposed to normoxia or hypoxia and medium was replaced with pre-incubated normoxic or hypoxic medium with final concentrations of 10–150 μM of inhibitor or DMSO. After 72 h, cells were incubated with 10% alamarBlue® for 2 h under normoxia at 37° C. The fluorescence signal was measured using the multi-mode microplate reader (FLUOstar® Omega, BMG Labtech) at 580 nm (excitation wavelength 540 nm). Response to treatments was quantified by evaluating EC_{50} values (concentration of inhibitor that leads to half-maximum viability response determined by Hill fit).

Clonogenic cell survival assays

Clonogenic survival of HeLa cell monolayers was evaluated using cell densities applied in the extracellular acidification assay to determine the effect of inhibitors on the clonogenic cell survival while having the same acidification conditions. Cells were exposed to 10–50 μM VR16-09, VD11-4-2, VD12-09, or 0.25% DMSO for 72 h upon normoxic or hypoxic conditions (0.2% O_2). Such doses of inhibitors significantly reduced hypoxia-induced acidification. Then cells were trypsinized, reseeded in triplicate with known cell densities and allowed to form colonies for 14 days. To test inhibitors in 3D cell models, non-hypoxic and hypoxic H460 spheroids were exposed to 5–15 μM doses of VR16-09 or 0.25% DMSO for 24 h on day 4 or day 11, respectively. Single cell suspensions were prepared and cells were plated in triplicate with known cell densities and allowed to form colonies for 14 days. Colonies were quantified after staining and fixation with 0.4% methylene blue in 70% ethanol. Surviving fraction was normalized to vehicle (DMSO).

Spheroid growth

To prepare plates for the growth of attachment-free H460 spheroids, autoclaved 1.5% w/v agarose (Sigma-Aldrich) was dispensed in the inner 60 wells of 96-well plates (50 μL/well) and left for polymerization at room temperature for 30 min. H460 cells were plated in modified 96-well plates to the surface of agarose menisci with a density of 500 cells/well. The DMEM was refreshed every two days. After 7 or 11 days in culture, spheroids were incubated with 20 μg/mL pimonidazole (PIMO, Hypoxyprobe-1, HP-1000, BioConnect) for 2 h at 37° C, collected and cryoconserved for immunofluorescence analysis (see below). In parallel 4 or 11 days after cell seeding, spheroids of homogeneous volume were treated with 5–15 μM VR16-09 or 0.25% DMSO for 24 h and collected for clonogenic survival assay.

Western blot

Protein isolates were prepared by incubating scraped cells in RIPA buffer on ice for 30 min, followed by centrifugation to remove cell debris. Protein concentrations were determined using Bradford protein quantification reagent (BioRad). Western blot was performed using primary antibodies, including mouse anti-CA IX (M75, 1:40, kindly provided by Silvia Pastorekova, Institute of Virology, Slovak Academy of Science, Slovak Republic), mouse anti-CA XII (clone 15A4, 1:100, kindly provided by Aurelija Žvirblienė, Institute of Biotechnology, Vilnius University, Lithuania), rabbit anti-MCT1 (1:100), rabbit anti-MCT4 (1:400, kindly provided by Holger M. Becker, University of Veterinary Medicine Hannover, Hannover, Germany), rabbit anti-lamin A (1:10.000, Sigma-Aldrich), and mouse anti-actin (1:2.000.000, MP Biomedicals). Primary antibodies were incubated overnight at 4° C, whereas horseradish peroxidase-linked secondary antibodies (1:2.000, Cell Signaling) were incubated for 1 h at room temperature. Amersham ECL Western Blotting Detection Reagent (GE Healthcare Life Sciences) was applied for the detection of CA XII, MCT1, MCT4, and lamin A, while SuperSignal™ West Pico PLUS Chemiluminescent Substrate (Life Technologies) was used for the visualization of CA IX and actin.

Immunofluorescence analysis

H460 spheroids of day 7 and day 11 were cryoconserved. Frozen sections (7 μm) of spheroids were fixed in acetone (4° C, 10 min), air-dried and rehydrated in phosphate buffered saline (PBS). Non-specific binding

was blocked by incubation with 0.5% goat serum in PBS for 30 min at room temperature. Sections were stained (37° C, 1 h) using primary rabbit anti-PIMO (1:250) or mouse anti-CA IX (1:100, M75), followed by incubation (37° C, 1 h) with secondary goat anti-rabbit Alexa488 or goat anti-mouse Alexa594, respectively (both 1:500, from Invitrogen). Nuclei were stained with DAPI (final concentration 5 μg/mL) for 2 min at room temperature. Staining without primary antibody was used as negative control. Sections were viewed at 10× magnification by Nikon Eclipse E800 microscope (Nikon Instruments Inc.).

Statistics

Statistical analysis was performed using GraphPad Prism (version 6.01). A non-parametric Mann-Whitney *U* test for small groups was applied to evaluate the statistical significance of differences between two independent groups of variables and $p < 0.05$ was assumed to be significant ($^{*}p < 0.05$; $^{**}p < 0.01$, $^{***}p < 0.001$, $^{****}p < 0.0001$).

CONCLUSIONS

In conclusion, the integrative set of synthesis, inhibitory activities, biophysical binding profiles, crystallographic analysis, and effects in 2D and 3D cancer cell culture models is described in the present study. X-ray analysis demonstrated novel, previously unseen conformational changes in CA IX active site due to ligand binding. Our compounds exhibited high affinity and selectivity towards recombinant CA IX, reached nanomolar CA IX-dependent functional effects as well reduced hypoxia-induced acidification in a variety of cancer cell lines. Interestingly, hypoxia-dependent reduction of clonogenic survival was only observed in spheroids, highlighting the importance of investigating CA IX-targeting compounds in 3D cell models resembling the naturally occurring hypoxic microenvironment with clonogenic survival as endpoint. The newly designed compounds are therefore promising agents for CA IX-specific therapy.

ACKNOWLEDGMENTS

We thank Rianne Biemans and Natasja Lieuwes for their skillful assistance with viability, clonogenic survival, and extracellular pH measuring experiments. The work was supported by grants from the Research Council of Lithuania (Jurgita Matulienė, SEN-04/2015), by the Deutsche Forschungsgemeinschaft (Holger M. Becker, BE 4310/6-1), by the European Research Council (Philippe Lambin, Hypoximmuno, ERC-ADG-2015, n° 694812), and the Dutch Cancer Society (Philippe Lambin, Ludwig J. Dubois, UM 2012-5394 and MAC 2013-6089).

CONFLICTS OF INTEREST

DM declares that he has patents and patent applications pending on CA inhibitors.

PDB ID CODES

Atomic coordinates along with experimental data of CA IX in complex with following compounds were deposited in Protein Data Bank: VR16-09 (PDB ID: 6G98), VR16-10 (PDB ID: 6G9U), VD12-09 (PDB ID: 6FE0) and VD11-4-2 (PDB ID: 6FE1) Coordinates of unliganded CA IX X-ray structure were also deposited (PDB ID: 6FE2).

REFERENCES

1. Harris AL. Hypoxia—a key regulatory factor in tumour growth. Nat Rev Cancer. 2002; 2:38–47. https://doi.org/10.1038/nrc704.
2. Pettersen EO, Ebbesen P, Gieling RG, Williams KJ, Dubois L, Lambin P, Ward C, Meehan J, Kunkler IH, Langdon SP, Ree AH, Flatmark K, Lyng H, et al. Targeting tumour hypoxia to prevent cancer metastasis. From biology, biosensing and technology to drug development: the METOXIA consortium. J Enzyme Inhib Med Chem. 2015; 30:689–721. https://doi.org/10.3109/14756366.2014.966704.
3. Höckel M, Vaupel P. Tumor hypoxia: definitions and current clinical, biologic, and molecular aspects. J Natl Cancer Inst. 2001; 93:266–76. https://doi.org/10.1093/jnci/93.4.266.
4. Wilson WR, Hay MP. Targeting hypoxia in cancer therapy. Nat Rev Cancer. 2011; 11:393–410. https://doi.org/10.1038/nrc3064.
5. Wojtkowiak JW, Verduzco D, Schramm KJ, Gillies RJ. Drug resistance and cellular adaptation to tumor acidic pH microenvironment. Mol Pharm. 2011; 8:2032–38. https://doi.org/10.1021/mp200292c.
6. Pastoreková S, Parkkila S, Parkkila AK, Opavský R, Zelník V, Saarnio J, Pastorek J. Carbonic anhydrase IX, MN/CA IX: analysis of stomach complementary DNA sequence and expression in human and rat alimentary tracts. Gastroenterology. 1997; 112:398–408. https://doi.org/10.1053/gast.1997.v112.pm9024293.
7. Wykoff CC, Beasley NJ, Watson PH, Turner KJ, Pastorek J, Sibtain A, Wilson GD, Turley H, Talks KL, Maxwell PH, Pugh CW, Ratcliffe PJ, Harris AL. Hypoxia-inducible expression of tumor-associated carbonic anhydrases. Cancer Res. 2000; 60:7075–83.
8. Simko V, Takacova M, Debreova M, Laposova K, Ondriskova-Panisova E, Pastorekova S, Csaderova L, Pastorek J. Dexamethasone downregulates expression of carbonic anhydrase IX via HIF-1α and NF-κB-dependent

mechanisms. Int J Oncol. 2016; 49:1277–88. https://doi.org/10.3892/ijo.2016.3621.

9. Andreucci E, Peppicelli S, Carta F, Brisotto G, Biscontin E, Ruzzolini J, Bianchini F, Biagioni A, Supuran CT, Calorini L. Carbonic anhydrase IX inhibition affects viability of cancer cells adapted to extracellular acidosis. J Mol Med (Berl). 2017; 95:1341–53. https://doi.org/10.1007/s00109-017-1590-9.

10. Ihnatko R, Kubes M, Takacova M, Sedlakova O, Sedlak J, Pastorek J, Kopacek J, Pastorekova S. Extracellular acidosis elevates carbonic anhydrase IX in human glioblastoma cells via transcriptional modulation that does not depend on hypoxia. Int J Oncol. 2006; 29:1025–33.

11. Zatovicova M, Sedlakova O, Svastova E, Ohradanova A, Ciampor F, Arribas J, Pastorek J, Pastorekova S. Ectodomain shedding of the hypoxia-induced carbonic anhydrase IX is a metalloprotease-dependent process regulated by TACE/ADAM17. Br J Cancer. 2005; 93:1267–76. https://doi.org/10.1038/sj.bjc.6602861.

12. Závada J, Závadová Z, Zat'ovicová M, Hyrsl L, Kawaciuk I. Soluble form of carbonic anhydrase IX (CA IX) in the serum and urine of renal carcinoma patients. Br J Cancer. 2003; 89:1067–71. https://doi.org/10.1038/sj.bjc.6601264.

13. Pastorek J, Pastoreková S, Callebaut I, Mornon JP, Zelník V, Opavský R, Zat'ovicová M, Liao S, Portetelle D, Stanbridge EJ, et al. Cloning and characterization of MN, a human tumor-associated protein with a domain homologous to carbonic anhydrase and a putative helix-loop-helix DNA binding segment. Oncogene. 1994; 9:2877–88.

14. Svastová E, Hulíková A, Rafajová M, Zat'ovicová M, Gibadulinová A, Casini A, Cecchi A, Scozzafava A, Supuran CT, Pastorek J, Pastoreková S. Hypoxia activates the capacity of tumor-associated carbonic anhydrase IX to acidify extracellular pH. FEBS Lett. 2004; 577:439–45. https://doi.org/10.1016/j.febslet.2004.10.043.

15. Ditte P, Dequiedt F, Svastova E, Hulikova A, Ohradanova-Repic A, Zatovicova M, Csaderova L, Kopacek J, Supuran CT, Pastorekova S, Pastorek J. Phosphorylation of carbonic anhydrase IX controls its ability to mediate extracellular acidification in hypoxic tumors. Cancer Res. 2011; 71:7558–67. https://doi.org/10.1158/0008-5472.CAN-11-2520.

16. Swietach P, Vaughan-Jones RD, Harris AL. Regulation of tumor pH and the role of carbonic anhydrase 9. Cancer Metastasis Rev. 2007; 26:299–310. https://doi.org/10.1007/s10555-007-9064-0.

17. Csaderova L, Debreova M, Radvak P, Stano M, Vrestiakova M, Kopacek J, Pastorekova S, Svastova E. The effect of carbonic anhydrase IX on focal contacts during cell spreading and migration. Front Physiol. 2013; 4:271. https://doi.org/10.3389/fphys.2013.00271.

18. Svastova E, Witarski W, Csaderova L, Kosik I, Skvarkova L, Hulikova A, Zatovicova M, Barathova M, Kopacek J, Pastorek J, Pastorekova S. Carbonic anhydrase IX interacts with bicarbonate transporters in lamellipodia and increases cell migration via its catalytic domain. J Biol Chem. 2012; 287:3392–402. https://doi.org/10.1074/jbc.M111.286062.

19. Pastorek J, Pastorekova S. Hypoxia-induced carbonic anhydrase IX as a target for cancer therapy: from biology to clinical use. Semin Cancer Biol. 2015; 31:52–64. https://doi.org/10.1016/j.semcancer.2014.08.002.

20. Gaspari R, Rechlin C, Heine A, Bottegoni G, Rocchia W, Schwarz D, Bomke J, Gerber HD, Klebe G, Cavalli A. Kinetic and Structural Insights into the Mechanism of Binding of Sulfonamides to Human Carbonic Anhydrase by Computational and Experimental Studies. J Med Chem. 2016; 59:4245–56. https://doi.org/10.1021/acs.jmedchem.5b01643.

21. Krishnamurthy VM, Bohall BR, Kim CY, Moustakas DT, Christianson DW, Whitesides GM. Thermodynamic parameters for the association of fluorinated benzenesulfonamides with bovine carbonic anhydrase II. Chem Asian J. 2007; 2:94–105. https://doi.org/10.1002/asia.200600360.

22. Krishnamurthy VM, Kaufman GK, Urbach AR, Gitlin I, Gudiksen KL, Weibel DB, Whitesides GM. Carbonic anhydrase as a model for biophysical and physical-organic studies of proteins and protein-ligand binding. Chem Rev. 2008; 108:946–1051. https://doi.org/10.1021/cr050262p.

23. Zhou Y, Wang J, Gu Z, Wang S, Zhu W, Aceña JL, Soloshonok VA, Izawa K, Liu H. Next Generation of Fluorine-Containing Pharmaceuticals, Compounds Currently in Phase II-III Clinical Trials of Major Pharmaceutical Companies: New Structural Trends and Therapeutic Areas. Chem Rev. 2016; 116:422–518. https://doi.org/10.1021/acs.chemrev.5b00392.

24. Dudutienė V, Zubrienė A, Smirnov A, Timm DD, Smirnovienė J, Kazokaitė J, Michailovienė V, Zakšauskas A, Manakova E, Gražulis S, Matulis D. Functionalization of fluorinated benzenesulfonamides and their inhibitory properties toward carbonic anhydrases. ChemMedChem. 2015; 10:662–87. https://doi.org/10.1002/cmdc.201402490.

25. Dudutienė V, Zubrienė A, Smirnov A, Gylytė J, Timm D, Manakova E, Gražulis S, Matulis D. 4-Substituted-2,3,5,6-tetrafluorobenzenesulfonamides as inhibitors of carbonic anhydrases I, II, VII, XII, and XIII. Bioorg Med Chem. 2013; 21:2093–106. https://doi.org/10.1016/j.bmc.2013.01.008.

26. Dudutienė V, Matulienė J, Smirnov A, Timm DD, Zubrienė A, Baranauskienė L, Morkūnaite V, Smirnovienė J, Michailovienė V, Juozapaitienė V, Mickevičiūtė A, Kazokaitė J, Bakšytė S, et al. Discovery and characterization of novel selective inhibitors of carbonic anhydrase IX. J Med Chem. 2014; 57:9435–46. https://doi.org/10.1021/jm501003k.

27. Lou Y, McDonald PC, Oloumi A, Chia S, Ostlund C, Ahmadi A, Kyle A, Auf dem Keller U, Leung S, Huntsman D, Clarke B, Sutherland BW, Waterhouse D, et al. Targeting tumor hypoxia: suppression of breast tumor growth and metastasis by novel carbonic anhydrase IX

inhibitors. Cancer Res. 2011; 71:3364–76. https://doi.org/10.1158/0008-5472.CAN-10-4261.

28. Pacchiano F, Carta F, McDonald PC, Lou Y, Vullo D, Scozzafava A, Dedhar S, Supuran CT. Ureido-substituted benzenesulfonamides potently inhibit carbonic anhydrase IX and show antimetastatic activity in a model of breast cancer metastasis. J Med Chem. 2011; 54:1896–902. https://doi.org/10.1021/jm101541x.

29. Alterio V, Hilvo M, Di Fiore A, Supuran CT, Pan P, Parkkila S, Scaloni A, Pastorek J, Pastorekova S, Pedone C, Scozzafava A, Monti SM, De Simone G. Crystal structure of the catalytic domain of the tumor-associated human carbonic anhydrase IX. Proc Natl Acad Sci USA. 2009; 106:16233–38. https://doi.org/10.1073/pnas.0908301106.

30. Leitans J, Kazaks A, Balode A, Ivanova J, Zalubovskis R, Supuran CT, Tars K. Efficient Expression and Crystallization System of Cancer-Associated Carbonic Anhydrase Isoform IX. J Med Chem. 2015; 58:9004–09. https://doi.org/10.1021/acs.jmedchem.5b01343.

31. Li Y, Tu C, Wang H, Silverman DN, Frost SC. Catalysis and pH control by membrane-associated carbonic anhydrase IX in MDA-MB-231 breast cancer cells. J Biol Chem. 2011; 286:15789–96. https://doi.org/10.1074/jbc.M110.188524.

32. Tu C, Foster L, Alvarado A, McKenna R, Silverman DN, Frost SC. Role of zinc in catalytic activity of carbonic anhydrase IX. Arch Biochem Biophys. 2012; 521:90–94. https://doi.org/10.1016/j.abb.2012.03.017.

33. Dubois L, Douma K, Supuran CT, Chiu RK, van Zandvoort MA, Pastoreková S, Scozzafava A, Wouters BG, Lambin P. Imaging the hypoxia surrogate marker CA IX requires expression and catalytic activity for binding fluorescent sulfonamide inhibitors. Radiother Oncol. 2007; 83:367–73. https://doi.org/10.1016/j.radonc.2007.04.018.

34. Rami M, Dubois L, Parvathaneni NK, Alterio V, van Kuijk SJ, Monti SM, Lambin P, De Simone G, Supuran CT, Winum JY. Hypoxia-targeting carbonic anhydrase IX inhibitors by a new series of nitroimidazole-sulfonamides/sulfamides/sulfamates. J Med Chem. 2013; 56:8512–20. https://doi.org/10.1021/jm4009532.

35. Dubois L, Peeters SG, van Kuijk SJ, Yaromina A, Lieuwes NG, Saraya R, Biemans R, Rami M, Parvathaneni NK, Vullo D, Vooijs M, Supuran CT, Winum JY, Lambin P. Targeting carbonic anhydrase IX by nitroimidazole based sulfamides enhances the therapeutic effect of tumor irradiation: a new concept of dual targeting drugs. Radiother Oncol. 2013; 108:523–28. https://doi.org/10.1016/j.radonc.2013.06.018.

36. Jamali S, Klier M, Ames S, Barros LF, McKenna R, Deitmer JW, Becker HM. Hypoxia-induced carbonic anhydrase IX facilitates lactate flux in human breast cancer cells by non-catalytic function. Sci Rep. 2015; 5:13605. https://doi.org/10.1038/srep13605.

37. Ullah MS, Davies AJ, Halestrap AP. The plasma membrane lactate transporter MCT4, but not MCT1, is up-regulated by hypoxia through a HIF-1alpha-dependent mechanism. J Biol Chem. 2006; 281:9030–37. https://doi.org/10.1074/jbc.M511397200.

38. Angeli A, Tanini D, Peat TS, Di Cesare Mannelli L, Bartolucci G, Capperucci A, Ghelardini C, Supuran CT, Carta F. Discovery of New Selenoureido Analogues of 4-(4-Fluorophenylureido)benzenesulfonamide as Carbonic Anhydrase Inhibitors. ACS Med Chem Lett. 2017; 8:963–68. https://doi.org/10.1021/acsmedchemlett.7b00280.

39. Meehan J, Ward C, Turnbull A, Bukowski-Wills J, Finch AJ, Jarman EJ, Xintaropoulou C, Martinez-Perez C, Gray M, Pearson M, Mullen P, Supuran CT, Carta F, et al. Inhibition of pH regulation as a therapeutic strategy in hypoxic human breast cancer cells. Oncotarget. 2017; 8:42857–75. https://doi.org/10.18632/oncotarget.17143.

40. van Kuijk SJ, Parvathaneni NK, Niemans R, van Gisbergen MW, Carta F, Vullo D, Pastorekova S, Yaromina A, Supuran CT, Dubois LJ, Winum JY, Lambin P. New approach of delivering cytotoxic drugs towards CAIX expressing cells: A concept of dual-target drugs. Eur J Med Chem. 2017; 127:691–702. https://doi.org/10.1016/j.ejmech.2016.10.037.

41. Chiche J, Ilc K, Laferrière J, Trottier E, Dayan F, Mazure NM, Brahimi-Horn MC, Pouysségur J. Hypoxia-inducible carbonic anhydrase IX and XII promote tumor cell growth by counteracting acidosis through the regulation of the intracellular pH. Cancer Res. 2009; 69:358–68. https://doi.org/10.1158/0008-5472.CAN-08-2470.

42. Zanoni M, Piccinini F, Arienti C, Zamagni A, Santi S, Polico R, Bevilacqua A, Tesei A. 3D tumor spheroid models for *in vitro* therapeutic screening: a systematic approach to enhance the biological relevance of data obtained. Sci Rep. 2016; 6:19103. https://doi.org/10.1038/srep19103.

43. Baker BM, Chen CS. Deconstructing the third dimension: how 3D culture microenvironments alter cellular cues. J Cell Sci. 2012; 125:3015–24. https://doi.org/10.1242/jcs.079509.

44. Kimlin LC, Casagrande G, Virador VM. In vitro three-dimensional (3D) models in cancer research: an update. Mol Carcinog. 2013; 52:167–82. https://doi.org/10.1002/mc.21844.

45. Wang Z, Tang J, Salomon CE, Dreis CD, Vince R. Pharmacophore and structure-activity relationships of integrase inhibition within a dual inhibitor scaffold of HIV reverse transcriptase and integrase. Bioorg Med Chem. 2010; 18:4202–11. https://doi.org/10.1016/j.bmc.2010.05.004.

46. Foreman EL, McElvain SM. The Reaction of Organic Halides with Piperidine. V. Negatively Substituted Ethyl Bromides. J Am Chem Soc. 1940; 62:1435–38. https://doi.org/10.1021/ja01863a029.

47. Takano S, Yamazoe S, Koyasu K, Tsukuda T. Slow-Reduction Synthesis of a Thiolate-Protected One-Dimensional Gold Cluster Showing an Intense

Near-Infrared Absorption. J Am Chem Soc. 2015; 137:7027–30. https://doi.org/10.1021/jacs.5b03251.

48. Robson P, Smith TA, Stephens R, Tatlow JC. Aromatic Polyfluoro-Compounds. Part XIII. Derivatives of Penta- and 2,3,5,6-Tetra-Fluorothiophenol. J Chem Soc. 1963; 0:3692–703. https://doi.org/10.1039/jr9630003692.

49. Khalifah RG. The carbon dioxide hydration activity of carbonic anhydrase. I. Stop-flow kinetic studies on the native human isoenzymes B and C. J Biol Chem. 1971; 246:2561–73.

50. Smirnovienė J, Smirnovas V, Matulis D. Picomolar inhibitors of carbonic anhydrase: importance of inhibition and binding assays. Anal Biochem. 2017; 522:61–72. https://doi.org/10.1016/j.ab.2017.01.022.

51. Baranauskienė L, Hilvo M, Matulienė J, Golovenko D, Manakova E, Dudutienė V, Michailovienė V, Torresan J, Jachno J, Parkkila S, Maresca A, Supuran CT, Gražulis S, Matulis D. Inhibition and binding studies of carbonic anhydrase isozymes I, II and IX with benzimidazo[1,2-c][1,2,3]thiadiazole-7-sulphonamides. J Enzyme Inhib Med Chem. 2010; 25:863–70. https://doi.org/10.3109/14756360903571685.

52. Leslie AG. Recent changes to the MOSFLM package for processing film and image plate data. Newsletter on Protein Crystallography; 1992. p. 26.

53. Evans PR. SCALA. Newsletter on Protein Crystallography. 1997; 33:22–24.

54. Vagin A, Teplyakov A. MOLREP: An Automated Program for Molecular Replacement. J Appl Cryst. 1997; 30:1022–25. https://doi.org/10.1107/S0021889897006766.

55. Vagin AA, Murshudov GN, Strokopytov BV. BLANC: The Program Suite for Protein Crystallography. J Appl Cryst. 1998; 31:98–102. https://doi.org/10.1107/S0021889897007796.

56. Ran FA, Hsu PD, Wright J, Agarwala V, Scott DA, Zhang F. Genome engineering using the CRISPR-Cas9 system. Nat Protoc. 2013; 8:2281–308. https://doi.org/10.1038/nprot.2013.143.

57. Becker HM, Hirnet D, Fecher-Trost C, Sültemeyer D, Deitmer JW. Transport activity of MCT1 expressed in Xenopus oocytes is increased by interaction with carbonic anhydrase. J Biol Chem. 2005; 280:39882–89. https://doi.org/10.1074/jbc.M503081200.

58. Tu CK, Silverman DN. Solvent deuterium isotope effects in the catalysis of oxygen-18 exchange by human carbonic anhydrase II. Biochemistry. 1982; 21:6353–60. https://doi.org/10.1021/bi00268a006.

59. Price GD, Badger MR. Isolation and Characterization of High CO(2)-Requiring-Mutants of the Cyanobacterium Synechococcus PCC7942 : Two Phenotypes that Accumulate Inorganic Carbon but Are Apparently Unable to Generate CO(2) within the Carboxysome. Plant Physiol. 1989; 91:514–25. https://doi.org/10.1104/pp.91.2.514.

60. Cimmperman P, Baranauskienė L, Jachimoviciūte S, Jachno J, Torresan J, Michailovienė V, Matulienė J, Sereikaitė J, Bumelis V, Matulis D. A quantitative model of thermal stabilization and destabilization of proteins by ligands. Biophys J. 2008; 95:3222–31. https://doi.org/10.1529/biophysj.108.134973.

61. The PyMOL Molecular Graphics System, version 1.5.0.1. New York: Schrödinger, LLC; 2012.

4. Discussion

CAs are widespread in many life forms. There are at least 16 mammalian CA isoforms and some of them are associated with different diseases. In general – the enzymatic activities of various CA isoforms are favorable for various physiological processes, but in some cases, they promote development of various diseases (Supuran, 2012). The main focus of my thesis was on structural studies of ligand complexes with hCA II and hCA IX. hCA IX is considered to favor tumor cell proliferation (Chiche et al., 2009), while inhibition of hCA II lowers the intraocular pressure, thus relieving symptoms of glaucoma and lowering damage to the eye nerve (Mincione et al., 2008). All of the mammalian CAs display relatively high sequence identity but differ by localization in the cell and tissue and despite the same catalyzed reaction play different physiological roles. hCA isoforms display high sequence identity (23%-60%), and residues forming the active site pocket are even more conservative (Pinard et al., 2015). Only six residues out of 21 in the active site pocket are highly diverse between the isoforms thus making isoform selective inhibitor design a challenging task. Selective inhibition of an unwanted isoform is crucial to avoid disfunction of vital processes. Currently available medications, such as Diamox (acetazolamide), have poor selectivity and they target most of the CA isoforms with nanomolar affinity, thus displaying numerous side effects (Supuran, 2008b). Designing a molecule which fits the active site of CA enzyme so perfectly, that it has significantly lower affinity to all other isoforms is an ongoing research challenge.

Available structural data of the protein – ligand interactions are essential for rational drug design. X-ray crystallography can give precise insight in ligand-enzyme complexes at atomic resolution. The obtained information notably increases the chance to design a compound targeted towards a specific isoform.

At the beginning of my thesis work I crystallized hCA II in complex with five similar thiophene-2-sulfonamides. The thiophene-2-sulfonamides were designed based on available structural data of similar compounds - thiadiazole-2-sulfonamides. Acetazolamide is thiadiazole-2-sulfonamide and it has been determined that acetazolamide with its thiadiazol moiety forms a hydrogen bond to highly conservative hCA active site residue Thr200. Since thiophene-2-sulfonamide has no nitrogen atoms to form a hydrogen bond at that position we expected some difference in the ligand positioning due to weaker Van der Waals forces. Analysis of X-ray data showed that four of the compounds were bound very similarly within the active site of hCA II

interacting with the polar part, while compound with more hydrophobic tail moiety fitted in the hydrophobic part of hCA II. From the obtained results it could be concluded that orientation and binding mode of compound in the active site of enzyme can be directly affected solely by hydrophobicity of its tail moiety. Importantly, the obtained results can be used to generate an improved compound with combined binding properties of parent compounds – potential "dual tail" compounds possessing both polar and non-polar tails for potentially wider active site coverage and higher selectivity.

Artificial sweetener saccharine was previously determined as a CA inhibitor by another research group with increase in selectivity comparing to sulfonamide class inhibitors (Köhler et al., 2007). It was previously determined that saccharine moiety with attached sulfonamide group prefers binding to the enzyme through its sulfonamide ZBG, as it is energetically more favorable (Alterio et al., 2015b). As newly synthesized compound tail moiety was attached to saccharine ZBG it was expected that compounds will bind to the Zn^{2+} ion through its sulfonamide group. The acquired crystal structures had atomic resolution and the attained electron density map clearly demonstrated an unexpected hydrolysis of the isothiazole cycle in the saccharine moiety. Although hydrolysis of the isothiazole cycle most probably occurred due to the high pH level of the precipitant in the crystallization mix, the binding mode of the compound allowed design of further CA-ligands with series of new open-ring saccharine derivatives with increase in selectivity to some of the CA isoforms (Ivanova et al., 2017). Although structural studies of hCA II are nothing unique, considering more than 775 structures available on the PDB, hCA II is still the most popular hCA isoform for studies of new ligand types due to easy experimental procedures. Even so, despite the massive structural data of hCA II, there is still no isoform specific inhibitor for hCA II and drug design for anti-glaucoma medicaments and diuretics is still an ongoing research field.

One of the main targets for pharmacologically important enzyme drug design in the CA field is tumor associated hCA IX. The available data in literature suggests that enzymatic activity of hCA IX favors tumor growth and its inhibition could prevent cancer cell spread (Chen et al., 2005). Limited expression of hCA IX in normal tissues and overexpression in many tumors makes it a valid target for anti-cancer drug research (Mahalingam et al., 2018). A serious problem for design of an isoform specific hCA IX inhibitor was the lack of structural data about hCA IX – ligand interactions. Until 2015 there was only one hCA IX structure available in the PDB **(**Alterio et al., 2009). Repeating crystallization conditions from the first published hCA IX catalytic domain structure failed and at that time the described expression method in baculovirus yielded very limited

quantity of protein. Therefore, we decided to develop a new protein expression and purification pathway suitable for structural studies. We managed to express a soluble and active hCA IX catalytic domain. Furthermore, we produced hCA IX crystals in complex with previously described thiophene-2-sulfonamides. Comparing binding modes of compounds among hCA II and hCA IX isoforms it was noted that all tested compounds were bound quite differently within the active sites of hCA IX and hCA II. By analyzing the binding modes, we concluded that all of the tested thiophene-2-sulfonamides were oriented to the part of the enzyme active site which differs most between all of the mammalian CA isoforms. Orientation differences of the tested thiophene-2-sulfonamides can be explained by potential collision of the tail moiety with hCA II residue Phe131. Further research of thiophene-2-sulfonamide derivatives is ongoing targeting the most diverse hCA residues.

Using our designed hCA IX catalytic domain expression, purification and crystallization system, multiple highly efficient fluorinated benzene-sulfonamides were co-crystallized with the enzyme. From the obtained data we solved several high resolution structures of ligand-hCA IX complexes of various nanomolar CA inhibitors. The obtained structure of inhibitor VR16-09 in complex with hCA IX could explain the observed 1,000,000 fold selectivity of binding to hCA IX over hCA II. Being a good example of selective inhibitor design, VR16-09 made specific interactions in both polar and hydrophobic parts of the active site.

By comparison of crystallographic and kinetic studies, it can be can concluded that the 8/12 carbon ring at the *ortho* position results in a lower affinity towards many hCA isoforms whilst remaining a pico/nano molar inhibitor to hCA IX. The fluorobenzene cycle is positioned similarly in hCA IX-VR16-09, hCA IX-VR16-10 and hCA IX-VD12-09 crystal structures, despite differences in tail moieties. Fluorobenzene cycle fit in the conservative part of hCA IX and can be used for further inhibitor design. There are small differences regarding affinities to some hCA isoforms among the compounds VD12-09 and VR16-10, although they are structurally similar and differ only in polar tail moiety parts. The hydrophobic cycloalkane moiety and binding mode is identical within hCA IX of these compounds. Judging from X-ray data, the hydrophilic tail moieties of compounds VD12-09 and VR16-10 are oriented to the conservative part of hCA.

If bound to hCA II, hydrophobic tails of VD12-09 and VR16-10 could potentially clash with one of the most diverse residues - Phe131. This provides higher selectivity against hCA II and many other hCA isoforms.

The cycloalkane group at *meta*- position results in much weaker selectivity against hCA II for compound VD11-4-2. The big eight carbon cycle at *meta*- position does not affect the positioning of the hydrophobic ring but has an overall effect on fluorobenzene cycle orientation. Another difference between VD11-4-2 and other compounds is the fact that the there is -SO_2- group instead of -S- at the *para*- tail which results in two additional hydrogen bonds with residues Asn62 and Gln92. Sulfonyl part of the VD11-4-2 hydrophilic tail moiety linker perfectly fits between two polar residues occupying that part of the hCA IX active site thus potentially providing further clue for rational design of polar tail of similar derivatives.

In conclusion, my work has provided several clues for isoform-specific inhibitor design of hCAs. The most important part of the performed study was creation of efficient hCA IX production, purification and crystallization system, which was successfully used for further structural and kinetic studies.

5. Conclusions

1. Thiophene-2-sulfonamides are effective human carbonic anhydrase inhibitors, with tail moiety orientation towards the hot spot for isoform selective drug design.
2. Ligand orientation within the active site of carbonic anhydrases can be affected solely by hydrophobicity of tail moiety.
3. Isothiazole cycle in saccharin moiety can be hydrolyzed in high pH environment forming open ring saccharine derivatives which work as semi-selective CA inhibitors.
4. Genetic fusion of catalytic domain of hCA IX with MBP in combination with expression in *Pichia pastoris* results in high yields of soluble and enzymatically active enzyme.
5. Fluorinated benzene-sulfonamides with cycloalkane moiety at the *ortho* position are nanomolar hCA IX inhibitors with notable increase in selectivity, comparing to widely used carbonic anhydrase inhibitors.
6. Fluorinated benzene-sulfonamides can alter enzyme active site pocket conformation by changing the side chain rotamers to their favorable orientation.

6. Main thesis for defense

1. Thiophene-2-sulfonamides can be used for targeting the most diverse region of hCA active site.
2. Open form 1-N-substituted saccharins are highly efficient hCA II inhibitors.
3. Expression system in *Pichia pastoris* is suitable for production of hCA IX catalytic domain in high amounts.
4. Increase in selectivity for fluorinated benzene-sulfonamides with cycloalkane tail moiety at *ortho*- position interacts with the most diverse hCA residues thus providing a promising anti-cancer drug candidate.

7. List of original publications

1. **Leitans J**, Sprudza A, Tanc M, Vozny I, Zalubovskis R, Tars K, Supuran CT. 2013. 5-Substituted-(1,2,3-triazol-4-yl)thiophene-2-sulfonamides strongly inhibit human carbonic anhydrases I, II, IX and XII: solution and X-ray crystallographic studies. Bioorganic & Medicinal Chemistry, 21(17):5130-5138.
2. Ivanova J, **Leitans J**, Tanc M, Kazaks A, Zalubovskis R, Supuran CT, Tars K. 2015. X-ray crystallography-promoted drug design of carbonic anhydrase inhibitors. Chemical Communications, 51(33):7108-7111.
3. **Leitans J**, Kazaks A, Balode A, Ivanova J, Zalubovskis R, Supuran CT, Tars K. 2015. Efficient Expression and Crystallization System of Cancer-Associated Carbonic Anhydrase Isoform IX. Journal of Medicinal Chemistry, 58(22):9004-9009.
4. Kazokaite J, Niemans R, Dudutiene V, Becker HM, **Leitans J**, Zubriene A, Baranauskiene L, Gondi G, Zeidler R, Matuliene J, Tars K, Yaromina A, Lambin P, Dubois LJ, Matulis D. 2018. Novel fluorinated carbonic anhydrase IX inhibitors reduce hypoxia-induced acidification and clonogenic survival of cancer cells. Oncotarget, 9(42):26800-26816.

8. Approbation of the research (thesis related)

Related publications, not included in the thesis:

1. Buğday N, Küçükbay FZ, Küçükbay H, Bua S, Bartolucci G, **Leitans J**, Kazaks A, Tars K, Supuran CT. 2018. Synthesis of novel dipeptide sulfonamide conjugates with effective carbonic anhydrase I, II, IX, and XII inhibitory properties. Bioorganic Chemistry, 81:311-318.
2. Gul HI, Yamali C, Sakagami H, Angeli A, **Leitans J**, Kazaks A, Tars K, Ozgun DO, Supuran CT. 2018. New anticancer drug candidates sulfonamides as selective hCA IX or hCA XII inhibitors. Bioorganic Chemistry, 77:411-419.
3. Bianco G, Meleddu R, Distinto S, Cottiglia F, Gaspari M, Melis C, Corona A, Angius R, Angeli A, Taverna D, Alcaro S, **Leitans J**, Kazaks A, Tars K, Supuran CT, Maccioni E. 2017. NAcylbenzenesulfonamide Dihydro-1,3,4-oxadiazole Hybrids: Seeking Selectivity toward Carbonic Anhydrase Isoforms. ACS Medicinal Chemistry Letters, 8(8):792-796.
4. Pustenko A, Stepanovs D, Žalubovskis R, Vullo D, Kazaks A, **Leitans J**, Tars K, Supuran CT. 2017. 3H-1,2-benzoxathiepine 2,2-dioxides: a new class of isoform-selective carbonic anhydrase inhibitors. Journal of Enzyme Inhibition and Medicinal Chemistry, 32(1):767-775.
5. Ivanova J, Carta F, Vullo D, **Leitans J**, Kazaks A, Tars K, Žalubovskis R, Supuran CT. 2017. NSubstituted and ring opened saccharin derivatives selectively inhibit transmembrane, tumorassociated carbonic anhydrases IX and XII. Bioorganic & Medicinal Chemistry, 25(13):3583-3589.
6. Ivanova J, Balode A, Žalubovskis R, **Leitans J**, Kazaks A, Vullo D, Tars K, Supuran CT. 2017. 5- Substituted-benzylsulfanyl-thiophene-2-sulfonamides with effective carbonic anhydrase inhibitory activity: Solution and crystallographic investigations. Bioorganic & Medicinal Chemistry, 25(3):857- 863.
7. Tars K, Vullo D, Kazaks A, **Leitans J**, Lends A, Grandane A, Zalubovskis R, Scozzafava A, Supuran CT. 2013. Sulfocoumarins (1,2-benzoxathiine-2,2-dioxides): a class of potent and isoformselective inhibitors of tumor-associated carbonic anhydrases. Journal of Medicinal Chemistry, 10;56(1):293-300.

Conferences:

E. Bērtulis, **J. Leitāns**, A. Kazāks, K. Tārs. 2018. Structural investigations of carbonic anhydrase isoforms XII and Va. 76th University of Latvia conference - molecular biology section. Riga, Latvia.

J. Leitāns, E.Bertulis, A. Kazāks, K. Tārs. 2017. Structural investigations of carbonic anhydrases for design of selective inhibitors. 75th University of Latvia conference - molecular biology section. Riga, Latvia.

J. Leitans, A. Kazaks, R. Zalubovskis and K. Tars. 2015. Structural basis of saccharine derivative inhibition of carbonic anhydrase IX. 10th International Carbonic Anhydrase Conferance. Māstrihta, Nīderlande. (Best poster in one of three categories).

J. Leitāns, A. Kazāks, R. Žalubovskis, K. Tārs. 2015. Structural investigations of carbonic anhydrases for design of specific inhibitors. 73th University of Latvia conference - molecular biology section. Riga, Latvia.

9. Acknowledgements

This work was supported by the Taiwan-Latvian-Lithuanian collaboration project - Design of Anticancer Pharmaceutical Compounds Using Structure and Energetics of Lead – Target Interaction. I want to thank my supervisor Kaspars Tars, for long years of guidance and outstanding leadership. I acknowledge Andris Kazaks for protein purification by using ion-exchange chromatography and the given effort in hCA IX expression and purification system development. I acknowledge Inara Akopjana for work regarding hCA IX expression and help with *E.coli* expression system. I thank Elviss Dvinskis for a marvelous collaboration as laboratory partners. I thank Janis Rumnieks, Gints Kalnins and Svetlana Kotelovica and other BMC structural biology group colleagues for help during experiments. I also acknowledge all the colleagues that have helped collect crystallographic data at BESSY II, MAX II and MAX IV synchrotrons. I would also want to thank the University of Latvia Foundation for support during my PhD studies. I acknowledge all my co-authors especially Raivis Zalubovskis, Claudiu T. Supuran and Daumantas Matulis.

I would like to thank my mother Inese for support and help during this study process and my friends for moral support.

10. References

Aggarwal M, Boone CD, Kondeti B, McKenna R. 2013. Structural annotation of human carbonic anhydrases. Journal of Enzyme Inhibition and Medicinal Chemistry, 28(2):267-277.

Alterio V, Hilvo M, Di Fiore A, Supuran CT, Pan P, Parkkila S, Scaloni A, Pastorek J, Pastorekova S, Pedone C, Scozzafava A, Monti SM, De Simone G. 2009. Crystal structure of the catalytic domain of the tumor-associated human carbonic anhydrase IX. Proceedings of the National Academy of Sciences of the United States of America, 106(38):16233-16238.

Alterio V, Langella E, De Simone G, Monti SM. 2015a. Cadmium-containing carbonic anhydrase CDCA1 in marine diatom Thalassiosira weissflogii. Marine Drugs, 13(4):1688-1697.

Alterio V, Tanc M, Ivanova J, Zalubovskis R, Vozny I, Monti SM, Di Fiore A, De Simone G, Supuran CT. 2015b. X-ray crystallographic and kinetic investigations of 6-sulfamoyl-saccharin as a carbonic anhydrase inhibitor. Organic & Biomolecular Chemistry, 13(13):4064-4069.

Aminlari A, East M, Wei W, Quillen D. 2008. Topiramate induced acute angle closure glaucoma. The Open Ophthalmology Journal, 2:46-7. doi: 10.2174.

Aspatwar A, Haapanen S, Parkkila S. 2018. An Update on the Metabolic Roles of Carbonic Anhydrases in the Model Alga Chlamydomonas reinhardtii. Metabolites, 8(1). pii: E22.

Aspatwar A, Tolvanen ME, Ortutay C, Parkkila S. 2010. Carbonic anhydrase related protein VIII and its role in neurodegeneration and cancer. Current Pharmaceutical Design, 16(29):3264-3276.

Avvaru BS, Kim CU, Sippel KH, Gruner SM, Agbandje-McKenna M, Silverman DN, McKenna R. 2010. A short, strong hydrogen bond in the active site of human carbonic anhydrase II. Biochemistry, 49(2):249-251.

Banerjee S, Deshpande PA. 2016. On origin and evolution of carbonic anhydrase isozymes: A phylogenetic analysis from whole-enzyme to active site. Computational Biology and Chemistry, 61:121-129.

Behnke CA, Le Trong I, Godden JW, Merritt EA, Teller DC, Bajorath J, Stenkamp RE. 2010. Atomic resolution studies of carbonic anhydrase II. Acta Crystallographica Section D, 66(Pt 5):616-627.

Berg JM, Tymoczko JL, Stryer L. 2002. Biochemistry. 5th edition. New York: W H Freeman, 372-378.

Bhat FA, Ganai BA, Uqab B. 2017. Carbonic Anhydrase: Mechanism, Structure and Importance in Higher Plants. Asian Journal of Plant Science and Research, 7(3):17-23.

Bismar TA, Bianco FJ, Zhang H, Li X, Sarkar FH, Sakr WA, Grignon DJ, Che M. 2003. Quantification of G250 mRNA expression in renal epithelial neoplasms by real-time reverse transcription-PCR of dissected tissue from paraffin sections. Pathology, 35(6):513-517.

Bleumer I, Knuth A, Oosterwijk E, Hofmann R, Varga Z, Lamers C, Kruit W, Melchior S, Mala C, Ullrich S, De Mulder P, Mulders PF, Beck J. 2004. A phase II trial of chimeric monoclonal antibody G250 for advanced renal cell carcinoma patients. British Journal of Cancer, 90(5):985-990.

Bui MH, Seligson D, Han KR, Pantuck AJ, Dorey FJ, Huang Y, Horvath S, Leibovich BC, Chopra S, Liao SY, Stanbridge E, Lerman MI, Palotie A, Figlin RA, Belldegrun AS. 2003. Carbonic anhydrase IX is an independent predictor of survival in advanced renal clear cell carcinoma: implications for prognosis and therapy. Clinical Cancer Research, 9(2):802-811.

Buonanno M, Langella E, Zambrano N, Succoio M, Sasso E, Alterio V, Di Fiore A, Sandomenico A, Supuran CT, Scaloni A, Monti SM, De Simone G1. 2017. Disclosing the Interaction of Carbonic Anhydrase IX with Cullin-Associated NEDD8-Dissociated Protein 1 by Molecular Modeling and Integrated Binding Measurements. ACS Chemical Biology, 12(6):1460-1465.

Capasso C, Supuran CT. 2015. An overview of the alpha-, beta- and gamma-carbonic anhydrases from Bacteria: can bacterial carbonic anhydrases shed new light on evolution of bacteria? Journal of Enzyme Inhibition and Medicinal Chemistry, 30(2):325-332.

Carta F, Supuran CT. 2013. Diuretics with carbonic anhydrase inhibitory action: a patent and literature review (2005 - 2013). Expert Opinion on Therapeutic Patents, 23(6):681-691.

Carta F, Vullo D, Osman SM, AlOthman Z, Supuran CT. 2017. Synthesis and carbonic anhydrase inhibition of a series of SLC-0111 analogs. Bioorganic & Medicinal Chemistry, 25(9):2569-2576.

Casey JR, Morgan PE, Vullo D, Scozzafava A, Mastrolorenzo A, Supuran CT. 2004. Carbonic anhydrase inhibitors. Design of selective, membrane-impermeant inhibitors targeting the human tumor-associated isozyme IX. Journal of Medicinal Chemistry, 47(9):2337-2347.

Chakravarty S, Kannan KK. 1994. Drug-protein interactions. Refined structures of three sulfonamide drug complexes of human carbonic anhydrase I enzyme. Journal of Molecular Biology, 243(2):298-309.

Chang DK, Moniz RJ, Xu Z, Sun J, Signoretti S, Zhu Q, Marasco WA. 2015. Human anti-CAIX antibodies mediate immune cell inhibition of renal cell carcinoma in vitro and in a humanized mouse model in vivo. 14:119. Molecular Cancer, doi: 10.1186.

Chen J, Rocken C, Hoffmann J, Kruger S, Lendeckel U, Rocco A, Pastorekova S, Malfertheiner P, Ebert MP. 2005. Expression of carbonic anhydrase 9 at the invasion front of gastric cancers. Gut, 54(7):920-927.

Chia SK, Wykoff CC, Watson PH, Han C, Leek RD, Pastorek J, Gatter KC, Ratcliffe P, Harris AL. 2001. Prognostic significance of a novel hypoxia-regulated marker, carbonic anhydrase IX, in invasive breast carcinoma. Journal of Clinical Oncology, 19(16):3660-3668.

Chiche J, Ilc K, Brahimi-Horn MC, Pouysségur J. 2010. Membrane-bound carbonic anhydrases are key pH regulators controlling tumor growth and cell migration. Advances in Enzyme Regulation, 50(1):20-33.

Chiche J, Ilc K, Laferriere J, Trottier E, Dayan F, Mazure NM, Brahimi-Horn MC, Pouyssegur J. 2009. Hypoxia-inducible carbonic anhydrase IX and XII promote tumor cell growth by counteracting acidosis through the regulation of the intracellular pH. Cancer Research, 69(1):358-368.

Csaderova L, Debreova M, Radvak P, Stano M, Vrestiakova M, Kopacek J, Pastorekova S, Svastova E. 2013. The effect of carbonic anhydrase IX on focal contacts during cell spreading and migration. Frontiers in Physiology, 4:271. doi: 10.3389.

De Simone G, Alterio V, Supuran CT. 2013. Exploiting the hydrophobic and hydrophilic binding sites for designing carbonic anhydrase inhibitors. Expert Opinion on Drug Discovery, 8(7):793-810.

De Simone G, Di Fiore A, Menchise V, Pedone C, Antel J, Casini A, Scozzafava A, Wurl M, Supuran CT. 2005. Carbonic anhydrase inhibitors. Zonisamide is an effective inhibitor of the cytosolic isozyme II and mitochondrial isozyme V: solution and X-ray crystallographic studies. Bioorganic & Medicinal Chemistry Letters, 15(9):2315-2320.

Deitmer JW, Theparambil SM, Ruminot I, Becker HM. 2015. The role of membrane acid/base transporters and carbonic anhydrases for cellular pH and metabolic processes. Frontiers in Neuroscience, 8:430. doi: 10.3389.

Del Prete S, Vullo D, De Luca V, Supuran CT, Capasso C. 2014. Biochemical characterization of the δ-carbonic anhydrase from the marine diatom Thalassiosira weissflogii, TweCA. Journal of Enzyme Inhibition and Medicinal Chemistry, 29(6):906-911.

DiMario RJ, Clayton H, Mukherjee A, Ludwig M, Moroney JV. 2017. Plant Carbonic Anhydrases: Structures, Locations, Evolution, and Physiological Roles. Molecular Plant, 10(1):30-46.

Dudutiene V, Zubrienė A, Smirnov A, Timm DD, Smirnovienė J, Kazokaitė J, Michailovienė V, Zakšauskas A, Manakova E, Gražulis S, Matulis D. 2015. Functionalization of fluorinated benzenesulfonamides and their inhibitory properties toward carbonic anhydrases. ChemMedChem, 10(4):662-687.

Emsley P.; Cowtan K. Coot: model-building tools for molecular graphics. Acta Crystallogr., Sect. D: Biol. Crystallogr. 2004, 60, 2126−2132.

Evans, P. R. Scala. Joint CCP4+ ESF-EAMCB Newsletter on Protein Crystallography 1997, 33, 22−24.

Ferry JG. 2010. The gamma class of carbonic anhydrases. Biochimica et Biophysica Acta, 1804(2):374-381.

Fisher SZ, Tu C, Bhatt D, Govindasamy L, Agbandje-McKenna M, McKenna R, Silverman DN. 2007. Speeding up proton transfer in a fast enzyme: kinetic and crystallographic studies on the effect of hydrophobic amino acid substitutions in the active site of human carbonic anhydrase II. Biochemistry, 46(12):3803-3813.

Fisher Z, Hernandez Prada JA, Tu C, Duda D, Yoshioka C, An H, Govindasamy L, Silverman DN, McKenna R. 2005. Structural and kinetic characterization of active-site histidine as a proton shuttle in catalysis by human carbonic anhydrase II. Biochemistry, 44(4):1097-1105.

Frost SC. 2014. Physiological functions of the alpha class of carbonic anhydrases. Subcellular Biochemistry, 75:9-30.

García-Fernández MJ, Tabary N, Martel B, Cazaux F, Oliva A, Taboada P, Concheiro A, Alvarez-Lorenzo C. 2013. Poly-(cyclo)dextrins as ethoxzolamide carriers in ophthalmic solutions and in contact lenses. Carbohydrate Polymers, 98(2):1343-1352.

Gudmundsdóttir E, Stefánsson E, Bjarnadóttir G, Sigurjónsdóttir JF, Gudmundsdóttir G, Masson M, Loftsson T. 2000. Methazolamide 1% in cyclodextrin solution lowers IOP in human ocular hypertension. Investigative Ophthalmology & Visual Science, 41(11):3552-3554.

Gut MO, Parkkila S, Vernerova Z, Rohde E, Zavada J, Hocker M, Pastorek J, Karttunen T, Gibadulinova A, Zavadova Z, Knobeloch KP, Wiedenmann B, Svoboda J, Horak I, Pastorekova S. 2002. Gastric hyperplasia in mice with targeted disruption of the carbonic anhydrase gene Car9. Gastroenterology, 123(6):1889-1903.

Haas NB, Manola J, Dutcher JP, Flaherty KT, Uzzo RG, Atkins MB, DiPaola RS, Choueiri TK. 2017. Adjuvant Treatment for High-Risk Clear Cell Renal Cancer: Updated Results of a High-Risk Subset of the ASSURE Randomized Trial. JAMA Oncology, 3(9):1249-1252.

Heck RW, Boriack-Sjodin PA, Qian M, Tu C, Christianson DW, Laipis PJ, Silverman DN. 1996. Structure-based design of an intramolecular proton transfer site in murine carbonic anhydrase V. Biochemistry, 35(36):11605-11611.

Hewett-Emmett D, Tashian RE. 1996. Functional diversity, conservation, and convergence in the evolution of the alpha-, beta-, and gamma-carbonic anhydrase gene families. Molecular Phylogenetics and Evolution, 5(1):50-77.

Hilvo M, Baranauskiene L, Salzano AM, Scaloni A, Matulis D, Innocenti A, Scozzafava A, Monti SM, Di Fiore A, De Simone G, Lindfors M, Jänis J, Valjakka J, Pastoreková S, Pastorek J, Kulomaa MS, Nordlund HR, Supuran CT, Parkkila S. 2008. Biochemical characterization of CA IX, one of the most active carbonic anhydrase isozymes. The Journal of Biological Chemistry, 283(41):27799-809.

Huang S, Hainzl , Grundström C, Forsman C, Samuelsson G, Sauer-Eriksson AE. 2011. Structural studies of β-carbonic anhydrase from the green alga Coccomyxa: inhibitor complexes with anions and acetazolamide. PLOS ONE, 6(12):e28458.

Hulikova A, Zatovicova M, Svastova E, Ditte P, Brasseur R, Kettmann R, Supuran CT, Kopacek J, Pastorek J, Pastorekova S. 2009. Intact intracellular tail is critical for proper functioning of the tumor-associated, hypoxia-regulated carbonic anhydrase IX. FEBS Letters, 583(22):3563-3568.

Innocenti A, Pastorekova S, Pastorek J, Scozzafava A, De Simone G, Supuran CT. 2009. The proteoglycan region of the tumor-associated carbonic anhydrase isoform IX acts as anintrinsic buffer optimizing CO2 hydration at acidic pH values characteristic of solid tumors. Bioorganic & Medicinal Chemistry Letters, 19(20):5825-5828.

Ivanova J, Carta F, Vullo D, Leitans J, Kazaks A, Tars K, Zalubovskis R, Supuran CT. 2017. N-Substituted and ring opened saccharin derivatives selectively inhibit transmembrane, tumor-associated carbonic anhydrases IX and XII. Bioorganic & Medicinal Chemistry, 25(13):3583-3589.

Jafarzadeh F, Field ML, Harrington DK, Kuduvalli M, Oo A, Kendall J, Desmond M, Mills K. 2014. Novel application of acetazolamide to reduce cerebrospinal fluid production in patients

undergoing thoracoabdominal aortic surgery. Interactive CardioVascular and Thoracic Surgery, 18(1):21-26.

Kaluz S, Kaluzova M, Liao SY, Lerman M, Stanbridge EJ. 2009. Transcriptional control of the tumor- and hypoxia-marker carbonic anhydrase 9: A one transcription factor (HIF-1) show? Biochimica et Biophysica Acta, 1795(2):162-172.

Kanski JJ. 1968. Carbonic anhydrase inhibitors and osmotic agents in glaucoma. Carbonic anhydrase inhibitors. British Journal of Ophthalmology, 52(8):642-643.

Katayama F, Miura H, Takanashi S. 2002. Long-term effectiveness and side effects of acetazolamide as an adjunct to other anticonvulsants in the treatment of refractory epilepsies. Brain & Development, 24(3):150-154.

Kaur IP, Smitha R, Aggarwal D, Kapil M. 2002. Acetazolamide: future perspective in topical glaucoma therapeutics. International Journal of Pharmaceutics, 248(1-2):1-14.

Kikutani S, Nakajima K, Nagasato C, Tsuji Y, Miyatake A, Matsuda Y. 2016. Thylakoid luminal θ-carbonic anhydrase critical for growth and photosynthesis in the marine diatom Phaeodactylum tricornutum. Proceedings of the National Academy of Sciences of the United States of America, 113(35):9828-9833.

Kivela J, Parkkila S, Parkkila AK, Leinonen J, Rajaniemi H. 1999. Salivary carbonic anhydrase isoenzyme VI. The Journal of Physiology, 520 Pt 2:315-320.

Köhler K, Hillebrecht A, Schulze Wischeler J, Innocenti A, Heine A, Supuran CT, Klebe G. 2007. Saccharin inhibits carbonic anhydrases: possible explanation for its unpleasant metallic aftertaste. Angewandte Chemie International Edition, 46(40):7697-9.

Krishnamurthy VM, Kaufman GK, Urbach AR, Gitlin I, Gudiksen KL, Weibel DB, Whitesides GM. 2008. Carbonic anhydrase as a model for biophysical and physical-organic studies of proteins and protein-ligand binding. Chemical Reviews, 108(3):946-1051.

Krungkrai SR, Krungkrai J. 2011. Malaria parasite carbonic anhydrase: inhibition of aromatic/heterocyclic sulfonamides and its therapeutic potential. Asian Pacific Journal of Tropical Biomedicine, 1(3):233-242.

Kumar V., Abbas A. K., Fausto N., Mitchell R. 2007. Robbins Basic Pathology. Elsevier 8(1): 802–803.

Laitaoja M, Valjakka, Jänis J. 2013. Zinc coordination spheres in protein structures. Inorganic Chemistry, 52(19):10983-10991.

Langella E, Buonanno M, Vullo D, Dathan N, Leone M, Supuran CT, De Simone G, Monti SM. 2018. Biochemical, biophysical and molecular dynamics studies on the proteoglycan-like domain of carbonic anhydrase IX. Cellular and Molecular Life Sciences, 75(17):3283-3296.

Lapointe M, Mackenzie TD, Morse D. 2008. An external delta-carbonic anhydrase in a free-living marine dinoflagellate may circumvent diffusion-limited carbon acquisition. Plant Physiology, 147(3):1427-1436.

Leaf DE, Goldfarb DS. 2007. Mechanisms of action of acetazolamide in the prophylaxis and treatment of acute mountain sickness. Journal of Applied Physiology, 102(4):1313-1322.

Leitans J, Kazaks A, Balode A, Ivanova J, Zalubovskis R, Supuran CT, Tars K. 2015. Efficient Expression and Crystallization System of Cancer-Associated Carbonic Anhydrase Isoform IX. Journal of Medicinal Chemistry, 58(22):9004-9009.

Leppilampi M, Karttunen TJ, Kivela J, Gut MO, Pastorekova S, Pastorek J, Parkkila S. 2005. Gastric pit cell hyperplasia and glandular atrophy in carbonic anhydrase IX knockout mice: studies on two strains C57/BL6 and BALB/C. Transgenic Research, 14(5):655-663.

Leslie, A. G. W. Recent changes to the MOSFLM package for processing film and image plate data. Joint CCP4+ ESF-EAMCB Newsletter on Protein Crystallography 1992, 26.

Liljas A, Laurberg M. 2000. A wheel invented three times. The molecular structures of the three carbonic anhydrases. EMBO Reports, 1(1):16-17.

Lindskog S. 1997. Structure and mechanism of carbonic anhydrase. Pharmacology & Therapeutics, 74(1):1-20.

Lolak N, Akocak S, Bua S, Sanku RKK, Supuran CT. 2019. Discovery of new ureido benzenesulfonamides incorporating 1,3,5-triazine moieties as carbonic anhydrase I, II, IX and XII inhibitors. Bioorganic & Medicinal Chemistry, 27(8):1588-1594.

Lusthaus JA, Goldberg I. 2017. Brimonidine and brinzolamide for treating glaucoma and ocular hypertension; a safety evaluation. Expert Opinion on Drug Safety, 16(9):1071-1078.

Mahalingam SM, Chu H, Liu X, Leamon CP, Low PS. 2018. Carbonic Anhydrase IX-Targeted Near-Infrared Dye for Fluorescence Imaging of Hypoxic Tumors. Bioconjugate Chemistry, 29(10):3320-3331.

Mahon BP, Pinard MA, McKenna R. 2015. Targeting carbonic anhydrase IX activity and expression. Molecules, 20(2):2323-2348.

Maren TH. 1967. Carbonic anhydrase: chemistry, physiology, and inhibition. Physiological Reviews, 47(4):595-781.

Maupin CM, Voth GA. 2007. Preferred orientations of His64 in human carbonic anhydrase II. Biochemistry, 46(11):2938-2947.

Mincione F, Scozzafava A, Supuran CT. 2008. The development of topically acting carbonic anhydrase inhibitors as antiglaucoma agents. Current Pharmaceutical Design, 14(7):649-654.

Morgan PE, Pastoreková S, Stuart-Tilley AK, Alper SL, Casey JR. 2007. Interactions of transmembrane carbonic anhydrase, CAIX, with bicarbonate transporters. American Journal of Physiology - Cell Physiology, 293(2):C738-748.

Murshudov G. N, Vagin AA, Dodson EJ. Refinement of macromolecular structures by the maximum-likelihood method. Acta Crystallogr., Sect. D: Biol. Crystallogr. 1997, 53, 240−255.

Nakagawa Y, Uemura H, Hirao Y, Yoshida K, Saga S, Yoshikawa K. 1998. Radiation Hybrid Mapping of the Human MN/CA9 Locus to Chromosome Band 9p12–p13. Genomics, 53 (1): 118–119.

Nakai H, Byers MG, Venta PJ, Tashian RE, Shows TB. 1987. The gene for human carbonic anhydrase II (CA2) is located at chromosome 8q22. Cytogenetics and Cell Genetics, 44(4):234-5.

Pan P, Leppilampi M, Pastorekova S, Pastorek J, Waheed A, Sly WS, Parkkila S. 2006. Carbonic anhydrase gene expression in CA II-deficient (Car2-/-) and CA IX-deficient (Car9-/-) mice. The Journal of Physiology, 571(Pt 2):319-327.

Parkkila S, Lasota J, Fletcher JA, Ou WB, Kivelä AJ, Nuorva K, Parkkila AK, Ollikainen J, Sly WS, Waheed A, Pastorekova S, Pastorek J, Isola J, Miettinen M. 2010. Carbonic anhydrase II. A novel biomarker for gastrointestinal stromal tumors. Modern Pathology, 23(5):743-750.

Pena KL, Castel SE, de Araujo C, Espie GS, Kimber MS. 2010. Structural basis of the oxidative activation of the carboxysomal gamma-carbonic anhydrase, CcmM. Proceedings of the National Academy of Sciences of the United States of America, 107(6):2455-2460.

Pierce WM Jr, Nardin GF, Fuqua MF, Sabah-Maren E, Stern SH. 1991. Effect of chronic carbonic anhydrase inhibitor therapy on bone mineral density in white women. Journal of Bone and Mineral Research, 6(4):347-354.

Pilka ES, Kochan G, Oppermann U, Yue WW. 2012. Crystal structure of the secretory isozyme of mammalian carbonic anhydrases CA VI: implications for biological assembly and inhibitor development. Biochemical and Biophysical Research Communications, 419(3):485-489.

Pinard MA, Mahon B, McKenna R. 2015. Probing the surface of human carbonic anhydrase for clues towards the design of isoform specific inhibitors. BioMed Research International, 2015:453543.

Puscas I, Coltau M, Baican M, Pasca R, Domuta G. 1999. The inhibitory effect of diuretics on carbonic anhydrases. Research Communications in Molecular Pathology and Pharmacology, 105(3):213-236.

Raymond E, ten Bokkel Huinink WW, Taïeb J, Beijnen JH, Faivre S, Wanders J, Ravic M, Fumoleau P, Armand JP, Schellens JH; European Organization for the Research and Treatment of Cancer Early Clinical Study Group. 2002. Phase I and pharmacokinetic study of E7070, a novel chloroindolyl sulfonamide cell-cycle inhibitor, administered as a one-hour infusion every three weeks in patients with advanced cancer. Journal of Clinical Oncology, 20(16):3508-3521.

Reungprapavut S, Krungkrai SR, Krungkrai J. 2004. Plasmodium falciparum carbonic anhydrase is a possible target for malaria chemotherapy. Journal of Enzyme Inhibition and Medicinal Chemistry, 19(3):249-256.

Rowlett RS. 2010. Structure and catalytic mechanism of the beta-carbonic anhydrases. Biochimica et Biophysica Acta, 1804(2):362-373.

Roy A, Taraphder S. 2006. Proton transfer pathways in the mutant His-64-Ala of human carbonic anhydrase II. Biopolymers, 82(6):623-630.

Schneider HP, Alt MD, Klier M, Spiess A, Andes FT, Waheed A, Sly WS, Becker HM, Deitmer JW. 2013. GPI-anchored carbonic anhydrase IV displays both intra- and extracellular activity in cRNA-injected oocytes and in mouse neurons. Proceedings of the National Academy of Sciences of the United States of America, 110(4):1494-1499.

Scozzafava A, Menabuoni L, Mincione F, Briganti F, Mincione G, Supuran CT. 1999. Carbonic anhydrase inhibitors. Synthesis of water-soluble, topically effective, intraocular pressure-lowering aromatic/heterocyclic sulfonamides containing cationic or anionic moieties: is the tail more important than the ring? Journal of Medicinal Chemistry, 42(14):2641-2650.

Serle JB. 1994. Pharmacological advances in the treatment of glaucoma. Drugs & Aging, 5(3):156-170.

Shah GN, Bonapace G, Hu PY, Strisciuglio P, Sly WS. 2004. Carbonic anhydrase II deficiency syndrome (osteopetrosis with renal tubular acidosis and brain calcification): novel mutations in CA2 identified by direct sequencing expand the opportunity for genotype-phenotype correlation.

Shimahara H, Yoshida T, Shibata Y, Shimizu M, Kyogoku Y, Sakiyama F, Nakazawa T, Tate S, Ohki SY, Kato T, Moriyama H, Kishida K, Tano Y, Ohkubo T, Kobayashi Y. 2007.

Tautomerism of histidine 64 associated with proton transfer in catalysis of carbonic anhydrase. The Journal of Biological Chemistry, 282(13):9646-9656.

Siedlecka A, Gardestrom P, Samuelsson G, Kleczkowski L, Krupa Z. 1999. A Relationship between Carbonic Anhydrase and Rubisco in Response to Moderate Cadmium Stress during Light Activation of Photosynthesis. A Journal of Biosciences, 54(9):759-763.

Singh S, Lomelino CL, Mboge MY, Frost SC, McKenna R. 2018. Cancer Drug Development of Carbonic Anhydrase Inhibitors beyond the Active Site. Molecules, 23(5). pii: E1045.

Smith KS, Jakubzick C, Whittam TS, Ferry JG. 1999. Carbonic anhydrase is an ancient enzyme widespread in prokaryotes. Proceedings of the National Academy of Sciences of the United States of America, 96(26):15184-15189.

So AK, Espie GS, Williams EB, Shively JM, Heinhorst S, Cannon GC. 2004. A novel evolutionary lineage of carbonic anhydrase (epsilon class) is a component of the carboxysome shell. Journal of Bacteriology, 186(3):623-630.

Souza VB, Moura Filho FJ, Souza FG, Pereira Filho SA, Coelho SS, Furtado FA, Gonçalves TB, Vasconcelos KF. 2008. Intraocular pressure in schizophrenic patients treated with psychiatric medications. Arquivos Brasileiros de Oftalmologia, 71(5):660-664.

Srinivasan B, Tonddast-Navaei S, Roy A, Zhou H, Skolnick J. 2019. Chemical space of Escherichia coli dihydrofolate reductase inhibitors: New approaches for discovering novel drugs for old bugs. Medicinal Research Reviews, 39(2):684-705.

Supuran & Capasso. 2015. The η-class carbonic anhydrases as drug targets for antimalarial agents. Expert Opinion on Therapeutic Targets, 19(4):551-563.

Supuran CT. 2008a. Diuretics: from classical carbonic anhydrase inhibitors to novel applications of the sulfonamides. Current Pharmaceutical Design, 14(7):641-648.

Supuran CT. 2008b. Carbonic anhydrases: novel therapeutic applications for inhibitors and activators. Nature Reviews Drug Discovery, 7(2):168-181.

Supuran CT. 2012. Structure-based drug discovery of carbonic anhydrase inhibitors. Journal of Enzyme Inhibition and Medicinal Chemistry, 27(6):759-772.

Supuran CT. 2018a. Carbonic anhydrase activators. Future Medicinal Chemistry, 10(5):561-573.

Supuran CT. 2018b. Carbonic anhydrase inhibitors as emerging agents for the treatment and imaging of hypoxic tumors. Expert Opinion on Investigational Drugs, 27(12):963-970.

Talbot DC, von Pawel J, Cattell E, Yule SM, Johnston C, Zandvliet AS, Huitema AD, Norbury CJ, Ellis P, Bosquee L, Reck M. 2007. A randomized phase II pharmacokinetic and pharmacodynamic study of indisulam as second-line therapy in patients with advanced non-small cell lung cancer. Clinical Cancer Research, 13(6):1816-1822.

Tanpure RP, Ren B, Peat TS, Bornaghi LF, Vullo D, Supuran CT, Poulsen SA. 2015. Carbonic anhydrase inhibitors with dual-tail moieties to match the hydrophobic and hydrophilic halves of the carbonic anhydrase active site. Journal of Medicinal Chemistry, 58(3):1494-1501.

Tars K, Matulis D. In press. X-Ray crystallographic structures of high-affinity and high-selectivity inhibitor complexes with CA IX that plays a special role in cancer, (in press).

Tars K, Vullo D, Kazaks A, Leitans J, Lends A, Grandane A, Zalubovskis R, Scozzafava A, Supuran CT. 2013. Sulfocoumarins (1,2-benzoxathiine-2,2-dioxides): a class of potent and isoform-selective inhibitors of tumor-associated carbonic anhydrases. Journal of Medicinal Chemistry, 56(1):293-300.

Taylor AT. 2011. High-altitude illnesses: physiology, risk factors, prevention, and treatment. Rambam Maimonides Medical Journal, 2(1):e0022.

Tu C, Qian M, An H, Wadhwa NR, Duda D, Yoshioka C, Pathak Y, McKenna R, Laipis PJ, Silverman DN. 2002. Kinetic analysis of multiple proton shuttles in the active site of human carbonic anhydrase. The Journal of Biological Chemistry, 277(41):38870-38876.

Tu CK, Silverman DN, Forsman C, Jonsson BH, Lindskog S. 1989. Role of histidine 64 in the catalytic mechanism of human carbonic anhydrase II studied with a site-specific mutant. Biochemistry, 28(19):7913-7918.

Tuccinardi T, Nuti E, Ortore G, Supuran CT, Rossello A, Martinelli A. 2007. Analysis of human carbonic anhydrase II: docking reliability and receptor-based 3D-QSAR study. Journal of Chemical Information and Modeling, 47(2):515-525.

Vagin AA, Murshudov GN, Strokopytov BV. 1998. BLANC: the program suite for protein crystallography. Journal of Applied Crystallography, 31, 98−112.

Vagin A, Teplyakov A. MOLREP: an Automated Program for Molecular Replacement. J. Appl. Crystallogr. 1997, 30, 1022−1025.

Van Berkel MA, Elefritz JL. 2018. Evaluating off-label uses of acetazolamide. American Journal of Health-System Pharmacy, 75(8):524-531.

van den Beucken T, Koritzinsky M, Niessen H, Dubois L, Savelkouls K, Mujcic H, Jutten B, Kopacek J, Pastorekova S, van der Kogel AJ, Lambin P, Voncken W, Rouschop KM, Wouters BG.

2009. Hypoxia-induced expression of carbonic anhydrase 9 is dependent on the unfolded protein response. The Journal of Biological Chemistry, 284(36):24204-24212.

Vullo D, Kumar RSS, Scozzafava A, Ferry JG, Supuran CT. 2018. Sulphonamide inhibition studies of the β-carbonic anhydrase from the bacterial pathogen Clostridium perfringens. Journal of Enzyme Inhibition and Medicinal Chemistry, 33(1):31-36.

Whittington DA, Waheed A, Ulmasov B, Shah GN, Grubb JH, Sly WS, Christianson DW. 2001. Crystal structure of the dimeric extracellular domain of human carbonic anhydrase XII, a bitopic membrane protein overexpressed in certain cancer tumor cells. Proceedings of the National Academy of Sciences of the United States of America, 98(17):9545-9550.

Zavadova Z, Zavada J. 2005. Carbonic anhydrase IX (CA IX) mediates tumor cell interactions with microenvironment. Oncology Reports, 13(5):977-982.

Zimmerman SA, Ferry JG. 2008. The beta and gamma classes of carbonic anhydrase. Current Pharmaceutical Design, 14(7):716-721.